Thermal Stimulation of the Rotokawa Andesite: A Laboratory Approach

Paul August Siratovich

A Thesis Submitted in Partial Fulfilment of the Requirements for the Degree of

Doctor of Philosophy

College of Science

Department of Geological Sciences

University of Canterbury

February, 2014

Contents

List of Figures

List of Tables

Dedication

For mom and dad, thanks for everything

Abstract

Thermal stimulation of geothermal wells is a production enhancement technique that is an attractive option to operators of geothermal fields as a way to enhance and revitalize well performance capabilities through injection of cold water into the geothermal reservoir. This thesis presents a review of thermal stimulation procedures that have been carried out at various geothermal fields worldwide, and then sets out to demonstrate through laboratory experiments the effects of thermal stimulation on typical reservoir rocks.

Thermal damage to crustal rocks is important in many fields of practical engineering applications. Thermal fractures have been discussed in many studies, however their formation under fully water saturated conditions as a result of rapid quenching is not fully understood. In this study, a new methodology is designed to replicate thermal stimulation in such an environment, using an apparatus that allows rocks to be heated to 350°C at up to 22 MPa confining pressure and rapidly quenched with cold water to ambient temperature while maintaining system pressure. The results indicate that through thermal cycling in the apparatus, porosity was increased, density decreased, acoustic velocities attenuated and mechanical properties significantly altered. Maximum damage occurred during the first thermal cycle, a product of the thermo-mechanical Kaiser effect such that rocks should not experience additional damage unless a previous maximum stress is surpassed.

The thesis details a comprehensive evaluation of the Rotokawa Andesite sourced from the Rotokawa Geothermal field located in the Taupo Volcanic Zone, New Zealand. The importance of microstructural fabrics on the physical properties of this reservoir lithology is demonstrated. The mineralogical and petrological fabrics of the rocks are coupled with detailed studies of the microstructural fracture networks, including measurements of porosity, density and permeability. Acoustic wave velocities and dynamic elastic moduli were determined. Uniaxial compressive strength testing coupled with acoustic emission have helped to determine the behavior of the rock under deformation and provided data to characterize the static elastic moduli of the rocks. These data are then utilized to build empirical, micromechanical and geometric relationships.

To better constrain important engineering concerns such as wellbore stability, reservoir forecasting and stimulation procedures, thermal property measurements were carried out on samples recovered from the

Rotokawa Andesite. In particular, measurements of linear thermal expansion, thermogravimetric analysis, and differential scanning calorimetry were measured utilizing varied experimental heating rates of 2, 5 and 20 K/min. The property analyses were carried out to determine if heating rates influenced the measurement of thermal properties, specifically thermal expansion coefficients and strain rate in the samples. Results indicate that thermal expansion is not heating rate dependent within the range investigated though the strain rate is significantly dependent on heating rate, with higher strain rates observed in conjunction with higher heating rates. By using a one dimensional stress model, a failure criterion can be established for the Rotokawa Andesite when subject to thermal stressing. The importance of this study is to further understand the critical heating and cooling rates at which thermal stress causes cracking within the Rotokawa reservoir. This can enhance permeability but can also affect wellbore stability, so constraining these conditions can be beneficial to resource utilization.

To test effects of thermal stimulation in the laboratory, Rotokawa Andesite core was heated to 325^{o}C at pressure of 20 MPa and quenched rapidly to 20^{o}C while maintaining a pressure of 20 MPa. Permeability increased by an order of magnitude over original pre-treatment values. Ultrasonic velocities also reflected a significant change after stimulation testing. Scanning electron microscopy showed significant microstructural change to samples and supplemented physical property investigations. The results imply that thermal stimulation can be successfully repeated in the laboratory and is coupled with both thermal and chemical components. The results of these investigations are of profound importance for effective utilization and maintenance of the Rotokawa Geothermal field and the results also have implications for geothermal fields worldwide.

Acknowledgements

To thank all of the people whom have helped me along through my doctoral studies would be a thesis in and of itself but I would like to make special mention of those who have made this dream become a reality, challenged me to think critically and supported my ideas the whole way through no matter how outlandish.

- Special thanks to Mighty River Power Company Limited for financial support during my research. This research project has changed my life and the Source to Surface program is one of the most incredible research projects that I could have imagined to take part in.
- Professor Jim Cole, Jim has been an essential part of this research every step of the way. I liked Jim from the first time I met him and we have become good mates through the course of this research. I value your friendship and sound guidance very much; I could not have pulled this off without you.
- Dr. Marlène Villeneuve, thank you very much for the sound guidance and great conversations both about work and life in general. Thanks for bringing be up to speed on my rock mechanics and helping me to grow as a scientist and as a person.
- Dr. Darren Gravley, thanks for making my time at Canterbury a fantastic one and bringing me into the Source to Surface group. It has been a life-changing experience and all of this would not have happened without your vision. You are an awesome guy and I look forward to more good times in the future.
- Dr. Ben Kennedy, thanks for wicked conversations, great ideas for cool experiments, inspiration for the laboratory testing and overall being a great dude.
- Mr. Thomas Powell, thank you for your support in pursuing this research, it has been a great time and I really look forward to doing more research with you and having many more fun times.
- Dr. Joe Gamman, I would definitely not have come to Canterbury without you. Source to Surface made my transition here seamless and allowed me to work with some great people. I cannot express how much I appreciate your help in making this research project a reality and I look forward to many more interesting times down the road.
- Florence Bégué for putting up with my office and social shenanigans. I know that I need to keep my mouth shut more often than not, but thanks for being a good sport about it. Definitely the best office mate I've ever had.
- Jonathan Davidson and Marie-Claude Hébert, also for putting up with me and my nonsense, you guys are awesome and I value your friendship every step of the way, and you too Johnny are a pretty awesome part of the office mate dynamic duo.
- Dr. Felix von Aulock. Thank you for all of the inspiration, putting me up in Liverpool and just being a great guy. Thanks for all the great conversations and good times, many more to come my friend.
- Dr. Mike Heap. Thanks for the inspiration and rigorous scientific banter, and the good laughs and snide remarks along the way.
- Professor Yan Lavallée. Thanks for the trips to Liverpool to get into some great experimental work. I'm looking forward to some more laughs and good times very soon.

- MRP staff: Steven Sewell, Irene Wallis, Novi Ganefianto, Ben Pezaro, Dan Warren.
- GNS Colleagues: Dr. Greg Bignall, Dr. David McNamara, Dr. Isabelle Chambrefort.
- Technical Staff of UC Geology: Matt Cockroft, Rob Spiers, Cathy Higgins, Dr. Kerry Swanson, Janet Brehaut, Sacha Baldwin-Cunningham.
- Mr. Sverrir Thórhallsson and Dr. Gudni Axelsson for introducing me to thermal stimulation during my time in Iceland and inspiring this research.
- The old guard: Dr. Jonathan Wardman, Dr. Paul Ashwell, Dr. Jacqueline Dohaney, Dr. Theodosios Kritikos (and Master Penelopi Zaka), Kristel Noges, you guys all made my time at Canterbury absolutely wonderful.
- The rest of the Canterbury folks in no particular order: Simon, Louise, Hamish, Emma, Bec, James, Josh, Josh, Eva, Shaun, Tom, Tom, Tom, Nick, Mark, Travis, Chris, Sam, Val, Carolyn, etc.
- The Crossfit Christchurch people for keeping me physically in tact: Chris Coxon, Pat Kailey, Johanna Coxon, Julie Dupree, Josh Dowdle, Peter and Sarah Evans, Jared Kelly, and all the other folks who push me along
- The Colorado people who helped make me the person I am today: Ben, Hunter, Daniel, Kristy, Meredith, Andrea, Alex, Brian, Brandon, Casey, David, Megan, Dave, Taylor, Courntey and all the rest
- My awesome family: Mom, Dad, Alex, Ashley, Avery, Uncle Bob, Aunt Sally, Uncle Steve, Sarah you guys rock
- My New Zealand kayaking mates, keeping me sane with the occasional foray into some amazing places.
- The people of Canterbury, times have been rough but will get better Kia Kaha!
- And anyone else who I have left off the list, you aren't forgotten, it would just take too long to put you all on here!

Declaration of Authorship

Deputy Vice-Chancellor's Office
Postgraduate Office

UNIVERSITY OF CANTERBURY
Te Whare Wānanga o Waitaha
CHRISTCHURCH NEW ZEALAND

Co-Authorship Form

This form is to accompany the submission of any PhD thesis that contains research reported in co-authored work that has been published, accepted for publication, or submitted for publication. A copy of this form should be included for each co-authored work that is included in the PhD thesis. Completed forms should be included at the front (after the thesis abstract) of each copy of the thesis submitted for examination and library deposit (including electronic copy).

Please indicate the chapter/section/pages of this thesis that are extracted from co-authored work and provide details of the publication or submission from the extract comes:

Chapter 3, submitted to International Journal of Rock Mechanics and Mining Sciences

Please detail the nature and extent (%) of contribution by the PhD candidate:

100% of research is of the candidate's original work. Co-authors provided dialogue, suggestions for revision and editorial comments.

Certification by Co-authors:

If there is more than one co-author then a single co-author can sign on behalf of all

The undersigned certifys that:

- The above statement correctly reflects the nature and extent of the PhD candidate's contribution to this co-authored work
- In cases where the PhD candidate was the lead author of the co-authored work he or she wrote the text

Name: **J.W.Cole** Signature:  Date: *January 31, 2014*

Deputy Vice-Chancellor's Office
Postgraduate Office

UNIVERSITY OF CANTERBURY
Te Whare Wānanga o Waitaha
CHRISTCHURCH NEW ZEALAND

Co-Authorship Form

This form is to accompany the submission of any PhD thesis that contains research reported in co-authored work that has been published, accepted for publication, or submitted for publication. A copy of this form should be included for each co-authored work that is included in the PhD thesis. Completed forms should be included at the front (after the thesis abstract) of each copy of the thesis submitted for examination and library deposit (including electronic copy).

Please indicate the chapter/section/pages of this thesis that are extracted from co-authored work and provide details of the publication or submission from the extract comes:
Chapter 4, to be submitted to Geothermal Energy

Please detail the nature and extent (%) of contribution by the PhD candidate:
100% of research is of the candidate's original work. Co-authors provided dialogue, suggestions for revision and editorial comments.

Certification by Co-authors:
If there is more than one co-author then a single co-author can sign on behalf of all
The undersigned certifys that:

- The above statement correctly reflects the nature and extent of the PhD candidate's contribution to this co-authored work
- In cases where the PhD candidate was the lead author of the co-authored work he or she wrote the text

Name: **J.W.Cole** Signature:  Date: *January 31, 2014*

Deputy Vice-Chancellor's Office
Postgraduate Office

UNIVERSITY OF CANTERBURY
Te Whare Wānanga o Waitaha
CHRISTCHURCH NEW ZEALAND

Co-Authorship Form

This form is to accompany the submission of any PhD thesis that contains research reported in co-authored work that has been published, accepted for publication, or submitted for publication. A copy of this form should be included for each co-authored work that is included in the PhD thesis. Completed forms should be included at the front (after the thesis abstract) of each copy of the thesis submitted for examination and library deposit (including electronic copy).

Please indicate the chapter/section/pages of this thesis that are extracted from co-authored work and provide details of the publication or submission from the extract comes:
Chapter 5, to be submitted to Journal of Volcanology and Geothermal Research

Please detail the nature and extent (%) of contribution by the PhD candidate:
100% of research is of the candidate's original work. Co-authors provided dialogue, suggestions for revision and editorial comments.

Certification by Co-authors:
If there is more than one co-author then a single co-author can sign on behalf of all
The undersigned certifys that:

- The above statement correctly reflects the nature and extent of the PhD candidate's contribution to this co-authored work
- In cases where the PhD candidate was the lead author of the co-authored work he or she wrote the text

Name: **J.W.Cole** Signature:  Date: *January 31, 2014*

Deputy Vice-Chancellor's Office
Postgraduate Office

UNIVERSITY OF CANTERBURY
Te Whare Wānanga o Waitaha
CHRISTCHURCH NEW ZEALAND

Co-Authorship Form

This form is to accompany the submission of any PhD thesis that contains research reported in co-authored work that has been published, accepted for publication, or submitted for publication. A copy of this form should be included for each co-authored work that is included in the PhD thesis. Completed forms should be included at the front (after the thesis abstract) of each copy of the thesis submitted for examination and library deposit (including electronic copy).

Please indicate the chapter/section/pages of this thesis that are extracted from co-authored work and provide details of the publication or submission from the extract comes:
Chapter 6, to be submitted to Geophysical Research Letters

Please detail the nature and extent (%) of contribution by the PhD candidate:
100% of research is of the candidate's original work. Co-authors provided dialogue, suggestions for revision and editorial comments.

Certification by Co-authors:
If there is more than one co-author then a single co-author can sign on behalf of all
The undersigned certifys that:

- The above statement correctly reflects the nature and extent of the PhD candidate's contribution to this co-authored work
- In cases where the PhD candidate was the lead author of the co-authored work he or she wrote the text

Name: **J.W.Cole** Signature:  Date: *January 31, 2014*

Chapter 1

Introduction

Geothermal reservoir environments present unique challenges to economically and optimally utilize high-enthalpy resources. Occasionally wellbores intended to tap these resources suffer from a lack of productivity or injectivity which can cause disruptions in resource utilization, reducing the value of the projects. This is generally related to permeability at the wellbore face and within the reservoir. Several processes can take place that reduce permeability such as wellbore collapse, casing degradation, mineral precipitation and filling of feed-zones with debris. Additionally, wells can be drilled that never encounter the permeable networks of the reservoir or encounter significant problems during their drilling. This can make such wells valueless. Through a carefully applied stimulation procedure, wells can be revitalized through an enhancement of permeability and hence become major assets to field operations.

The completion and maintenance of geothermal wells in a geothermal power project are the most cost-intensive aspects of geothermal projects, aside from the power-plant infrastructure. In order to keep costs down, the output of the wells must be optimized using the least expensive techniques available. One method that has been explored and has shown great success in many areas of the world is thermal stimulation. This involves the injection of fluids that are cooler than the reservoir rock to increase permeability at the well-reservoir interface and within the reservoir itself. The procedure has been postulated to achieve success through: 1) cleaning cuttings emplaced into permeable zones during drilling, 2) re-opening old or sealed fractures, and 3) creation of new fractures in the reservoir. The focus of this thesis will be the last of these mechanisms.

Thermal stimulation is a technique that is very attractive to operators as it can be realized at a much lower cost than chemical and hydraulic stimulations (Flores et al., 2005). Chemical stimulations are aimed at dissolving materials that hinder fluid flow and when appropriately applied achieve significant gains. However, chemical stimulation can also greatly increase chemical wear on important mechanical components such as wellheads and casings (Pasikki et al., 2010). Hydraulic stimulations use high injection pressures to generate

mechanical cracks, but their application in traditional high-temperature geothermal environments can be challenging as there can be increased risk to consider from factors such as wellbore stability issues, thermal degradation of treatment fluids and a lack of temperature stable propping agents (Zoback et al., 2003; Flores et al., 2005). Thermal stimulation involves the injection of water at low temperature and relatively low pressure into the wellbore with the goal to thermally contract or fracture the reservoir rock and hence enhance the permeability. Several geothermal fields worldwide (e.g. Kitao et al., 1990; Flores et al., 2005, Axelsson and Thorhallsson, 2009; Grant et al., 2013) have shown that this technique can be a very effective tool to enhance permeability and subsequently result in greater fluid handling capabilities for commercial powerplant installations.

Many investigations have been made into the role of thermal cracking of rock samples during heating and resultant changes in rock properties (e.g. Darot et al., 1992; David et al., 1999; Chaki et al., 2008; Nara et al., 2011; Heap et al., 2013), but no investigation has been done in a laboratory setting to explore the role of rapidly induced thermal stress by rapid cooling. This mechanism appears to be one process responsible for the creation of enhanced permeability through thermal stimulation and this is the primary goal of this thesis.

Understanding thermal fractures in laboratory environments can yield new insight into the formation of thermal stimulation in geothermal field operations. By devleoping rigorous experimental procedures in a controlled laboratory setting to test the role of thermal shocking on geothermal rocks, a comprehensive understanding of the procedure can be developed and an ideal methodology for its application can be developed.

1.1 Thesis Approach and Organization

This thesis aims to replicate thermal stimulation of geothermal reservoirs through laboratory based investigations, by understanding the microscopic scale processes that enhance permeability through injection of cold water into hot geothermal reservoir rocks. The thesis mainly comprises mansuscripts intended for publication in international, peer-reviewed journals. In portions of the following chapters there is some repetition of key concepts and elucidation of previous findings that need to be repeated to give readers the appropriate background on the subjects presented when viewed as separate manuscripts.

As this thesis follows a manuscript style of presentation, the references used in each chapter are included at the end of the chapter in lieu of a comprehensive reference list at the end of the thesis. This is also done

to allow the reader easy reference to the cited material within the same section of the text without having to change between chapters.

The manuscripts are presented with co-authors listed but as readers will note, I am the first author on all of these publications. I have preformed all of the data collection, interpretation and for the most part, processing of the data. My co-authors have been invaluable in discussing results and conclusions but the work presented here is the result of my own investigations and comprise the entirety of the thesis.

- Chapter 2 presents a brief overview of thermal stimulation case studies from geothermal fields worldwide. This chapter details the methodology of its application and the varied results of thermal stimulation. Several different hypotheses are presented from the various locations but in all cases one theme is consistent; thermal stimulation enhances permeability. Portions of this chapter were published in the Geothermal Resources Council Transactions as part of the 2011 annual meeting.

- Chapter 3 presents the development and initial testing methodology for a device specially built at the University of Canterbury to replicate thermal stimulation in the laboratory. This paper entitled "A New Methodology for Replicating Geothermal Reservoir Stimulation in the Laboratory" has been submitted to the International Journal of Rock Mechanics and Mining Sciences. The paper has been reviewed by one anonymous reviewer and also by Dr. Michael Heap who is listed as a co-author on subsequent publications in this thesis. The reviewers suggested major revisions and the paper to be published as a technical note in the journal. The revised version of the paper has been substantially changed with new material added which will then be re-submitted for consideration as a full research paper.

- Chapter 4 details our investigations on core sourced from the Rotokawa Andesite. The Rotokawa Geothermal field has seen the application of several thermal stimulation projects resulting in improved fluid handling capabilities of the field infrastructure. Therefore, it was chosen as the material to be utilized in this study for application of thermal stimulation procedures in the laboratory. Before thermal stimulation could be applied to the rocks it was essential to gain an understanding of the fundamental properties of these rocks. So, a detailed investigation was carried out to characterize the rocks from microscopic to macroscopic scale. These investigations utilized scanning electron and optical microscopy to understand the textures and compositions at the microscopic scale. Further, studies of physical properties such as porosity, density, permeability, acoustic velocities and strength were conducted. Through an application of our experimental results, we present empirical, micromechanical and geometrical relationships for the Rotokawa Andesite. This paper is in the final stages of preparation

for the Springer Journal "Geothermal Energy" and has benefitted from collaboration with Dr. Michael Heap and Dr. Thierry Reuschlé of the University of Strasbourg for permeability measurements and modeling discussions.

- Chapter 5 discusses the results of a study on the thermo-elastic properties of the Rotokawa Andesite. Thermo-mechanical and thermo-chemical studies were preformed on samples of the andesite to constrain thermal expansion coefficients and the behavior of the andesite under different heating and cooling rates. The results are then applied to classical models of thermal expansion behavior based on porosity models for isotropic media. The results are further utilized in models of tensile stress as a result of thermally induced stress. This paper is also in final stages of co-author review and is anticipated to be submitted to the Journal of Volcanology and Geothermal Research. The research benefitted from use of laboratory facilities at the University of Liverpool and collaboration with Professor Yan Lavallee and Dr. Felix von Aulock, also at the University of Liverpool.

- Chapter 6 details the results of thermal stimulation testing on the Rotokawa Andesite and the resulting increases in permeability and changes to physical properties. These results are detailed as physical and chemical changes to the samples with discussion relevant to thermal stimulation in geothermal fields. The results illustrate that permeability can be enhanced using our testing methodology. This paper is to be submitted to the American Geophysical Union's publication "Geophysical Research Letters".

- Chapter 7 presents the conclusions and key findings of the thesis work. Implications and considerations for industrial applications of this work are presented. Finally, suggestions for further experimental work are presented with regard to thermo-chemical interactions and permeability changes measured with differential confining pressures and temperatures.

- Appendices A-D are a compilation of datasets that were collected during this thesis
  - Appendix A is a compilation of thin section photo-micrographs and scanning electron microscope images collected from my studies of the Rotokawa Andesite.
  - Appendix B is a comprehensive database of the ultrasonic measurements that I have carried out throughout my thesis work.
  - Appendix C provides stress-strain spreadsheets and acoustic emission datasets that were collected during mechanical testing.
  - Appendix D compilation of reflected light photomicrographs and spreadsheets used in crack volume calculations of Rotokawa Andesite.

1.2 References

Axelsson, G.and Thorhallsson, S., (2009). Review of Well stimulation Operations in Iceland. Geotherm. Resour. Counc. Trans. 33, 795–800.

Chaki, S., Takarli, M., and Agbodjan, W.P., (2008). Influence of thermal damage on physical properties of a granite rock: Porosity, permeability and ultrasonic wave evolutions. Constr. Build. Mater. 22, 1456–1461.

Darot, M, Gueguen, Y., and Baratin, M.-L., (1992). Permeability of Thermally Cracked Granite. Geophys. Res. Lett. 19, 869–872.

David, C., Menendez, B., and Darot, M., (1999). Influence of stress-induced and thermal cracking on physical properties and microstructure of La Peyratte granite. Int. J. Rock Mech. Min. Sci. 36, 433–448.

Flores, M., Davies, D., Couples, G., and Palsson, B., (2005). Stimulation of Geothermal Wells, Can We Afford It ?, in: Proceedings World Geothermal Congress, Antalya, Turkey 24-29 April. p. 8.

Grant, M.A., Clearwater, J., Quinao, J., Bixley, P.F., and Le Brun, M., (2013). Thermal Stimulation of Geothermal Wells: A Review of Field Data, In: Proceedings, Thirty-Eighth Workshop on Geothermal Reservoir Engineering. Stanford University, Stanford, California. p. 7.

Heap, M.J., Mollo, S., Vinciguerra, S., Lavallée, Y., Hess, K., Dingwell, D.B., Baud, P., Iezzi, G., (2013). Thermal weakening of the carbonate basement under Mt . Etna volcano (Italy): Implications for volcano instability. J. Volcanol. Geotherm. Res. 250, 42–60.

Kitao, K., Ariki, K., Hatakeyama, K., and Wakita, K., (1990). Well Stimulation Using Cold-Water Injection Experiments in the Sumikawa Geothermal Field, Akita Perfecture, Japan. Geotherm. Resour. Counc. Trans. 14, 1219–1224.

Nara, Y., Meredith, P.G., Yoneda, T., and Kaneko, K., (2011). Influence of macro-fractures and micro-fractures on permeability and elastic wave velocities in basalt at elevated pressure. Tectonophysics 503, 52–59.

Pasikki, R.G., Libert, F., Yoshioka, K., and Leonard, R., (2010). Well Stimulation Techniques Applied at the Salak Geothermal Field, in: Proceedings World Geothermal Congress, Bali, Indonesia., vol 25-29. p. 11.

Zoback, M.D., Barton, C.A., Brudy, M., Castillo, D., Finkbeiner, T., Grollimund, B., Moos, D., Peska, P., Ward, C., and Wiprut, D., (2003). Determination of stress orientation and magnitude in deep wells. Int. J. Rock Mech. Min. Sci. 40, 1049–1076.

Chapter 2

A Review of Practical Experience in Thermal Stimulation

Abstract

Thermal stimulation of geothermal wells is a production enhancement technique that is an attractive option to operators of geothermal fields as a way to enhance and revitalize well performance capabilities through injection of cold water into the geothermal reservoir. Fracture formation, cleaning, and re-opening has been attributed to successful thermal stimulation. But to date, there has not been one preferred methodology for application of thermal stimulation, as surface infrastructure, injection fluid availability, and well completion details have been the primary controls on the application of the technique. This chapter presents a review of thermal stimulation procedures that have been carried out at various geothermal fields worldwide. While the application varies worldwide, it has seen several successful applications and is attractive to geothermal operators for field maintenance and ensuring reservoir longevity.

2.1 Thermal Stimulation Overview

Thermal stimulation has been utilized in many different ways in the geothermal fields that have seen its application. The end goal of the technique is to enhance permeability between the well and reservoir and even to deeper portions of the reservoir itself. This method exploits the thermo-elastic stress on the reservoir which can increase permeability by opening new fractures and contracting the reservoir rock mass, widening existing fractures and, increasing permeability (Pasikki et al., 2010; Grant et al., 2013). Thermal stimulation has also been postulated to result in the re-opening of sealed fractures, cleaning of fractures plugged by debris from drilling and completion operations and chemical erosion of permeability reducing materials (Kitao et al., 1990; Flores-Armenta and Tovar-Aguado, 2008; Axelsson and Thórhallsson, 2009; Pasikki et al., 2010).

The injection temperature of fluids into the wellhead during stimulation can range from 20°C, sourced from nearby fresh water sources, to 165°C, sourced from separated geothermal brine from power plant infrastructure (Björnsson, et al., 2004; Pasikki et al., 2010, Grant et al., 2013). Injection of a cooler than reservoir fluid in almost all cases provides a catalyst to enhance well fluid handling characteristics.

Thermal Stimulation can take place from a few hours after wells have been drilled to several months of long term, often cyclic injection. Thermal cycling in production wells has been shown to be an effective technique by rapidly cooling and heating the wellbore; the stresses are enhanced at the reservoir-well interface and there is permeability improvement (Bjornsson, 2004; Kitao et al., 1990). In addition, long term injection of cold water has shown significant improvement in fluid handling capacities in injection wells at the Rotokawa and Kawerau fields, New Zealand (Siega et al., 2009; Grant et al., 2013). There has as yet been no one 'tried-and true' method to apply thermal stimulation, despite it being an effective means of achieving enhanced permeability at the well-bore reservoir interface.

2.2 Thermal Stimulation Case Studies

2.2.1 Iceland

The heating and cooling of geothermal wells to enhance permeability has been a very successful and low risk stimulation technique in Iceland (Axelsson et al., 2006; Axelsson and Thórhallsson, 2009). The main focus of the technique is to thermally shock the reservoir formation to open new and re-open old fractures to enhance a formation's ability to transmit fluids to the well bore. The mechanism responsible for successful thermal stimulation is not well understood, but in Iceland has been more successful in the younger Quaternary reservoir rocks than those of the Tertiary. It is known that thermal shocking enhances or initiates fracture in the rocks, but how geological conditions affect the outcome is not well understood. It has been suggested that fractures are less mineralized (sealed) in the younger rocks, allowing easier permeability enhancement. There may also be a more favorable stress regime in the younger rocks, allowing them to respond to thermal stress in a shorter time span.

The Krafla high-temperature field of Northern Iceland is a field in which thermal stimulation of geothermal well bores has been performed as a standard procedure over the many decades the field has been in operation. More than 34 production wells have been drilled in the region. Most of these wells have been stimulated at the end of drilling operations by injection of cold water into the well through open-ended drill pipe lowered into the well (over variable lengths of time), with additional pressure and temperature monitoring tools.

Each well was allowed to heat up by stopping circulation and then subsequently cooled by water injection. This created thermal stresses in the reservoir and subsequently enhanced hydraulic pathways in the vicinity of the well (Axelsson et al., 2006).

Krafla well KJ-14 was drilled to a depth of 2100m, and provided an excellent example of thermal stimulation success. The well displayed circulation losses of between 4-8 kg/s at the end of the drilling operation, which gave initial indications that permeability near the well was lower than desired. Three days of stimulation were subsequently carried out, which included heating and cooling of the wellbore, and the final circulation losses were in excess of 40 kg/s at the end of the stimulation (Figure 2.1) .

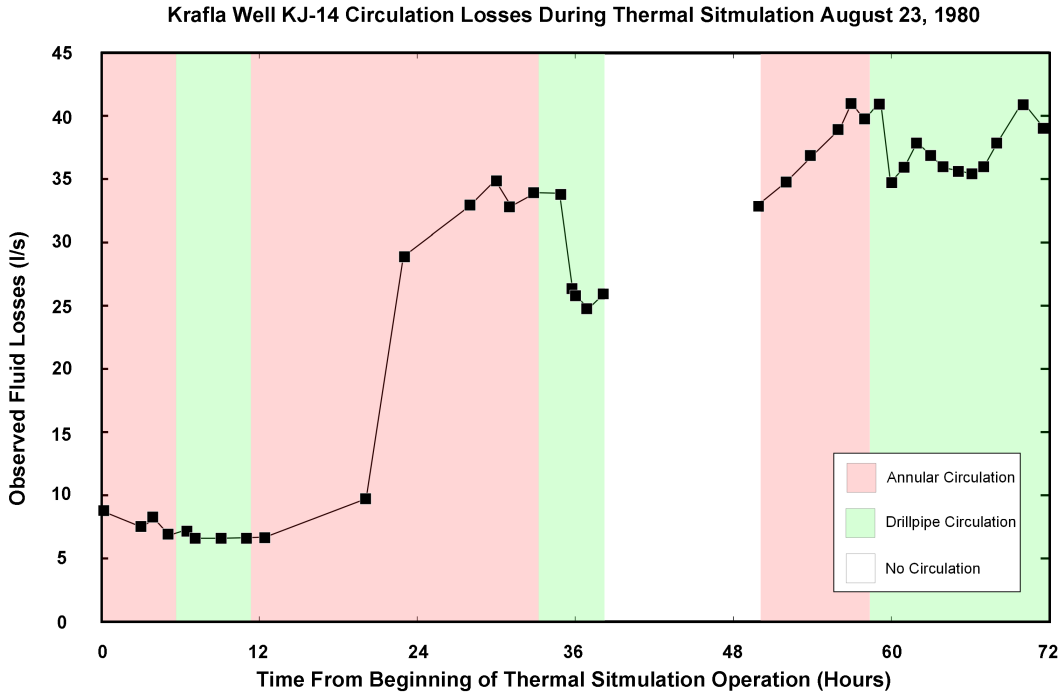

Figure 2.1: Observed circulation losses following drilling of well KJ-14 at Krafla geothermal field, Iceland. Thermal stimulation of the well began almost immediately after drilling and the circulation losses recorded during the procedure (modified after Stefánsson et al., 1982).

This well was one of the most productive in the Krafla region, yielding 15 kg/s of steam during initial production testing. The success of well KJ-14 has been attributed to the opening of existing fractures by the thermal stress, as well as the opening of new fractures by the thermal shocking of the reservoir rock when subjected to temperature extremes. Well KJ-14 proved to be one of the best producers in the Krafla field after the thermal stimulation was carried out (Stefánsson et al., 1982).

There have also been numerous successful stimulations at Hellisheidi field in Southern Iceland. One is well HE-8, which only showed minor circulation losses during drilling of the deeper portions of the well (2400m). During a change of drill bit, the well was circulated with cold water and circulation losses significantly

increased to 43 kg/s, which was attributed to the cleaning of cuttings that had previously filled in permeable zones. The well was further deepened and again became tight through the lower zones of the well. Once the well was drilled to its total depth of 2808 meters, injectivity in the well was poor at only 1-2 (kg/s)/bar and it was decided to lower open-ended drill string into the well to focus cold water injection to the deeper portions of the well. The practice involved injection for 10-20 hours of 20°C water and a heating cycle lasting 12-24 hours. After the initial stimulation, the well was completed and injection testing showed that injectivity had improved to 4-6 (kg/s)/bar. The well was then allowed to heat for 3 months and another stimulation cycle was undertaken, injecting 50 kg/s of 20°C water over a 15 day cycle. After the final stimulation cycle, the well showed an injectivity of 6-7 (kg/s)/bar (Björnsson, 2004; Axelsson et al., 2006; Axelsson and Thórhallsson, 2009). Clearly, the stimulation has had significant effect on the permeability of the well and success can be measured by the improvement in well performance, particularly after a well has been completed and allowed to heat for some time.

2.2.2 Salak, Indonesia

Thermal stimulation was applied in wells Awi 11-5 and Awi 11-6OH in the Salak Geothermal Field, Indonesia. The stimulation was carried out utilizing cyclic injection of hot brine at 165°C and condensate water at 38°C. The cycle lasted from 1-4 weeks and used a range of injection rates between 80 kg/s for condensate injection to upwards of 250 kg/s of hot brine. This cycle was carried out and the evolution of the injectivity index was measured for each well, Awi 11-6OH showed an initial injectivity of 2.0 (kg/s)/bar and increased to 4.0 (kg/s)/bar by the end of the cycle, Well Awi 11-5 showed initial injectivity of 1.1 (kg/s)/bar and increased to 2.6 (kg/s)/bar by the end of initial testing. However, cooling and decreased productivity from adjacent wells within the field was observed, so the thermal injection cycle was abandoned before long-term cooling of the reservoir occurred. The wells were then subjected to slow acid stimulation (SAS). The acidizing also had problems as corrosion was observed at the wellhead that was attributed to failure of corrosion inhibitor in the acid solution at the high injection temperature. The injectivity of Awi 11-6OH did not increase after the acid stimulation and a flow test held two months later still indicated that the well could not produce suitable amounts of steam for production (Pasikki et al., 2010).

2.2.3 Sumikawa, Japan

The Sumikawa geothermal field in Akita Prefecture, Japan was the site of a series of thermal stimulations aimed to improve injectivity and productivity abilities of three wells directionally drilled to approximately 2000m. The wells identified for this study were SA-1, SA-2, and SA-4. The true vertical depths of the feed-points were identified to be 1727m, 1449m, and 1260m respectively. Injection took place using two forced pumps with maximum flow-rates of 70 kg/s at 2.5 bars and two reciprocating pumps capable of producing 40 kg/s at a maximum pressure of 70 bars. The water was injected directly through the wellhead without the use of additional tubing or down-hole equipment. The flow-rates of the injection ranged from 3 kg/s and 110 kg/s during the experiment. The wellhead pressure and flow-rates were monitored from the surface during the procedure. The testing initially used the lowest flow-rate to displace hot fluid from the well bore into the reservoir, and increases in well-head pressure were observed at this time. The well-head pressure then slowly decreased as thermal contraction of the reservoir rocks occurred, and the intake capacity of the wells increased. As the stimulation continued, the intake capacity of the wells increased and was attributed to fracture formation in the reservoir rock and the subsequent permeability increase (Kitao et al., 1990).

In order to quantify the success of the stimulation, production flow rate, fluid enthalpy and injectivity indexes were measured both before and after the operation. There was a clear increase in two of the wells with overall improvements in injectivity through the three wells tested. Well SA-1 showed the greatest improvement; gaining an additional thermal output of 20 MWth three months after the stimulation was concluded. Similarly, well SA-4 also showed overall improvement in output characteristics and showed a power output increase of 3 MWth. Well SA-2 showed a regressive trend after the stimulation that was attributed to casing collapse in the well which prevented the running of tools into the well below 1100m. Overall, the experiment was successful providing a thermal output increase of over 12.7 MWth compared to that before testing. The cost of the experiment was 5.4 million Yen in 1990, which converts to just over 235,000 USD; this gives the improvement in well output to be approximately 18,500 USD/MWth, a significant increase for a low cost stimulation experiment, which compared to drilling an additional well, is a relatively small price for significant improvement of reservoir-well bore connectivity.

2.2.4 Guadeloupe, Lesser Antilles

Well BO-4 on the island of Guadeloupe was drilled to a total depth of 2500 meters in the 1970's, a geothermal power plant nearby began operation in 1988, but the well was found to be below acceptable levels for

commercial production. It was decided to thermally stimulate the well in August, 1998 and to then evaluate if the well had increased in productive ability. Seawater was utilized from the nearby ocean as it is abundant and relatively inexpensive to obtain for the injection of the stimulation procedure. Anhydrite scale inhibitor IDOS 130 was added to the injection water, at a dosage of 10% of the flow rate of injected water, to prevent scaling of anhydrite during the injection procedure. An extensive study was carried out prior to the injection to ensure that the chosen inhibitor could prevent the scaling of anhydrite due to the seawater's chemistry and to ensure that reservoir formation damage could not occur due to the inhibitor. The pressure in the well was monitored at a depth of 600 meters during the operation and provided useful information. At the conclusion it was determined that the injectivity of the well had increased by almost 50% and that the skin effect was significantly decreased. Testing of the well also indicated that fluid flow rates of between 11.1-16.6 tons/hour were possible and indicated that the individual well could possibly produce up to 1 MWe. A year after the stimulation procedures, production testing confirmed that a 50% improvement of the wells ability to produce fluids was still valid, and gave clear indication that the stimulation procedure was a great success (Tulinius et al., 2000).

2.2.5 Los Humeros, Mexico

Well H-40 at Los Humeros geothermal field in Pue, Mexico provides a good example of well revitalization by thermal stimulation that was otherwise a failure after drilling was completed. Well H-40 was drilled to a depth of 2226 meters, but during attempts to deepen the well, a mechanical fish was left in the borehole from 2128 to 2226 meters. The well was completed with a 7" slotted liner from 1600 to 2127m, just above the unrecoverable fish. The results obtained during drilling indicated a highly permeable zone that showed circulation losses between 2.7-7.2 kg/s. After completion the wellhead pressure was quite low during testing and weak, mixed fluid discharged at the surface through the completed wellhead. The well was utilized as a reservoir pressure monitoring well from January 1999 to February 2001, and no improvement to the well production characteristics was observed after this period (Flores-Armeta and Tovar-Aguado, 2008).

Well H-40 was then converted to an injection well that also performed poorly; the maximum fluid intake to the well was 1.38 kg/s. In July 2005, a thermal stimulation program was undertaken in an attempt to improve the well performance. The initial injection was at a mass flow rate of 1.38 kg/s and gradually increased. The fluid injection went on for four days and then was subsequently suspended for 72 hours to allow the well to re-heat and pressure measurements to be taken. The fluid injection then restarted for an additional five days and a maximum input of 9.7 kg/s was achieved. The well was subsequently stimulated a

second time in October 2005 and the injection capacity of the well had increased to accept up to 30.5 kg/s of fluid; it is possible more fluid could have been taken in by the well, but no other water source was available to supplement the maximum intake capacity.

During and after the stimulation, pressure transient tests were conducted to determine permeability thickness, static water levels and skin factor within the well. The permeability thickness decreased after the stimulation, but the skin factor decreased from 1.23 to -3.41, indicating that the well permeability had become reliant on fracture permeability (after Bodvarsson et al., 1984).

2.2.6 New Zealand

There has been successful thermal stimulation in four injection wells at Kawerau and Rotokawa geothermal fields, New Zealand, through the long-term injection of ambient-temperature water into the wells by wellhead injection. The stimulations were carried out over 21-25 days for each well. The water source for the stimulation was from reserve water pits at near-by drilling rig sites and the water was pumped to the wells through water lines, allowing multiple tasks to be completed by tapping into the rig's resources. There were some periods of injection shut-down where the water source was not available due to the needs of drilling activities (Siega et al., 2009)

Wells KA-43 and KA-44, at Kawerau, showed relatively good performance characteristics prior to stimulation, each showing injectivity indexes of 6.4 (kg/s)/bar and 5.5 (kg/s)/bar; these figures improved significantly after the injection cycle. Well KA-43 was stimulated continuously for 21 days and showed a final injectivity of 12.5 (kg/s)/bar. Well KA-44 was initially stimulated for one day, shut in for two days, then continuously stimulated for 20 days and displayed strong increase of injectivity to 26.9 (kg/s)/bar after the cycle.

Wells RK-21 and RK-23 at Rotokawa were also subjected to thermal stimulation. Well RK-21 initially showed an injectivity of 4.2 (kg/s)/bar. Stimulation was similar to the wells at Kawerau, with a near-continuous injection of cold water, and a two-day lapse during the cycle due to fluid availability. The well significantly improved and showed an injectivity index of 10 (kg/s)/ bar after the stimulation was concluded. Well RK-23 was initially a problematic well with a poor injectivity of 0.75 (kg/s)/bar that would also accept very little fluid. After stimulation, the well did not show a great improvement in injectivity as it only increased to 0.83 (kg/s)/bar. However, the down-hole pressure in the well reduced by 40 bar and the injection capacity of the well significantly improved. The well was subsequently able to accept 38.8 kg/s of fluid after the procedure, having previously shown very little injection capacity.

The following observations were attributed to the success of the stimulation operation: feed zones that were not previously observed were opened and contributed to injection capacity; existing feed zones were enhanced, and decreased down-hole pressure in the wells allowed more injection capacity. In addition to these observations, comparison of drilling data to the post-stimulation data indicated criteria that may make wells good candidates for thermal stimulations. In particular, new feed zones that were opened corresponded to zones where circulation losses were observed during drilling, and injectivity in post-drilling operations is not always linear. This suggests that obstructions such as physical debris may have existed at the wellbore face.

2.3 Summarizing Thermal Stimulation Results

Injection of cold water has proven to be an effective way to increase permeability and the results are positive when comparing pre-stimulation well capabilities to post-stimulation capabilities. In almost all cases, a notable increase in well capacity has been observed. Table 2.1 presents the results of the previously mentioned studies and gives an overview of thermal stimulation success.

Table 2.1: Thermal stimulation results from presented case studies. Injectivity Index (II) presented where data was available.

Field (Test Wells)	Injection Rate (kg/s)	Initial II (kg/s)/bar	Post Stimulation II (kg/s)/bar
Hellisheidi (HE-08)	50-60	2	6-7
Sumikawa (SA 1, 2, 4)	3-110	11.1;13.3;9.2	18.2;15.5;11.2
Los Humeros (H-40)	1.3-33	Capacity less than 1.4 kg/s	In excess of 30.5 kg/s
Boulliante (BO-4)	26	0.9	1.4
Salak (Awi-11-6-OH; 11-5)	60-250	2.01; 1.09	4.03; 2.56
Kawerau (KA 44, KA 45)	25-60	6.4; 5.5	12.5; 26.9
Rotokawa (RK 21; 23)	11-39	0.75; 4.2	0.83; 10

It must be noted that the majority of the examples presented here are from injection wells, and that the injectivity index in most cases continues to improve after the stimulations have been carried out, consistent with theory proposed by Grant et al., (2013).

2.4 References

Axelsson, G., Thórhallsson, S., and Bjornsson, G. (2006), Stimulation of Geothermal Wells in Basaltic Rock in Iceland, in ENGINE- Enhanced Geothermal Innovative Network for Europe: Workshop 3 "Stimulation of Reservoir and Induced Microseismicity". Kartause Ittingen, Zurich June 29-July 1, p. 8.

Axelsson, G., and Thórhallsson, S. (2009), Review of Well stimulation Operations in Iceland, Geotherm. Resour. Counc. Trans., 33, 795–800.

Bjornsson, G. (2004), Reservoir Conditions at 3-6 KM Depth in the Hellisheidi Geothermal Field, SW-Iceland, Estimated by Deep Drilling, Cold Water Injection and Seismic Monitoring, in Proceedings, Twenty-Ninth Workshop on Geothermal Reservoir Engineering Stanford University, Stanford, California, January 26-28, 2004, p. 8.

Bodvarsson, G.S., Benson, S.M., Sigurdsson, O., and Stefansson,V. (1984), The Krafla Geothermal Field, Iceland. 1: Analysis of Well Test Data, Water Resour. Res., 20(11), 1515–1530.

Flores-Armenta, M., and Tovar-Aguado, R. (2008), Thermal Fracturing of Well H-40 , Los Humeros Geothermal Field, Geotherm. Resour. Counc. Trans., 32, 8–11.

Grant, M.A., Clearwater, J., Quinao, J., Bixley, P.F., and Le Brun, M. (2013), Thermal Stimulation of Geothermal Wells: A Review of Field Data, in PROCEEDINGS, Thirty-Eighth Workshop on Geothermal Reservoir Engineering. Stanford University, Stanford, California., p. 7.

Kitao, K., Ariki, K., Hatakeyama, K., and Wakita, K. (1990), Well Stimulation Using Cold-Water Injection Experiments in the Sumikawa Geothermal Field, Akita Perfecture, Japan, Geotherm. Resour. Counc. Trans., 14 (Part II), p. 1219–1224.

Pasikki, R. G., Libert, F., Yoshioka, K., and Leonard R. (2010), Well Stimulation Techniques Applied at the Salak Geothermal Field, in Proceedings World Geothermal Congress, Bali, Indonesia, vol. 25-29 Apri, p. 11.

Siega, C. H., Grant, M., and Powell, T. (2009), Enhancing Injection Well Performance by Cold Water Stimulation in Rotokawa and Kawerau Geothermal Fields, in Proceedings, PNOC-EDC Conference, p. 7, Manilla, Philippines.

Stefánsson, V., Gudmundsson, A., Steingrímsson, B., Halldórsson, G.K., Ármannsson, H., Franzson, H., and Hauksson, T. (1982), Krafla – well KJ- 14. Drilling, research and production characteristics, Reykjavík, Iceland. (in Icelandic).

Tulinius, H., Correia, H., Sigurdsson, O. (2000) Stimulating a high enthalpy well by thermal cracking. in Proceedings, World Geothermal Congress, Kyushu-Tohoku, Japan, May 28 - June 10, 2000. 1883-1888.

Chapter 3

A New Methodology for Replicating Geothermal Reservoir Stimulation in the Laboratory

P.A Siratovich[a], M. Villeneuve[a], J. Cole[a], B. Kennedy[a]

[a]Department of Geological Sciences, University of Canterbury, Private Bag 4800, Christchurch 8140, New Zealand

Submitted to the *International Journal of Rock Mechanics and Mining Sciences.*
Draft submitted August 23, 2013. Revised draft presented here.

Abstract

Thermal damage to crustal rocks is important in many fields of practical engineering applications. Geothermal energy production in particular can benefit from the understanding of how thermally induced fractures may enhance permeability at the wellbore and within reservoirs. Thermal stimulation is a reservoir enhancement technique that relies on the generation of permeable fractures by thermal gradients. Thermal fractures are discussed in many studies, however their formation under fully water saturated conditions as a result of rapid quenching is not fully understood. Replication of thermal stimulation in a controlled laboratory environment will allow parameterization of the controls on this process at the field scale and assist in stimulation optimization. In this study we present a new methodology designed to replicate thermal stimulation in such an environment. We have developed an apparatus to allow rocks to be heated to 350°C at up to 22 MPa confining pressure and rapidly quenched with cold water to ambient temperature while maintaining system pressure. In order to test this device, we have characterized a homogeneous rhyolite using acoustic velocity profiling, physical property measurements and uni-axial compressive strength (UCS) testing. Our results indicate that through thermal cycling in our apparatus, we have increased porosity, decreased density,

attenuated acoustic velocities and changed the mechanical properties of our original material. We also discuss the implications of the Kaiser effect regarding damage thresholds in the studied rocks. We conclude that through our methods we have confirmed the processes believed to be responsible for the application of successful thermal stimulation in geothermal fields.

Highlights

- We have replicated geothermal stimulation in the laboratory with excellent results.
- We have induced thermal damage in rocks by cold water quenching.
- Thermal damage has reduced seismic velocities and mechanical strength.
- We have created new fracture damage to rocks as a result of thermal quenching.
- Thermal stimulation in the laboratory replicates what has been observed in the field.

3.1 Introduction

The mechanical degradation and change in fluid transport capabilities of rocks as a result of thermal stressing is a very important research question that spans the practical fields of geothermal energy production, nuclear waste repository security, volcanic stability, and building materials engineering. Geothermal wells can be enhanced by induced thermal gradients in the reservoir rocks [1–4]. Nuclear waste repositories must be stable and seal hazardous wastes and by-products from the outside world; thermal emission and build up of nuclear waste can induce cracking in rocks surrounding these facilities and create environmental hazards due to enhanced permeability from this thermal cracking [5–7]. Building materials made of natural stone and synthetic concretes are also prone to weakening and property alteration due to induced thermal gradients from sources such as fire [8–10]. In addition to materials used for engineering purposes, alteration of rocks by heating and cooling of volcanic edifices can significantly change the fundamental physical properties of those rocks, potentially contributing to weakening [11,12]. Here we present the initial results of testing of a

geothermal stimulation device designed to replicate thermal stimulation procedures carried out at geothermal fields to enhance productivity and injectivity of wells [13–15]. While it has long been accepted that thermal stimulation is an excellent reservoir enhancement technique, there have been no systematic laboratory studies to replicate this process.

Thermal and physical damage of rocks in the laboratory has been extensively studied in an effort to understand the evolution of physical and mechanical properties. Heating damage to rocks has been shown to significantly alter porosity, permeability, uniaxial compressive strength, acoustic velocities and acoustic emission output during strength testing. Homande-Etienne and Troalen [16] published one of the ground-breaking papers on the role of thermal cracking on the texture, porosity and permeability of granites and limestones. This work indicated that most damage within the samples occurred as a result of expansion of inter-crystalline boundaries, increasing the effective (open) porosity of the rocks. Later, several authors [17–20] indicated that dispersed cracking of mineral grains and inter-granular expansion during heating is the dominant mechanism that results in increased porosity during heating of rock specimens. These studies found clear correlations between the induced maximum temperature of the sample and physical properties such as porosity and acoustic wave velocity. Complementary to these studies, it is well documented that increased permeability and decreased seismic velocities are an effect of thermal damage on rocks [11,21,22]. Several other authors have also observed physical and mechanical degradation of rocks due to heat induced damage [23–25]. These studies have investigated rocks heated under consistent temperature gradients of 1-2°C/min and cooled to ambient conditions at the same rate. Yong and Wang [26] investigated heating rates of 0.4-12.5°C/min in Westerly Granite and reported that greatest total acoustic emission is seen during the highest heating rate. They observed little acoustic emission (AE) activity during cooling, but did not report the rates at which cooling occurred.

There have been no studies that have explored the influence of very rapid cooling on rock samples while under fully saturated, pressurized conditions. In order to fully understand how thermal stimulation in a geothermal environment may occur, we have developed a new system and method to induce thermal shock on rock cores by rapid cooling under confined conditions. We present a novel device for thermally shocking rock samples under pressures equivalent to hydrostatic stress conditions within a geothermal system [14]. We also present the initial results as proof of concept for our apparatus that we have changed physical, mechanical and acoustic properties of our source rocks. We characterize porosity, uniaxial compressive strength (UCS), dynamic and static elastic moduli as well as compressional (P-wave) and shear (S-wave) velocity profiling for intact rocks, and compare our results to those of authors who have previously considered thermal stressing under dry conditions.

3.2 The Geothermal Stimulator System Properties

3.2.1 Design parameters

A simple to use, easy to operate, high-temperature, moderate pressure, stimulation system has been developed to allow the heating and cooling of rocks under pressures representative of those found in geothermal systems. The system is capable of maintaining internal temperatures greater than 325°C for several hours and pressures in excess of 25 MPa. The confining media of the vessel is distilled water with the ability to convert the system to use different fluids, such as those from geothermal steam-fields, power plant condensates, via a simple feed to the system. The system is also able to sustain a 'quenching' cycle where system pressure is maintained while cooling of specimens is achieved by passing cooling water through the sample chamber. The system is relatively user-friendly, low maintenance and has a high safety factor despite the temperatures and pressures involved being well over ambient laboratory conditions.

3.2.2 Apparatus overview

The key elements of the stimulator system are a bolted closure reactor vessel, ceramic jacket heater and pressurization system (Figure 3.1). The specimen is placed inside the pressure vessel on a hardened stainless steel (316 grade) platen that is notched to allow fluid to fully encircle the sample on the vessel bottom. The sample chamber is then bolted shut with the specimen located on the platen. The system is flooded with water and all head-space and air in the system removed from the vessel and tubing. A Williams CP500-V300 pump is fed with an air supply of 5-10 bar(g) that pumps distilled water through the system at a variable rate of 0.1 to 8.71 L/H using a timer control. The heater provides thermal input to the vessel chamber and heats both the specimen and the surrounding water.

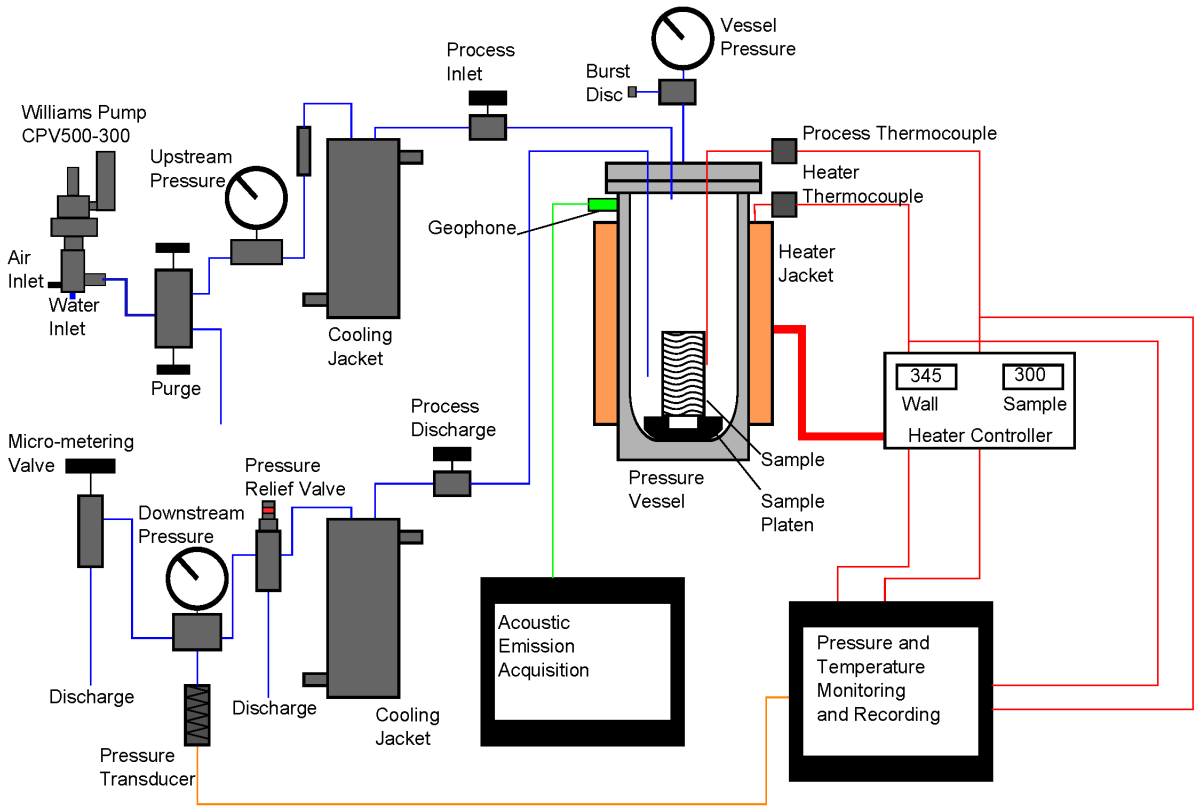

Figure 3.1: The Geothermal Stimulator system. The system consists of three distinct components, pressurization and maintenance, heating elements, and controllers and digital recording of pressure, temperature and acoustic emissions.

3.2.3 Pressure Vessel Specifications

The pressure vessel (PV) is a Bolted Closure Reactor (model BCH-2) provided by High-Pressure Equipment Ltd. and is machined using 316 stainless steel. The vessel has an internal capacity of 1000 ml, interior diameter of 76.2 mm and internal depth of 228.6 mm. Maximum allowable pressure within the vessel is 34.4 MPa at 343°C. The pressure vessel is equipped with a bolted closure with three ports; one for fluid injection, one for fluid rejection and a third for a sample thermocouple.

3.2.4 Heating System

The heating system is comprised of a High-Pressure Equipment Ltd. ceramic jacket heater that runs at 2000 W and 220 volts, controlled by Eurotherm 3208i and 3208 proportional power controllers. One thermocouple is led through the top of the PV and is placed next to the sample; this thermocouple is used to monitor the sample temperature and controls the heating cycle of the system. A second thermocouple is located on the outside of the PV between the vessel wall and the ceramic heater jacket. This thermocouple is slaved to the heating system and is used to monitor the external temperature and controls heat input to the system. The heater controls are set to allow a heating rate of 1°C/min though the controller is capable of rates from 0.1 to 10 °C/min.

3.2.5 Pressurizing System

Pressure maintenance and regulation of the geothermal stimulator system is one of the most important design characteristics of the apparatus. Geothermal system pressure regimes are typically near or slightly under-pressured with respect to hydrostatic pressure [27] in liquid dominated systems. In order to replicate these systems we had to allow for pressurization of the vessel and sample, and ensure that no steam-cap built up in the system that could hinder the effects of our quenching design. Therefore, the system was built with a Williams CPV500-V300 pneumatic plunger pump, capable of delivering up to 8.71 litres per hour at 3.2 cm^3/stroke, a variable stroke rate of 1-45 strokes per minute and a maximum discharge pressure of 224 bar(g). The Williams pump is driven by an air supply of 5-10 bar(g). System pipe-work consists of 1/8" stainless steel 316 tubing. The discharge and pressure regulation of the system is achieved by a Swagelok proportional relief valve (model R4) with a variable pressure of 155 to 275 bar(g). When the system is in the heating cycle, the expansion of water within the vessel creates pressure on the relief valve which is set to 150 bar(g) and opens to relieve pressure (a necessary safety feature). To ensure that the system is kept free of air, the Williams pump cycles a pulse of water into the system once every 2 minutes to make-up for fluid discharge due to pressure build-up. This design was found to be necessary after extensive testing revealed that the system lost too much fluid during the heating stage from the vessel and allowed pressure to drop once the desired temperature had been reached within the system.

The pressurization of the system is achieved by the Williams pump as previously discussed but it is worth noting here that the system operates under an isobaric condition. This was done in an effort to ensure that

when the quenching cycle is initiated, the sample experiences as rapid a temperature change as possible, which is the purpose of the device. As such, the quenching and pressurization are achieved with the same system. The sample experiences an isobaric confinement from the fluid pressure such that during testing the confinement can range from 0.1-24 MPa.

3.2.6 Data Collection System

Monitoring of the stimulation testing is done both manually and digitally by visual gauges that provide the user with information on temperatures and pressures inside the system while under operation. Digital data is collected by a LabView dataDAQ, which monitors the two thermocouple feeds described in Section 3.2.4. A 100 MPa pressure transducer that monitors pressure to within 0.001 MPa is also fed to the LabView software. Acoustic emissions are monitored via the Mistras AE software and USB nodes. The AE node is connected to the pressure vessel via a high-temperature node with a frequency range of 20 kHz to 1 MHz. The AE acquisition is set up to record any emissions above 55 dB as background laboratory noise saturates the acquisition system below this threshold.

3.2.7 System Operation: Pressure Profiles, Temperature Profiles and Heating Cycles

The operation of the geothermal stimulator is relatively simple and requires little maintenance over several cycles of heating and cooling. The operator places a sample on a steel platen in the bottom of the pressure vessel (Figure 3.1) and bolts the vessel shut. The operator then fills the system using the Williams pump and purges all air from the system. During this operation, the desired system pressure for the experimental run is achieved through adjustment of the relief valve. At this stage the sample is under a fully saturated high pressure condition that allows the percolation of water into the open porosity of the sample. The operator checks for pressure stability and once this is achieved, the heating process can begin. The heating controller is switched on and heats at 1°C/min until the desired temperature is reached and maintained. The Williams pump cycles over a 2 minute interval to ensure the system is maintained at the desired pressure range and purges when over-pressured via the relief valve. Once the heating and temperature stabilization cycle ends, the user switches the Williams pump to full capacity to pump cool water into the system and quench the sample. Tables 3.1 and 3.2 detail temperatures change at the sample during a rapid-cooling

cycle and during a slow decline, non-quenched sample run. Figure 3.2 graphically illustrates the heating, temperature stabilization phase and, quenching cycle.

Table 3.1: Cooling time step-points for a sample during quenching to ambient temperature (20°C).

Sample Temperature (°C)	**Time to Cool During Quenching (minutes)**	**Cooling Rate Per Step (°C/min)**
300	-	-
250	3.5	14.28
200	9.0	9.09
150	17.0	6.25
100	27.25	4.88
50	47.5	2.47
Target 20	121.5	0.41

Table 3.2: Cooling time step-points for a sample during slow cooling to ambient temperature (20°C).

Sample Temperature (°C)	**Time to Cool During Quenching (minutes)**	**Cooling Rate Per Step (°C/min)**
300	-	-
250	18.42	2.71
200	44.66	1.90
150	84.58	1.25
100	146.75	0.80
50	286.58	0.36
Target 20	830.42	0.09

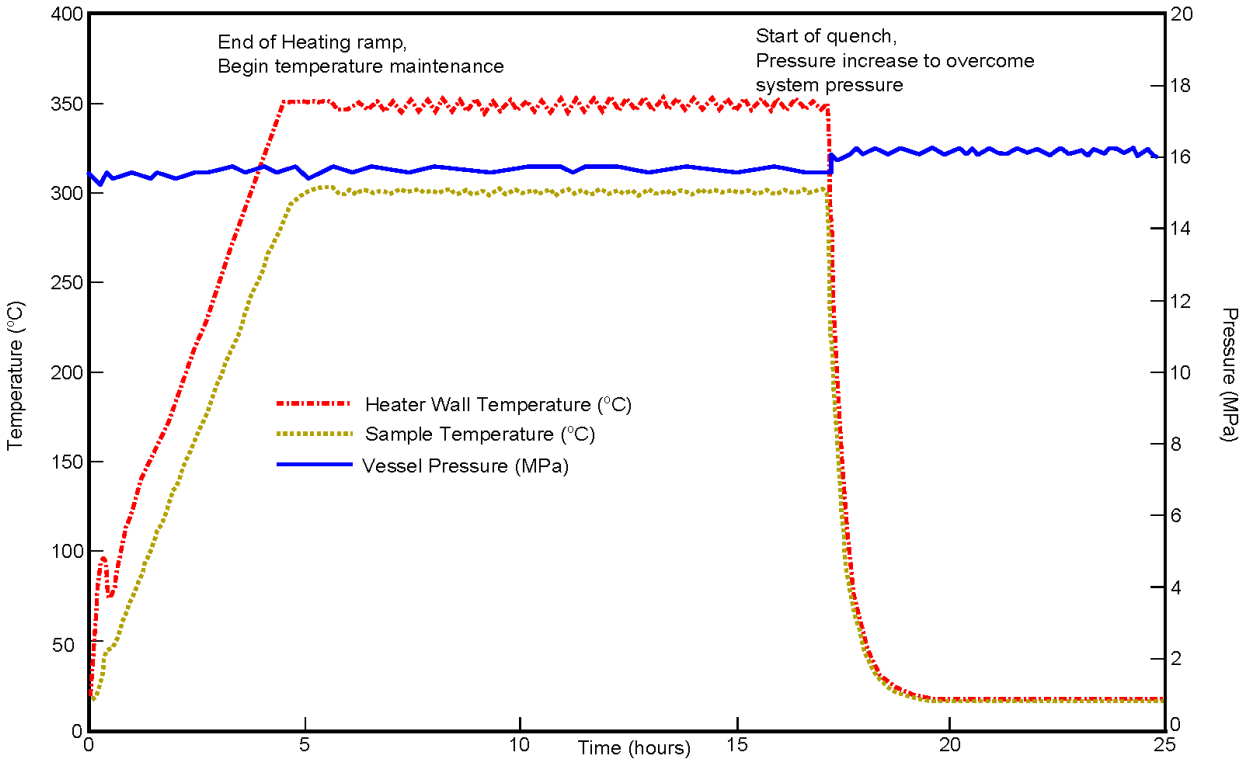

Figure 3.2: Temperature and pressure profiles for the first heating and quenching cycle of sample R5A. The temperature increase takes approximately five hours, is sustained for twelve hours and is quenched in approximately 2 hours. The system is pressurized prior to heating and is slowly de-pressurized at the end of the quench cycle.

3.3 Materials and Methods

3.3.1 Allandale Rhyolite

The material used for this study was Allandale Rhyolite, a unit of the pre-Lyttelton Volcanic Complex (˜12-13 Ma) located in Gebbies Pass, Banks Peninsula, New Zealand [28]. These rhyolites are micro-spherulitic and composed predominantly of devitrified glass, quartz and plagioclase phenocrysts (Figure 3.3). The phenocrysts of quartz and plagioclase show evidence of cracking but the devitrified glass groundmass does not appear to be pervasively cracked. The Allandale Rhyolite was chosen for this study for several reasons: its close proximity to facilities at University of Canterbury, ease of sample preparation, and similarity to rhyolites found within the Taupo Volcanic Zone that serve as reservoir rocks for several geothermal systems in

New Zealand [29–31]. We have characterized the physical, mechanical and elastic properties of the Allandale rhyolites used in this study to determine any changes to these properties that have taken place as a result of thermal stressing, and if so, how this occurred. In order to do so it was necessary to gain a fundamental understanding of the ranges of porosity, density, acoustic wave velocities and mechanical properties of the samples.

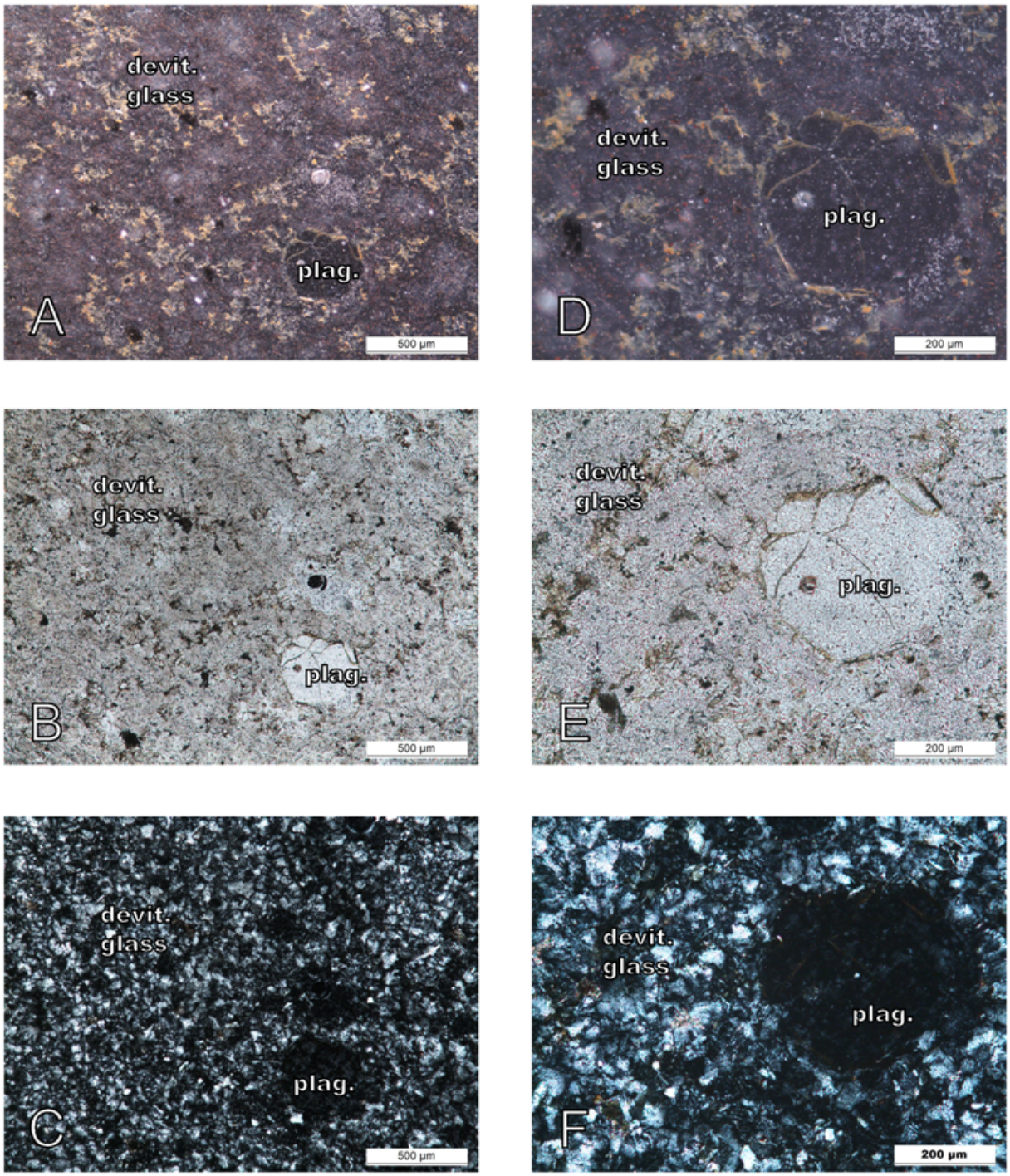

Figure 3.3: Photomicrographs of Allandale Rhyolite. These rhyolites are composed of a matrix of devitrified glass with occasional quartz and plagioclase phenocrysts reaching 2mm in size. (A) reflected light with devitrified glass groundmass and plagioclase (plag.) phenocryst. (B) plane-polarized light. (C) cross-polarized. (D-F) detail of plagioclase phenocryst and groundmass reflected, plane-polarized and cross-polarized light, respectively.

3.3.2 Sample Preparation

Cylindrical cores were taken from a single specimen of the Allandale Rhyolite sourced from Gebbies Pass with a nominal diameter of 20.6 mm and cut and ground (within 0.01mm) to a nominal length of 50.7mm, yielding samples with length to diameter ratios slightly greater than 2.5:1. This geometry allows for the validation of uniaxial compression strength (UCS) according with methods established by the International Society for Rock Mechanics (ISRM)[32]. Additionally, the 20.6 mm diameter is acceptable for the lithology studied to allow a 10:1 maximum grain size to diameter of the core as the largest phenocrysts observed are in the sub 2 mm range. Samples were washed with tap water after cutting and grinding, and ultrasonically cleaned in distilled water. Density and porosity of the specimens were determined in accordance with the ISRM dual-weight method [32].

3.3.3 Acoustic Velocity Profiling

Dynamic elastic moduli, compressional wave (Vp), and shear wave (Vs) velocities were determined using a GCTS Testing Systems Computer Aided Testing System Ultrasonic Velocity Testing System (CATS ULT-100) apparatus with axial P and S wave piezoelectric crystals. Pulse frequency was 900 kHz and 108 waveforms were captured during each measurement cycle. The velocities were determined using a constant stress on each sample of 10 MPa via a Tecnotest servo-controlled 3000 kN loading frame. The stress of 10 MPa was used to ensure a consistent waveform across the specimens and that the applied load was consistent for all measurement cycles. This was determined to be below crack-closure stress and ensured a good quality interpretation of the first arrival time of acoustic pulses. From the acquisition of these data we determined the dynamic Poisson's ratio and Young's modulus using Equations 3.1 and 3.2 [33], respectively:

$$v_d = \frac{(Vp^2 - 2Vs^2)}{2(Vp^2 - Vs^2)} \tag{3.1}$$

$$E_d = \frac{(\varrho * Vs^2 * (3Vp^2 - 4Vs^2))}{(Vp^2 - Vs^2)} \tag{3.2}$$

Where Vp is compressional wave velocity in m/s, Vs is shear wave velocity in m/s, E_d is the Young's Modulus, v_d is the dynamic Poisson's ratio and ϱ is density in kg/m^3. Our physical and acoustic property characterizations are summarized in Table 3.3.

3.3.4 Mechanical Property Testing

UCS was determined using a Technotest 3000 kN, servo-controlled loading frame. Tokyo Sokki Kenkyujo Co. Ltd (TML) 10mm strain gauges with a gauge factor of 2.12 were attached to the specimens (two axial and two radial). The specimens were deformed at a constant strain rate of 1x10^{-5}/s, such that failure resulted within 5-10 minutes of initial loading [32]. The specimens were also monitored for acoustic emissions during UCS testing with the Mistras AE node acquisition system. Two AE nodes were attached to the samples at the top and base and hit counts, wave forms, energy and amplitude were recorded during sample deformation. Once stress-strain curves were obtained and acoustic emissions data processed, we obtained the static elastic moduli for each specimen by utilizing Equations 3.3 and 3.4 [32]. In addition, we selected portions of the stress-strain sequence to identify crack closure, crack initiation (crack volume reversal), unstable crack propagation (volumetric strain reversal) and ultimately crack coalescence at UCS [34–36]. From the data collected during testing we calculated the static Poisson's Ratio and Young's Modulus:

$$v_s = -(\frac{\Delta\varepsilon_r}{\Delta\varepsilon_a}) \tag{3.3}$$

$$E_s = (\frac{\Delta\sigma_a}{\Delta\varepsilon_a}) \tag{3.4}$$

Where v_s is the static Poisson's Ratio, E_s is the static Young's Modulus σ_a is axial differential stress (MPa) ε_a is axial strain (%) and ε_r is radial strain (%).

3.3.5 Sample Thermal Treatment Cycles

Eleven samples of Allendale Rhyolite were subjected to thermal treatment in this study. Eight of these samples were subject to rapid quenching, and three samples were cooled at a much slower rate. Three specimens were subjected to one cycle of heating and rapid quenching (R4A, R9B, and R10B), three specimens to two cycles of heating and quenching (R2A, R12B, R13A) and two specimens to three cycles of heating and quenching (R1B and R5B). As a reference, the slowly cooled samples were subject to one (R7A), two (R10A) and three (R14A) thermal cycles.

3.4 Initial Properties of Allandale Rhyolite

In an effort to quantify the physical and mechanical changes that take place as a product of stimulation cycling, we characterized the 'as-cut' physical properties of the Allandale Rhyolites. These data are then used as baselines for comparison of properties after thermal treatments. The physical and dynamic properties of the Allandale rhyolite are summarized in Table 3.3. We observe a marginally consistent porosity for the dataset ranging from 7.8-10.4 (vol%) with an associated density range of 2316-2382 kg/m^3. Compressional wave velocity varies from 2555-3279 m/s and shear wave velocities range from 1451-1827 m/s. We calculated the dynamic elastic moduli of the Young's Modulus from 13.07-20.57 GPa and Poisson's Ratio to vary from 0.26-0.29.

We also determined UCS and the static elastic moduli on five samples as shown in Table 3.4 and a representative stress-strain curve coupled with acoustic emissions during deformation is shown in Figure 3.4. The stress-strain curves were used to determine crack-closure stresses, and associated damage criteria as discussed in Section 3.3.4. We observe UCS to have a mean value of 151.3 MPa with a standard deviation of 7.7 MPa. Static Young's Modulus varies from 14.56-21.16 GPa with a mean of 17.29 GPa (close to that of the dynamic values) and static Poisson's Ratio from 0.26-0.31 with a mean of 0.28, similar to our dynamic measurements.

Table 3.3: Physical and Dynamic Properties of Allandale Rhyolite

Sample Number	Connected Porosity (vol%)	Bulk Density (kg/m^3)	Vp (m/s)	Vs (m/s)	Dynamic Poisson's Ratio	Dynamic Young's Modulus (GPa)
R1A	8.3	2370	3102	1723	0.27	18.63
R1B	7.9	2382	3279	1807	0.28	20.24
R2A	8.3	2376	3058	1710	0.28	18.23
R2B	8.6	2358	2929	1630	0.28	16.37
R3A	10.2	2328	2522	1451	0.27	13.07
R3B	9.3	2343	2762	1561	0.27	15.04
R4A	8.1	2374	3101	1719	0.28	18.35
R4B	9.3	2357	2960	1655	0.27	16.99
R5A	8.5	2361	3010	1630	0.28	16.63
R5B	9.0	2346	2829	1583	0.27	15.45
R6A	9.4	2342	2718	1547	0.26	14.83
R6B	8.7	2360	3007	1647	0.29	16.66
R7A	8.2	2372	3188	1746	0.28	19.33
R7B	7.8	2378	3170	1744	0.28	19.10
R8A	7.9	2376	3226	1804	0.28	19.97
R8B	8.6	2367	3128	1716	0.29	18.39
R9A	9.2	2341	2873	1629	0.27	16.33
R9B	8.7	2352	2880	1611	0.28	15.92
R10A	8.1	2371	3133	1781	0.26	19.48
R10B	7.8	2377	3271	1827	0.27	20.57
R11A	10.4	2316	2691	1541	0.26	14.09
R11B	9.2	2345	2786	1555	0.27	15.13
R12A	8.0	2374	3238	1789	0.28	19.92
R12B	8.4	2372	3086	1734	0.27	18.75
R13A	8.1	2378	3188	1800	0.27	20.00
R13B	8.6	2371	3015	1676	0.28	17.27
R14A	8.8	2363	3053	1692	0.28	17.80
R14B	8.2	2378	3099	1739	0.27	18.89
R15A	9.1	2355	2885	1587	0.28	15.68
R15B	8.4	2368	3054	1697	0.27	17.91
Average	**8.6**	**2362**	**3007**	**1678**	**0.28**	**17.50**
Standard Deviation	0.65	16.0	188	95	0.012	2.02

Table 3.4: Mechanical Properties of Allandale Ryholite

Sample Name	UCS (MPa)	Dynamic Poisson's Ratio	Static Poisson's Ratio	Dynamic Young's Modulus (GPa)	Static Young's Modulus (GPa)
R1A	162.3	0.28	0.31	18.63	18.97
R2B	144.8	0.28	0.27	16.37	16.64
R5B	143.6	0.27	0.31	15.45	15.11
R8A	155.6	0.28	0.26	19.97	21.16
R13B	150.3	0.28	0.27	17.27	14.56
AVG	151.3	0.28	0.28	17.54	17.29
STDEV	7.7	0.01	0.02	1.80	2.76

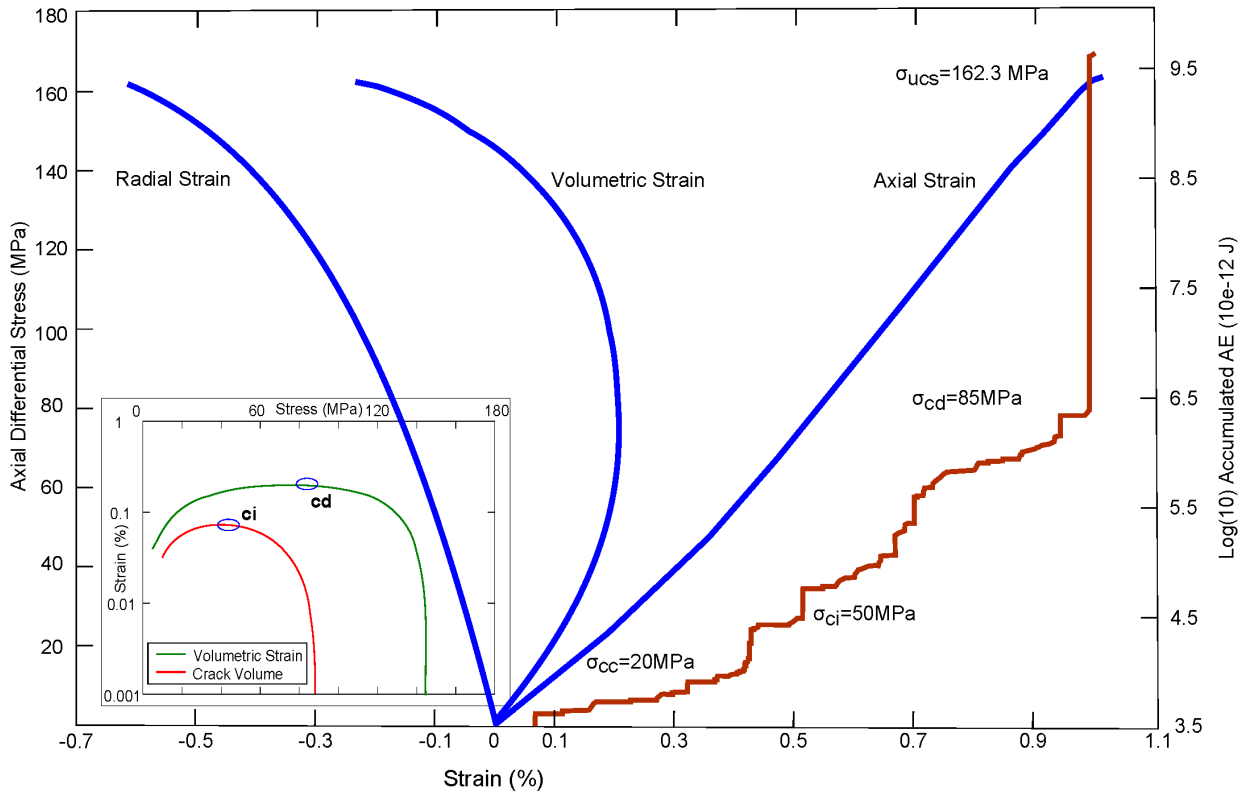

Figure 3.4: Typical stress-strain curves and cumulative acoustic emission output for Allandale Rhyolite. Specimen depicted in this figure is R1A. We observe crack closure to be ˜20MPa (10% of UCS), crack initiation at ˜50 MPa (30% of UCS), unsteady crack propagation at ˜85 MPa (53% of UCS) and UCS to be 162.3 MPa. The figure inset shows volumetric strain and crack volume during testing which were used to calculate crack initiation (ci) and crack propagation (cd) where the curves begin to reversal.

3.5 Results of Thermal Treatments

3.5.1 Acoustic Emissions During Testing

In order to quantify cracking of samples during thermal treatment in the pressure vessel, we utilized the Mistras equipment described in Section 3.2.6. A graphical depiction of the acoustic emissions recorded during treatment is given in Figure 3.5. The first thermal treatment cycle of sample R5A coupled with rapid cooling (Figure 3.5a) shows the largest amount of acoustic activity and when quenching began (17 hours) we observe a significant burst of activity from the system that decreases as system temperature decreases. The total number of events for this cycle is 4219. We see much less activity in the second treatment cycle (Figure 3.5b) with a similar acoustic output during the heating of the sample and some acoustic activity at the start of the quenching but an overall significantly lower output of 985 events. We monitored sample R7A for acoustic output during its thermal cycling (Figure 3.5c) where the system was allowed to cool more slowly without quenching. Some output activity was observed throughout the entire cycle but overall less activity than observed during a quenching cycle with 732 events during the whole test. We also carried out quench testing on the system with no sample in the vessel to determine the background noise and emissions during testing. This 'empty' testing resulted in the AE output seen in Figure 3.5d. The number of AE events (519) is lower than any of the cycles with samples but we do observe a slight increase of activity when the quenching cycle begins.

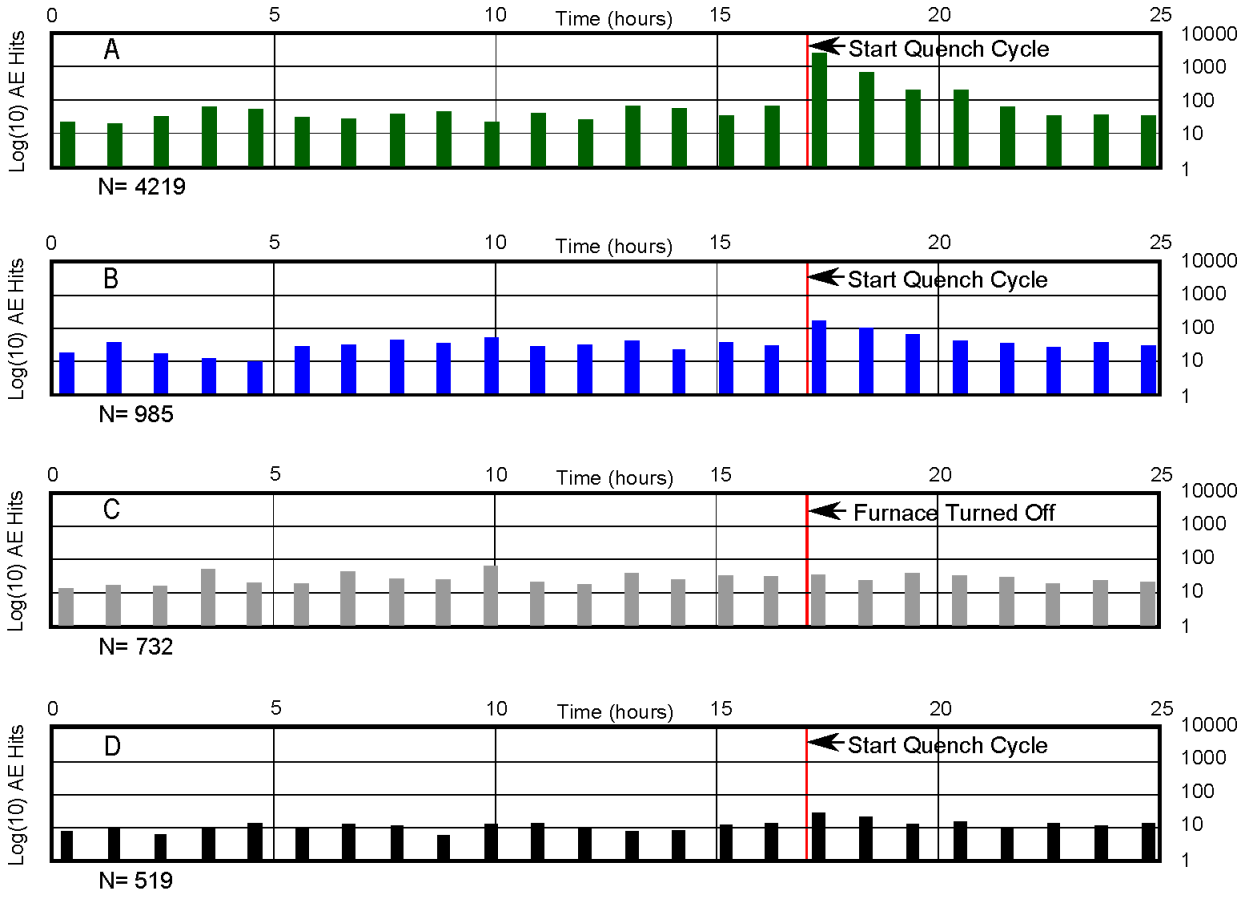

Figure 3.5: Acoustic emission output during heating and cooling cycles. (A) First rapid cooling cycle of sample R5A. (B) Second cooling cycle of sample R5A, much less AE output is recorded. (C) Slow cooling cycle of sample R7A even fewer AE events recorded than in A. (D) AE output during rapid cooling cycle with no sample inside the pressure vessel.

3.5.2 Physical and Chemical Changes

After the specimens were put through each thermal treatment cycle, they were removed from the pressure vessel and non-destructive properties re-evaluated. Tables 3.5 and 3.6 detail the values observed after final treatment cycles. All samples showed surface alteration from dull gray to an earthy brown (Figure 3.6). The change in surface sample color was due to oxidation of iron that was easily removed from the sample either by handling or when further characterization was carried out. This resulted in a slight volumetric loss from the specimen.

After re-measuring the sample geometry and evaluating porosity and density, we found that all the specimens displayed increased porosity and decreased bulk density after one treatment cycle (Figure 3.7).

The greatest change to porosity occurs after the first thermal treatment cycle with a smaller magnitude of change during subsequent cycling (Figure 3.8).

In samples that were rapidly quenched, we observed an average decrease in sample bulk densities of 68 kg/m^3 and an increase in porosity averaging 1.7 (vol%). The slowly cooled specimens also showed bulk density decreases with an average reduction of density of 61 kg/m^3 and porosity increase with an average of 1.3 (vol%).

Table 3.5: Compilation of physical properties of rapidly quenched Allandale Rhyolites after thermal treatments and total changes observed.

Sample Name	# of Quench Cycles	Porosity (vol%)	Bulk Density (kg/cm^3)	Vp (m/s)	Vs (m/s)	Dynamic Poisson's Ratio	Dynamic Young's Modulus (GPa)
R1B	3	9.2	2290	2834	1707	0.22	15.86
change		+1.5	-92	-445	-100	-0.06	-4.38
R2A	2	9.9	2274	2832	1695	0.22	16.12
change		+1.7	-101	-226	-15	-0.06	-2.12
R4A	1	9.4	2321	2729	1658	0.21	15.31
change		+1.3	-53	-371	-61	-0.07	-3.04
R5A	3	10.4	2283	2607	1548	0.20	13.67
change		+2.2	-79	-403	-99	-0.09	-2.96
R9B	1	10.0	2313	2575	1555	0.22	13.54
change		+1.3	-39	-304	-56	-0.06	-2.39
R10B	1	10.0	2325	2887	1659	0.25	16.00
change		+2.2	-53	-384	-168	-0.03	-4.57
R12B	2	10.2	2311	2648	1567	0.23	13.72
change		+1.8	-60	-438	-167	-0.05	-5.03
R13A	2	9.6	2310	2776	1679	0.21	15.47
change		+1.5	-68	-412	-121	-0.06	-4.53

Table 3.6: Compilation of physical properties of slowly cooled Allandale Rhyolites after thermal treatments and total changes observed.

Sample Name	# of Quench Cycles	Porosity (vol%)	Bulk Density (kg/m^3)	Vp (m/s)	Vs (m/s)	Dynamic Poisson's Ratio	Dynamic Young's Modulus (GPa)
R7A	1	9.2	2330	2892	1690	0.24	16.29
change		+0.9	-43	-296	-57	-0.04	-3.04
R10A	2	9.3	2314	3018	1693	0.26	16.36
change		+1.2	-57	-115	-87	-0.01	-3.11
R14A	3	10.5	2281	2785	1643	0.25	15.12
change		+1.7	-82	-268	-50	-0.03	-2.68

Figure 3.6: Allandale Rhyolite specimens before (R2A top) and after thermal treatment (R4A bottom). The texture and color of the specimen has clearly changed and this is also reflected in the physical properties. Width of cores is 20.6 mm.

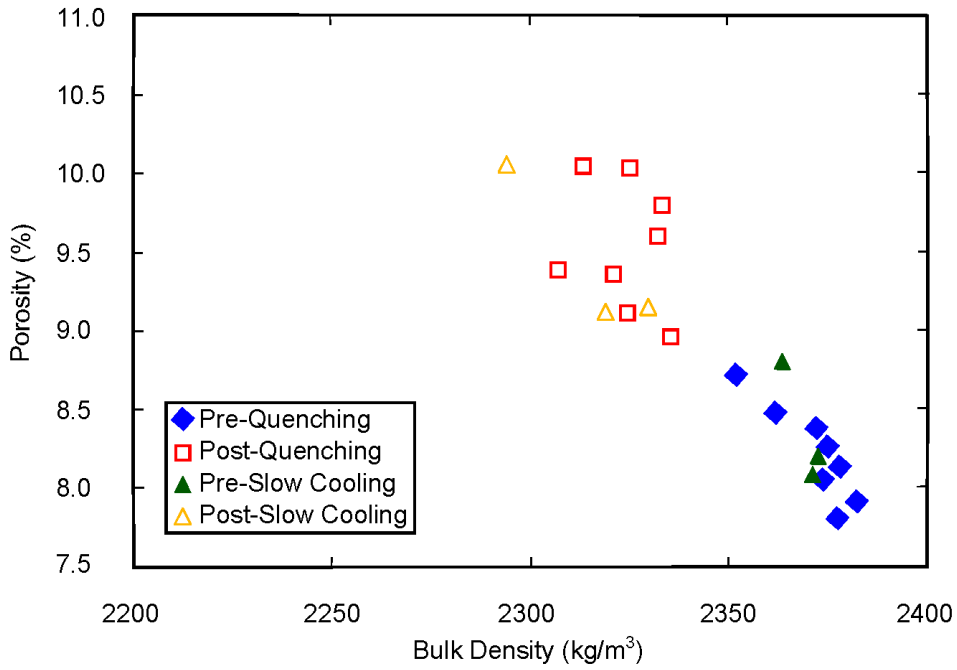

Figure 3.7: Bulk density and porosity for Allandale Rhyolite specimens that underwent thermal stressing. Post- treatment values are shown after one cycle.

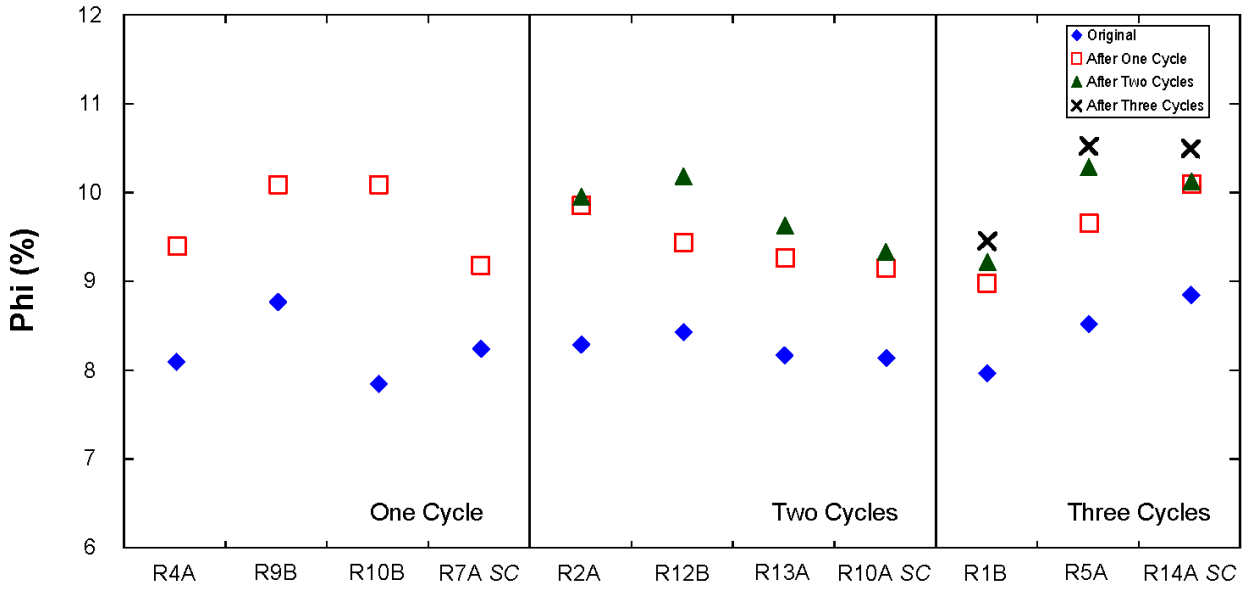

Figure 3.8: Connected porosity of pre-treatment and post-treatment values of Allandale Rhyolite after successive cycles. *SC* refers to samples that were cooled slowly.

3.5.3 Changes to Acoustic Velocities and Dynamic Elastic Moduli

After thermal treatment, we re-evaluated the acoustic velocities and dynamic elastic properties to observe trends and changes in their properties. Figure 3.9 shows the changes to Vp and Vs after thermal treatments with the greatest change occurring during the first cycle.

Vp is reduced in the rapidly quenched samples by an average of 373 m/s, an average reduction of 13.6% with Vs also showing average reduction of 98 m/s, a 6% overall reduction. In the slowly cooled samples, Vp is reduced by an average of 226 m/s, 10.6% with a 65 m/s reduction in Vs, a 3.8% decrease. Figure 3.10 illustrates the magnitude of changes in both compression and shear wave velocities after one cycle for all samples.

As a result of both density decreases and changes in P and S wave velocities, the dynamic acoustic moduli of Poisson's ratio and Young's modulus also decreased (Figure 3.11 shows pre-treatment and post-treatment values after one cycle). As such, Poisson's ratio decreased an average of 26.6% in rapidly quenched samples and 9.5% in slow cooled samples. The trend is also consistent with Young's modulus as we see an average decrease of 24.3% from rapid quenching and average of 18.4% from slow cooling.

We subjected samples to differing numbers of thermal treatment cycles to investigate whether the 'thermal Kaiser effect' affected samples in our testing. Literature on the Kaiser effect show that a sample will not be further damaged by re-heating it to the same temperature [17,26,37,38]. Figure 3.12 shows the magnitude of changes in porosity and acoustic properties in sample R5A after being subjected to three treatment cycles. The greatest change to the sample occurs during the first cycle with very little change during subsequent cycles.

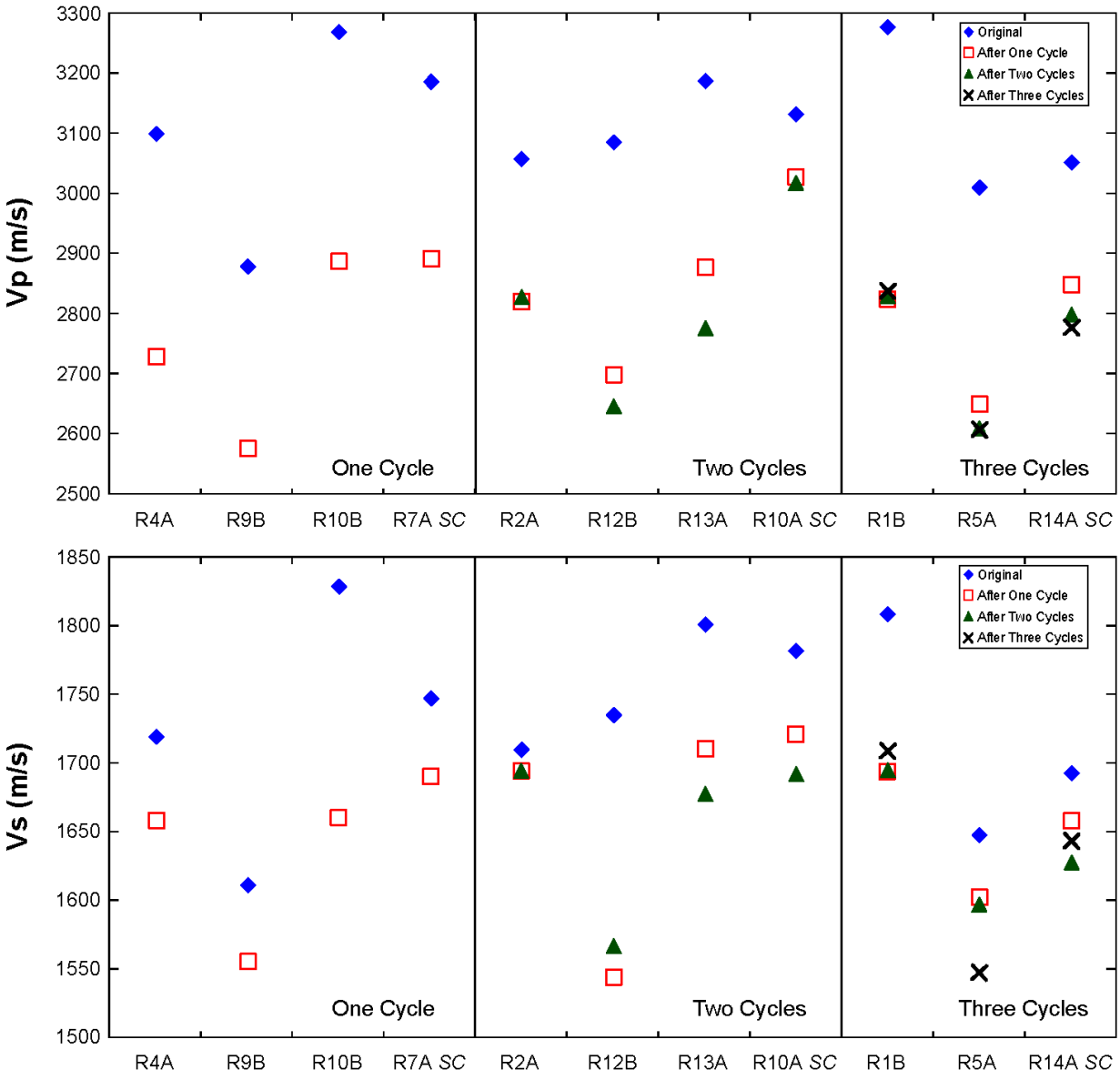

Figure 3.9: Comparison of pre-treatment and post treatment values of compressional (Vp) and shear (Vs) wave velocities and porosity for all samples of Allandale Rhyolite subject to thermal cycling. Samples with no suffix were rapidly cooled and those with *SC* were slowly cooled.

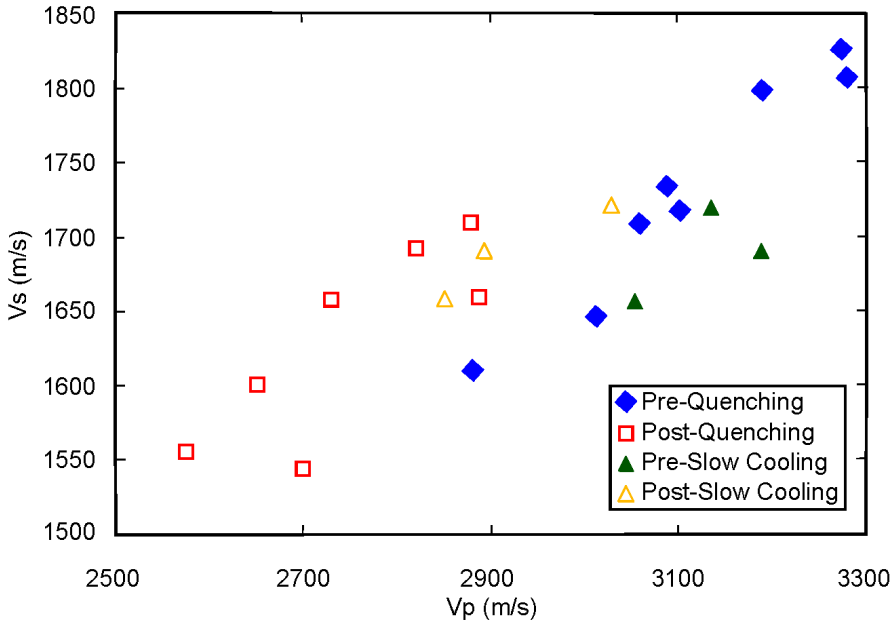

Figure 3.10: Comparison of acoustic velocities for all Allandale Rhyolite samples after one thermal cycle.

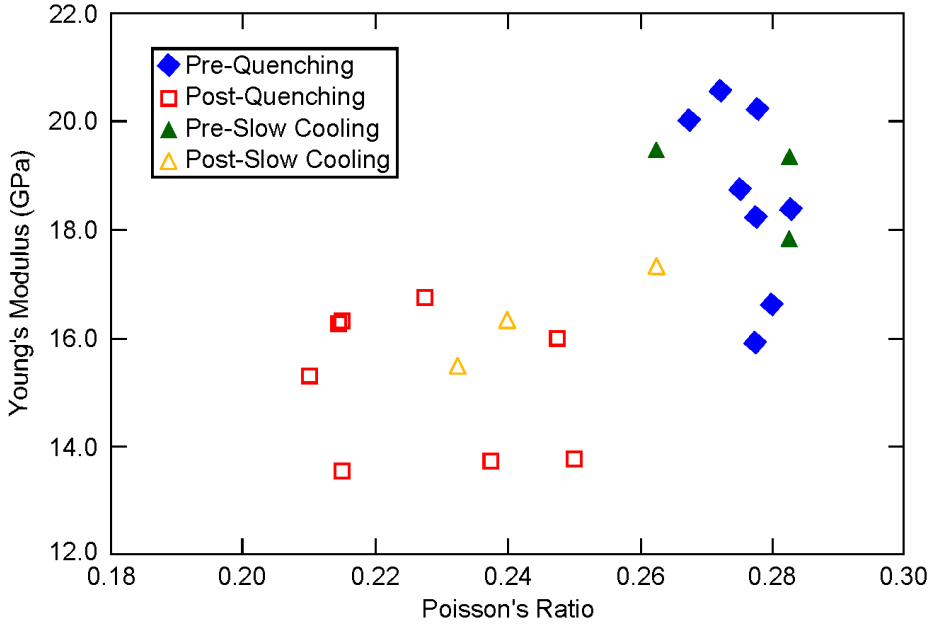

Figure 3.11: Change in dynamic Poisson's ratio and Young's modulus of Allandale Rhyolite after one thermal cycle.

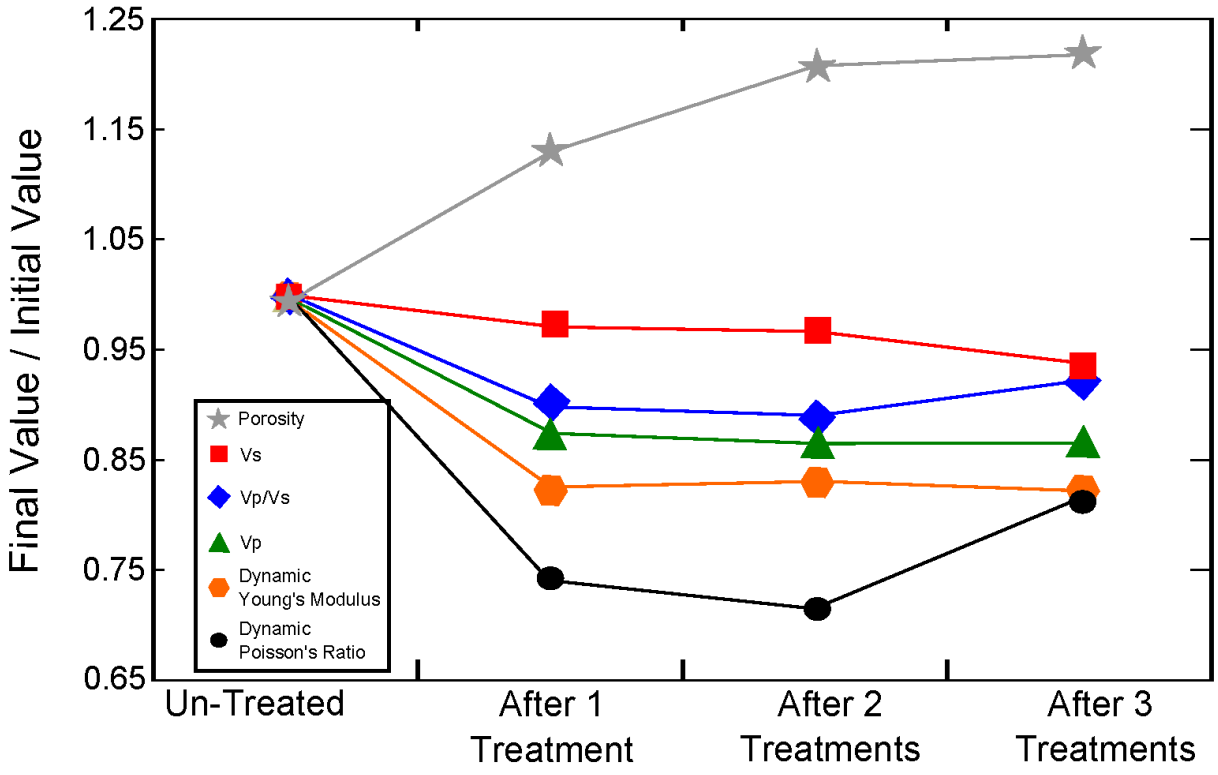

Figure 3.12: Absolute changes in porosity, acoustic velocities and dynamic moduli over three cycles of rapid quenching in sample R5A.

3.5.4 Changes in Strength Properties

Table 3.7: Observed mechanical, static and dynamic elastic properties of rapidly cooled specimens of Allandale Rhyolite

Sample Name	# of Treatment Cycles	UCS (MPa)	Dynamic Poisson's Ratio	Static Poisson's Ratio	Dynamic Young's Modulus (GPa)	Static Young's Modulus (GPa)
R1B	3	118.2	0.22	0.17	15.86	15.79
R2A	2	133.9	0.22	0.27	16.12	17.05
R4A	1	126.3	0.21	0.23	15.31	16.32
R5A	3	124.8	0.20	0.27	13.67	17.44
R9B	1	134.0	0.22	0.22	13.54	14.88
R10B	1	156.6	0.25	0.17	16.00	16.67
R12B	2	140.5	0.23	0.23	13.72	15.53
R13A	2	153.8	0.21	0.25	15.47	18.78
Average	-	137.4	0.22	0.23	14.96	16.56
Std. Dev.	-	13.22	0.02	0.04	1.12	1.22

Table 3.8: Observed mechanical, static and dynamic elastic properties of slowly cooled specimens of Allandale Rhyolite

Sample Name	# of Treatment Cycles	UCS (MPa)	Dynamic Poisson's Ratio	Static Poisson's Ratio	Dynamic Young's Modulus (GPa)	Static Young's Modulus (GPa)
R7A	1	140.3	0.24	0.24	16.29	19.42
R10A	2	137.9	0.26	0.24	16.36	21.03
R14A	3	119.9	0.25	0.20	15.12	14.07
Average	-	132.7	0.25	0.23	15.92	18.17

The thermally treated samples (Tables 3.7 and 3.8) show a slight decrease in average strength when compared to those not thermally treated (Table 3.4), with an average overall reduction of 11% for rapidly quenched samples and 14% for slow cooled samples. The two samples subject to three rapid quenching cycles show an average strength reduction of 24% when compared to the average of the un-treated specimens (the one sample slow cooled for three cycles shows a reduction of 26% from the mean). Static Poisson's ratio is reduced by an average of 27% in rapidly cooled samples, and an average of 24% in slow cooled samples when referenced to the un-treated specimens. An average reduction of 5% in the static Young's modulus is seen for rapid quenching and a slight increase of the static Young's modulus in slowly cooled samples of 2%. Figure 3.13 shows the stress/strain behavior of specimen R5A after three cycles of thermal treatment, and Figure 3.14 shows the stress-strain curves for samples R1A (non-treated) and R1B (quenched three times) with similar behavior during loading, but the thermally treated sample being weaker in UCS.

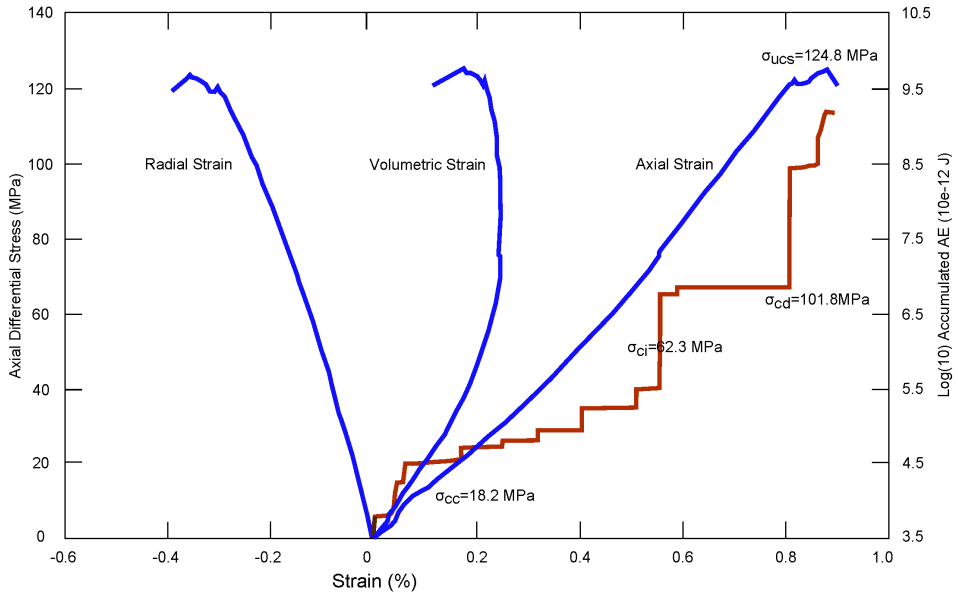

Figure 3.13: Stress-strain curves for R5A after three quenching cycles. We see crack closure to be ˜18 MPa (15% of UCS), crack initiation at ˜62 MPa (50% of UCS) and unsteady crack propagation at ˜102 MPa (81.6% of UCS).

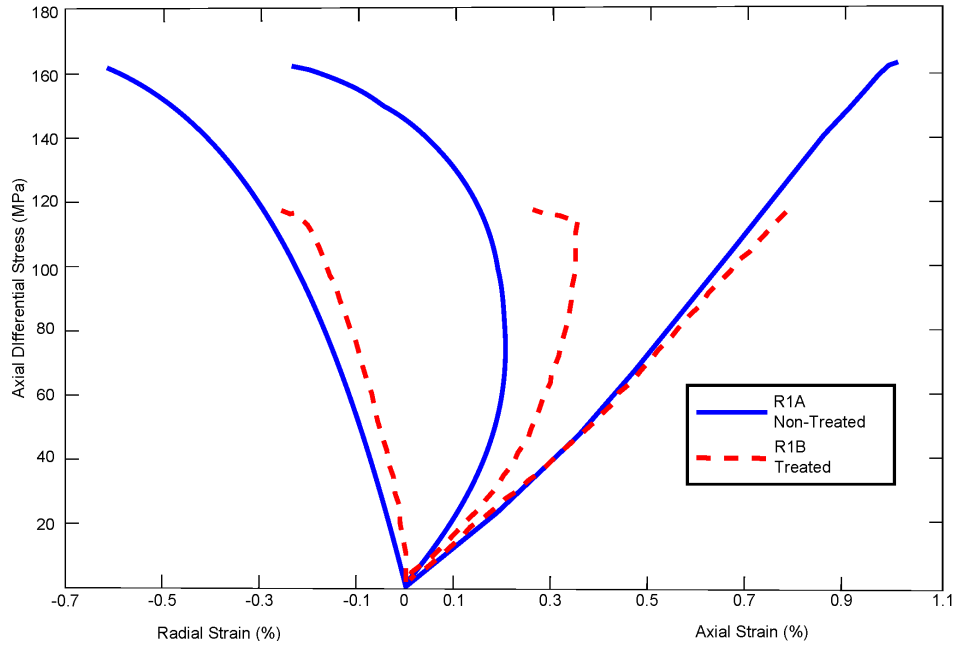

Figure 3.14: Stress-strain curves for samples R1A and thermally treated R1B. We see similar behavior but a decreased UCS after thermal cycling.

3.6 Discussion

3.6.1 Influence of Thermal Treatment on Sample Physical Properties

We observed density decreases in all specimens subject to thermal treatment and subsequently an increase in porosity. Sample acoustic velocities are likewise attenuated in all thermally treated samples and as a result of this the dynamic elastic moduli decrease. These results are consistent with those of several authors [11,19,38,43] where increases in porosity and decreases in acoustic velocities are attributed to microcracking in samples from heating in a dry environment.

The increase of porosity and decrease in density of the rapidly quenched samples is slightly greater than those that were slowly cooled. More damage therefore occurs during a rapid quenching cycle than a slow cooling cycle (Figure 3.8). This is also observed in our measurements of acoustic velocities specifically for compressional wave velocities where the attenuation is nearly 50% greater in rapidly quenched samples than those that were cooled slowly (Figure 3.9). Analysis of our acoustic emissions during the thermal testing (Figure 3.5) also shows a far greater number of acoustic emissions during testing of samples that have been rapidly quenched. This is a clear indication that more microfracturing is occurring during the quenching cycle than the slowly cooled cycle. This is similar to to the dry thermal treatments of Yong and Wang [26], who saw increased damage and higher heating total acoustic emissions in their rocks at higher heating rates, which we have also seen but under water saturated conditions.We therefore surmise that heating inherently causes damage in the samples under confined, saturated conditions, but that much more damage is created as a result of rapid quenching.

3.6.2 Thermomechanical Kaiser Effect

Our data indicate that the greatest damage in our thermal cycling occurs during the first cycle and that there is less damage in subsequent thermal cycling. Figure 3.8 illustrates that porosity shows the greatest increase after one thermal cycle but shows less increase in subsequent cycles. This is also seen in our acoustic properties in Figure 3.9 where the greatest change comes after the first thermal cycle, and is further illustrated in Figure 3.12 where the magnitude of changes is plotted for one sample (R5A). Finally, in the analysis of acoustic emissions during the treatment cycles we see much more activity during the initial

quenching cycle (Figure 3.5a) and significantly less in the second cycle (Figure 3.5b). This would indicate that the most damage occurs in the first cycle but that there is still some damage in the second cycle during quenching.

The Kaiser effect should constrain that rocks will not experience additional damage unless a previous maximum stress is exceeded (be it thermal or mechanical) [10,26] which suggests that in our experiments there will be no further damage after the first cycle. In fact, despite heating and quenching under the same conditions we observe damage in samples, albeit at reduced magnitudes (Figure 3.12). This possibly indicates that using our quenching methodology, the Kaiser effect does not fully apply. An alternate explanation may be that chemical changes are occurring during our testing (color change of samples as seen in Figure 3.6) and that this results in increased porosity and acoustic velocity attenuation. Further research will be needed to constrain how the thermal and chemical effects continue to damage samples and how this relates to the Kaiser effect.

3.6.3 Thermal Treatment and Mechanical Property Evolution

We show an overall degradation of the UCS for those samples subjected to thermal treatment, as noted by several authors [10,17,19,25,38]. We also show that the specimens that were subjected to multiple cycles of thermal stressing showed the largest decrease in strength (Tables 3.7 and 3.8). We observe a weakening of all specimens subjected to thermal treatment: for example, R1B showed a 28% lower UCS (118.2 MPa) after three cycles of thermal treatment compared to R1A (162.3 MPa), as both specimens were sourced from a single length of core. We have seen an overall reduction in strength of the specimens subjected to thermal treatment and thus the samples have been degraded by the generation of thermal cracks. This supports the data of several authors [10,21,23,24] that there is a significant decrease in rock and engineering material strengths when subjected to heating.

In this study, we do not reach the temperatures used by these authors (greater than 300°C and up to 1000°C), but perhaps the influence of the water saturated conditions of our testing may exacerbate the influence of heating and cooling. We show that after a quenching cycle, sample R5A shows a similar crack closure stress to that of an untreated sample, but that the crack initiation threshold is nearly 50% of UCS against nearly 30% in an untreated sample. This is another indication of microcrack damage occurring in our samples during our thermal quench cycle, where much greater stresses are required before new cracks begin to form. Additionally, the crack coalescence that leads to failure is at 82% of UCS in a quenched sample versus 53% in a non-treated sample, indicating that the sample is significantly damaged and greater

stress is required to initiate more fractures, but that the thermally induced damage does ultimately result in a weaker sample [9,10].

The sample set in which we compared slow cooled against rapid quenching does not have a large enough population to make final conclusions on the different effects between these two rates but there are indications rapid cooling has a greater influence. Samples subjected to thermal treatment are weaker than those which have not been, in line with the findings of many other studies on heat damage.

3.6.4 Implications of Permeability and Geothermal Applications

In our rapidly cooled samples, we have shown a decrease of 7.9-16.5 % in Vp and an increase in porosity of between 1.3-2.2 (vol%) the majority of which we attribute to exacerbated cracking during the quenching cycle. Chaki et al. [40] show a similar decrease in acoustic velocities of 4-16 % and permeability increase 1.1-1.9 times higher than original values. Similarly, Fortin et al. [41] showed that a 5-10% decrease in Vp corresponded to a permeability increase of 2.25-4.5 times the original values. We infer from our study that, although we did not measure permeability directly, our reduced acoustic velocities and increased porosity may correspond to twice the permeability of the original values, which would not be unexpected after thermal stressing events [11,22,41].

The ultimate goal of a thermal stimulation procedure is to increase permeability at the wellbore and within the reservoir. The results here are a first attempt to replicate thermal stimulation in a laboratory environment under similar pressure and temperature conditions found at depth. As such, damage in our testing is maximal in the first cycle and is significantly less through progressive cycling. It is well documented that several thermal cycles can significantly enhance the permeability of geothermal reservoirs [1,3,39,44], and it is possible that the complex thermal, physical, and chemical regimes present in a geothermal system aid in the propagation and generation of new fractures such that the Kaiser effect plays a lesser role. After field-scale stimulation, wellbores and reservoirs are subject to tectonic and thermal stresses that are very difficult to replicate in the laboratory and as such, there may be fracture healing, changes in mechanical stress and many other factors. These factors may result in fundamental changes to physical properties of the rock and as such, the materials are prone to active changes. Our observations of the Kaiser effect in the laboratory do not as such negate the results observed after multiple cycles of thermal stimulation. We do see that there is a continued increase in porosity and decrease in sample density in both our quenched and slow cooled datasets; this indicates that there may be a chemical component changing these properties that

is not readily identifiable with our other characterization methods. Further work on the geochemical aspect of the quenching cycles is needed to constrain this aspect.

3.6.5 Stimulation Apparatus

The thermal stimulation apparatus was designed to induce rapid thermal cooling gradients in rock samples under fully saturated conditions. The sample experiences an isotropic temperature change through the quenching system. This was done so that the sample will not experience differential cooling, furthering complex thermal stress regimes. As such, there is a clear difference between slow cooled samples and those that were rapidly quenched, as evidenced by acoustic velocity attenuation and total AE output during testing. The results suggest that our initial goals to demonstrate induced thermal cracking by forced quenching under saturation have been realized using our relatively simple design.

3.7 Conclusions

1. We have developed a novel device that allows heating and rapid cooling under water saturated conditions with the goal of replicating thermal stimulation in a geothermal reservoir. The device has successfully demonstrated that it is capable of inducing large changes to sample physical properties on the microscopic and macroscopic scale.

2. The measurement of sample properties both before and after thermal treatment has shown that we can increase sample porosity and decrease sample density through thermal cycling. An increase of porosity by a factor of 1.3 is observed in samples that have been rapidly quenched versus those that have been slowly cooled. Coupled with acoustic emissions, this shows that we have created additional porosity through our quenching cycles by microcracking.

3. We have decreased acoustic wave velocities and observed reduced dynamic elastic moduli. Our thermal treatments have successfully decreased the compressional wave and shear wave velocities of all samples in this study. Compressional wave velocities show the greatest attenuation in samples that have been rapidly quenched, indicating that more damage is imparted as a result of quenching versus slow cooling.

4. The increased microcracking, and decreased density and acoustic wave velocities, are representative of the lower overall strength that we observe in our sample dataset. The change in strength shows that

after one thermal treatment cycle maximum damage is done to the sample. Subsequent thermal cycles impart lesser damage which may be due to chemical changes, but further work is needed to explore this.

5. Our geothermal stimulation device will be a valuable tool in understanding the field of thermal treatment of rock materials and will play a crucial role in the field of rock physics research. The flexibility and design of the apparatus will allow for investigations not only for geothermal applications but to other fields such as concrete and materials engineering where materials can be subjected to induced thermal stresses by artificial and man-made temperature gradients.

With these initial results from our study, we now aim to perform a similar study on rocks sourced from a geothermal system which show secondary hydrothermal alteration. We intend in the future to supplement the measurements presented here with permeability, thermal property measurements and detailed micro-structural studies.

3.8 Acknowledgements

The authors greatly acknowledge the support of Mighty River Power Ltd. for financial support and inspiration. Additionally we wish to thank Mr. Peter Jones for his expertise and assistance in building the stimulation apparatus and providing technical assistance. Mr. Julian Phillips provided invaluable help in development of the recording instrumentation for the stimulation apparatus. We also wish to thank the support of the technical staff of the Department of Geological Sciences for their advice, humour and expertise. This project was funded in part by a grant from Mighty River Power Ltd. and the Department of Geological Sciences at the University of Canterbury. We would also like to acknowledge a Hubert Curien partnership (PHC) Dumont d'Urville grant (grant number 31950RK). Funding for BK was provided by Marsden Fast start (09-UO-017C). The manuscript benefited hugely from reviews by Mike Heap and one anonymous reviewer.

3.9 References

[1] Kitao, K, Ariki, K, Hatakeyama, K, Wakita K. Well Stimulation Using Cold-Water Injection Experiments in the Sumikawa Geothermal Field, Akita Perfecture, Japan. Geotherm Resour Counc Trans 1990;14:1219–24.

[2] Flores M, Davies D, Couples G, Palsson B. Stimulation of Geothermal Wells, Can We Afford It? In: Proceedings of the World Goethermal Congress 2005. Antalya, Turkey; 24-29 April, 2005, p. 8.

[3] Axelsson, G, Thórhallsson S. Review of Well stimulation Operations in Iceland. Geotherm Resour Counc Trans 2009;33:795–800.

[4] Siega CH, Grant M, Powell T. Enhancing Injection Well Performance by Cold Water Stimulation in Rotokawa and Kawerau Geothermal Fields. In: Proceedings, PNOC-EDC Conference; Manilla, Philippines; 2009, p. 7.

[5] Brodsky N, Riggins M, Connolly J. Thermal Expansion , Thermal Conductivity , and Heat Capacity Measurements at Yucca Mountain , Nevada. Int J Rock Mech Min Sci 1997;34:5.

[6] Miura K, Okui Y, Horii H. Micromechanics-based prediction of creep failure of hard rock for long-term safety of high-level radioactive waste disposal system. Mech Mater 2003;35:587–601.

[7] Martin CD, Christiansson R. Estimating the potential for spalling around a deep nuclear waste repository in crystalline rock. Int J Rock Mech Min Sci 2009;46:219–28.

[8] Chen Y, Wu X, Zhang F. Experiments on thermal fracture in rocks. Chinese Sci Bull 1999;44:1610–2.

[9] Heap MJ, Lavallee Y, Laumann A, Hess K-U, Meredith PG, Dingwell DB. How tough is tuff in the event of fire? Geology 2012;40:311–4.

[10] Heap MJ, Lavallée Y, Laumann A, Hess K-U, Meredith PG, Dingwell DB. The influence of thermal-stressing (up to 1000°C) on the physical, mechanical, and chemical properties of siliceous-aggregate, high-strength concrete. Constr Build Mater 2013;42:248–65.

[11] Vinciguerra S, Trovato C, Meredith P, Benson P. Relating seismic velocities, thermal cracking and permeability in Mt. Etna and Iceland basalts. Int J Rock Mech Min Sci 2005;42:900–10.

[12] Heap MJ, Vinciguerra S, Meredith PG. The evolution of elastic moduli with increasing crack damage during cyclic stressing of a basalt from Mt. Etna volcano. Tectonophysics 2009;471:153–60.

[13] Axelsson G, Thorhallsson S, Bjornsson, G. Stimulation of Geothermal Wells in Basaltic Rock in Iceland. In: ENGINE- Enhanced Geothermal Innovative. Network for Europe Workshop 3 "Stimulation of reservoir and microseismicity". Kartause Ittingen, Zurich, Switzerland; June 29-July 1, 2006, p. 8.

[14] Grant MA, Bixley PF. Geothermal Reservoir Engineering. 2nd ed. Oxford, UK: Elsevier Science Ltd; 2011.

[15] Grant MA, Clearwater J, Quinao J, Bixley PF, Le Brun M. Thermal Stimulation of Geothermal Wells: A Review of Field Data. In: Proceedings, Thirty-Eighth Workshop on Geothermal Reservoir Engineering. Stanford University, Stanford, California., 11-13 February 2013. p. 7.

[16] Homand-Etienne F, Troalen JP. Behaviour of Granites and Limestones Subjected to Slow and Homogeneous Temperature Changes. Eng Geol 1984;20:219–33.

[17] Fredrich JT, Wong T. Micromechanics of Thermally Induced Cracking in Three Crustal Rocks. J Geodyn 1986;91:12743–64.

[18] Géraud Y. Variations of connected porosity and inferred permeability in a thermally cracked granite. Geophys Res Lett 1994;21:979–82.

[19] David C, Menendez B, Darot M. Influence of stress-induced and thermal cracking on physical properties and microstructure of La Peyratte granite. Int J Rock Mech Min Sci 1999;36:433–48.

[20] Yavuz H, Demirdag S, Caran S. Thermal effect on the physical properties of carbonate rocks. Int J Rock Mech Min Sci 2010;47:94–103.

[21] Darot M, Gueguen Y, Baratin M-L. Permeability of Thermally Cracked Granite. Geophys Res Lett 1992;19:869–72.

[22] Jones C, Keaney G, Meredith, PG, Murell SAF. Acoustic emission and fluid permeability measurements on thermally cracked rocks. Phys Chem Earth 1997;22:13–7.

[23] Balme M, Rocchi V, Jones C, Sammonds P, Meredith P, Boon S. Fracture toughness measurements on igneous rocks using a high-pressure, high-temperature rock fracture mechanics cell. J Volcanol Geotherm Res 2004;132:159–72.

[24] Keshavarz M, Pellet FL, Loret B. Damage and Changes in Mechanical Properties of a Gabbro Thermally Loaded up to 1,000°C. Pure Appl Geophys 2010;167:1511–23.

[25] Patel A, Manga M, Carey RJ, Degruyter W. Effects of thermal quenching on mechanical properties of pyroclasts. J Volcanol Geotherm Res 2013;258:24–30.

[26] Yong C, Wang CY. Thermally Induced Acoustic Emission in Westerly Granite. Geophys Res Lett 1980;7:1089–92.

[27] Baria R, Michelet S, Baumgaertner J, Dyer B, Gerard A, Nicholls J, Hettkamp T, Teza D, Soma N, Asanuma H, Garnish T, Megel T. Microseismic Monitoring of The Worlds Largest Potential HDR Reservoir. In: Proceedings of the Twenty-Ninth Workshop on Geothermal Reservoir Engineering. Stanford University, Stanford, California; 26-28 January 2004. 8p.

[28] Hampton SJ, Cole JW. Lyttelton Volcano, Banks Peninsula, New Zealand: Primary volcanic landforms and eruptive centre identification. Geomorphology 2009;104:284–98.

[29] Wood CP. Calderas and geothermal systems in the Taupo Volcanic Zone, New Zealand. Proc. World Geotherm. Congr. Florence Italy. May 18-31, vol. 2, 1995, p. 1331–6.

[30] Rosenberg MD, Hunt TM. Ohaaki geothermal field: some properties of Huka Falls Formation mudstones. 21st New Zeal Geotherm Work Proc 1995:89–94.

[31] Bignall G, Milicich S, Ramirez E, Rosenberg M, Kilgour G, Rae A. Geology of the Wairakei-Tauhara Geothermal System, New Zealand. In: Proccedings of the World Geothermal Congreess. Bali, Indonesia; April 25-29 2010. p. 8.

[32] Ulusay R, Hudson J. The Complete ISRM Suggested Methods for Rock Characterization, Testing and Monitoring: 1974-2006. Antalya, Turkey: Elsevier; 2007.

[33] Guéguen Y, Palciauskas V. Introduction to the Physics of Rocks. Princeton, New Jersey: Princeton University Press; 1994.

[34] Martin CD. The strength of massive Lac du Bonnet Granite around underground openings. PhD Thesis. University of Manitoba, 1993.

[35] Eberhardt E, Stead D, Stimpson B, Read RS. Identifying Crack Initiation and Propagation Thresholds in Brittle Rock. Can Geotech J 1998;35:222–33.

[36] Takarli M, Prince W, Siddique R. Damage in granite under heating/cooling cycles and water freeze thaw condition. Int J Rock Mech Min Sci 2008;45:1164–75.

[37] Zuberek WM, Zogala B, Dubiel R, Pierwola J. Maximum Temperature Memory in Sandstone and Mudstone Observed with Acoustic Emission and Ultrasonic Measurements. Int J Rock Mech Min Sci Geomech Abstr 1999;3:416–7.

[38] Chaki S, Takarli M, Agbodjan WP. Influence of thermal damage on physical properties of a granite rock: Porosity, permeability and ultrasonic wave evolutions. Constr Build Mater 2008;22:1456–61.

[39] Flores-Armenta, M, Tovar-Aguado R. Thermal Fracturing of Well H-40, Los Humeros Geothermal Field. Geotherm Resour Counc Trans 2008;32:8–11.

[40] Reuschlé T, Gbaguidi HS, Darot M. The effect of heating on the microstructural evolution of La Peyratte granite deduced from acoustic velocity measurements. Earth Planet Sci Lett 2006;243:692–700.

[41] Lockner D. The Role of Acoustic Emission in the Study of Rock Fracture. Int J Rock Mech Min Sci Geomech Abstr 1993;30:883–99.

[42] Chaki S, Takarli M, Agbodjan WP. Influence of thermal damage on physical properties of a granite rock: Porosity, permeability and ultrasonic wave evolutions. Constr Build Mater 2008;22:1456–61.

[43] Fortin J, Stanchits S, Vinciguerra S, Guéguen Y. Influence of thermal and mechanical cracks on permeability and elastic wave velocities in a basalt from Mt. Etna volcano subjected to elevated pressure. Tectonophysics 2011;503:60–74.

[44] Siratovich PA, Sass I, Homuth S, Bjornsson A. Thermal Stimulation of Geothermal Reservoirs and Laboratory Investigation of Thermally Induced Fractures An Overview of Thermal Stimulation. Geotherm. Resour. Counc. Trans. Vol. 35, 2011, p. 1529–35.

Chapter 4

The Physical Properties of the Rotokawa Andesite, New Zealand, and Relationships of Microstructure, Strength, and Permeability

P.A. Siratovich[a], M. Heap[b], M. Villeneuve[a], J. Cole[a], T. Reuschlé[b]

[a]Department of Geological Sciences, University of Canterbury, Private Bag 4800, Christchurch 8140, New Zealand

[b]Laboratoire de Déformation des Roches, Équipe de Géophysique Expérimentale, Institut de Physique de Globe de Strasbourg (UMR 7516 CNRS, Université de Strasbourg/EOST), 5 rue René Descartes, 67084 Strasbourg cedex, France.

To be submitted to the Journal *Geothermal Energy.*

Abstract

The optimal utilization of a geothermal resource depends on a fundamental understanding of the physical properties that characterize the host rocks. These properties can be determined from laboratory studies on core sourced directly from a geothermal reservoir. This study details a comprehensive evaluation of the Rotokawa Andesite sourced from the Rotokawa Geothermal field located in the Taupo Volcanic Zone, New Zealand. Here, we evaluate the importance of microstructural fabrics on the physical properties of this reservoir lithology. We characterized the mineralogical and petrological fabrics of the rocks coupled with detailed studies of the microstructural fracture networks. These were coupled with measurements of porosity, density and permeability conducted under laboratory conditions. Further, acoustic wave velocities

and dynamic elastic moduli were determined. Uniaxial compressive strength testing coupled with acoustic emission recording aided in determining the behavior of the rock under deformation and provided data to characterize the static elastic moduli of the rocks. Through our investigations, we developed empirical, micromechanical and geometrical relationships between the physical properties of the Rotokawa Andesite. The aim of this study is to develop a comprehensive understanding of easily measurable physical properties of the Rotokawa Andesite and relate them to more complex reservoir processes.

Keywords

Rotokawa, geothermal, fractures, permeability, microstructure, physical properties, elastic moduli

4.1 Introduction

Fractures on multiple scales are the dominant control on fluid flow in most geothermal systems worldwide. Geothermal environments are prone to variable heat fluxes, dynamic fluid flow regimes and active tectonics which impact the physical and mechanical properties of the reservoir rocks in which they are hosted. The influence of such a dynamic environment can then render the host rocks highly altered and microstructurally complex. As a result of these changes, the relationships between physical properties may not be entirely straightforward. Studies of these properties and attempts to quantify how they interact in the subsurface can greatly assist in the optimization and maintenance of geothermal resources (e.g. DiPippo, 2008; Grant and Bixley, 2011; Gupta and Roy, 2007). Here we detail the results of a systematic physical and mechanical properties study on the Rotokawa Andesite, a major reservoir within the Rotokawa Geothermal Field, a high-enthalpy two-phase steam field (Krupp and Seward, 1987; Quinao et al., 2013), located within the Taupo Volcanic Zone (TVZ), North Island, New Zealand (Figure 4.1). TVZ is a rifted arc associated with the Hikurangi subduction system in which the Pacific plate descends beneath the Australasian plate (Cole, 1990; Wilson et al., 1995), and hosts active volcanism and multiple associated hydrothermal systems (Bibby et al., 1995; Rowland and Sibson, 2004; Rowland et al., 2010). Our goal, using a comprehensive experimental dataset, is to build solid relationships (empirical, micromechanical and geometrical) between the physical and mechanical properties of the Rotokawa Andesite.

The Rotokawa field has been the subject of exploration for mineral resources (sulfur and gold deposits) and, for many years, was the subject of detailed investigation into its commercial geothermal resource (Collar and Browne, 1985; Hedenquist et al., 1988; Krupp and Seward, 1987). More recently, electricity generation has been realized at Rotokawa with the installations of the Rotokawa I and Nga Awa Purua generation

stations (Legmann and Sullivan, 2003, Bloomberg et al., 2012). The more recent of these installations, the Nga Awa Purua power station hosts the single largest geothermal turbine installation in the world and has a generation capacity >140 MWe which is approximately 3% of New Zealand's electricity consumption (Horie and Muto, 2010).

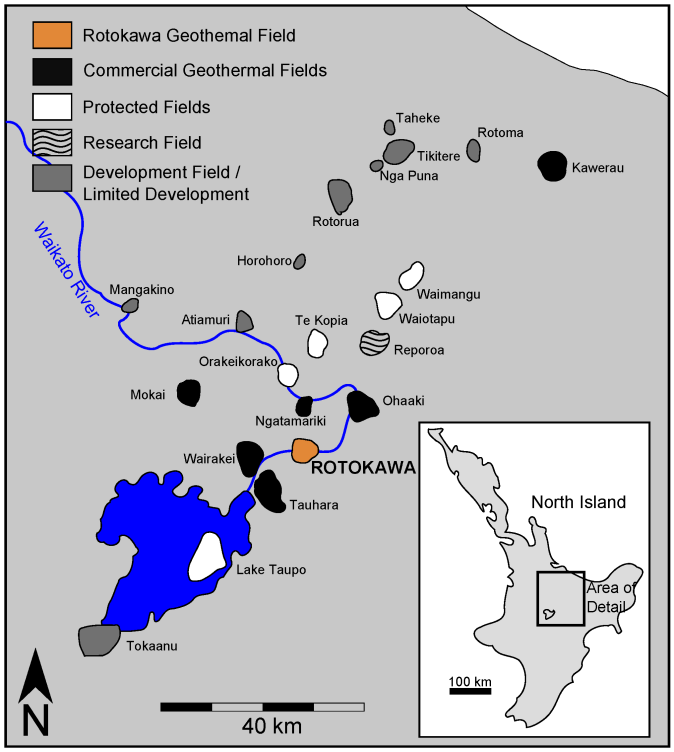

Figure 4.1: Geothermal Fields of the Taupo Volcanic Zone (TVZ), North Island, New Zealand and location of Rotokawa Geothermal Field (adapted from Sewell et al., 2012)

The study of core sourced from geothermal systems can yield valuable information to assist the modeling and understanding of these systems. For example, Stimac et al. (2004) present an excellent study on the relations of permeability and porosity from continuous core from Tiwi geothermal field, Philippines. Their data show that permeability and porosity decrease with depth, with occasional deviations attributed to alteration and compaction. However, the authors are careful to note that their work does not detail the influence of microfractures and their effect on relevant reservoir parameters. Lutz et al. (2010) present a very interesting case history of well core from Desert Peak (Nevada, USA) field in preparation for stimulation of an enhanced geothermal system (EGS). The results of their study further the understanding of the reservoir rock at Desert Peak and support proposed additional drilling and stimulation work within the reservoir. The effect of hydrothermal alteration on the physical properties of geothermal core is also a very significant

area of research. Fluids can alter the acoustic velocities and permeabilities of rock in both the natural and laboratory environment (Jaya et al., 2010, Kristinsdóttir, et al., 2010). However coupled studies of physical properties such as porosity, permeability and strength on geothermal reservoir rocks have not been extensively presented. A detailed study of the role of microfractures in relation to the physical properties of a geothermal system such as Rotokawa could serve to greatly improve the understanding of reservoir processes at multiple scales.

Geothermal systems are more often than not associated with volcanic systems and are often the buried remnants of extinct volcanic systems. By proxy, the study of rocks from volcanic edifices can help to boost the understanding of processes within geothermal reservoirs especially with regard to microfractures, which play an essential role in controlling strength, porosity, permeability, acoustic velocities and elastic moduli of rocks (Wu et al., 2000; Guéguen and Schubnel, 2003; Pereira and Arson, 2013; Faoro et al., 2013). Vinciguerra et al. (2005), Watanabe et al. (2008), Smith et al. (2009) and Heap et al. (2009 and 2013a) have investigated the mechanical, physical, and elastic properties of rocks sourced from volcanic edifices. For example, Vinciguerra et al. (2005) have provided an excellent example of the influence of thermal stressing on basaltic samples. They show, using ultrasonic wave velocities, that the response of microstructurally variable basalts to thermal stressing can be quite different. While a fresh, microlitic basalt exhibited severe reductions in P-wave velocity after exposure to 900 °C, the P-wave velocity of a porphyritic basalt with a pervasive microcrack network did not change.

Similar dependence on the effect of microfractures on strength (Smith et al, 2009) and permeability (Nara et al., 2011) has been investigated, with microfractures proving to be deleterious to both strength and permeability. David et al. (1999) showed that mechanical and thermal microcracking in granites results in significant changes to permeability and acoustic wave velocities. Mechanical microcracking resulted in the development of P-wave velocity anisotropy, while thermally microcracked samples showed little P-wave anisotropy. Additionally, permeability was much more varied in mechanically microcracked rocks than those induced thermally, suggesting that thermal microcracks develop isotropically. Chaki et al. (2008) investigated the role of thermal microcracking on granites and showed that ultrasonic wave propagation is attenuated by microcracks within the samples and the orientation of these thermal microcracks (with regard to the original microstructure) plays a critical role in the propagation and attenuation of the waves. Faoro et al. (2013) provide a model for how microcrack density within an isotropically microcracked sample can be modeled as a function of aspect ratio and microcrack connectivity. Elastic moduli and acoustic velocities are strongly influenced by the morphology, distribution and shape of pore space in rocks and are substantially attenuated by the presence of microcracks (Stanchits et al., 2006 and references therein).

The relationship between porosity and strength has also been observed by many authors, with general agreement that as porosity of a sample (both rock and other engineering materials) increases, strength decreases (e.g., Al-Harthi et al., 1999; Diamantis et al., 2009; Ju et al., 2013; Kahraman et al., 2005; Li and Aubertin, 2003; Chang et al., 2006). The geometry of the pores also has a significant role in the strength of the materials both intrinsically and with respect to the direction of stress (Luping, 1986). The microstructure of rocks can be changed by increased crack damage caused by both mechanical and thermal stresses (Heap et al., 2009, Nara et al., 2011) and this can be observed by the evaluation of physical properties both destructive and non-destructive (Pola et al., 2012 and references therein; Sousa et al., 2005). Our study details a comprehensive evaluation of reservoir rock core taken from the Rotokawa Andesite by a thorough evaluation of rock properties at various scales. We examine texture, mineralogy, petrology, and microstructure. Physical properties are explicitly investigated: porosity, density, ultrasonic wave propagation and dynamic moduli, uniaxial compressive strength, static elastic moduli and permeability. We correlate between the microcrack severity of the andesite and the physical properties observed. Here, we report our findings (Section 4.3), present empirical relationships of physical properties (Section 4.4.2), and classical micromechanical (Section 4.4.3.1) and geometrical models (Section 4.4.3.2) to predict both uniaxial compressive strength and permeability. Our data is discussed in relation to the Rotokawa Geothermal field and applicability of our results to other geothermal resources.

4.2 Materials and Methods

4.2.1 Sample Description and Preparation

The samples used in this study were sourced from Rotokawa production wells RK28, RK30 and RK27_L2 (Figure 4.2). The depths, orientations and corrected true vertical depths (TVD) are listed in Table 4.1. The original cores were approximately 6 m long and 100 mm in diameter, and were initially described by staff of GNS Science Wairakei Research Centre, New Zealand, in a series of internal industry reports detailing the respective production wells from surface to total depth (TD). These reports elucidate the stratigraphic sequences of the wells and rock types, hydrothermal alteration and locations of the wells (Rae et al., 2010, 2009; Ramirez and Hitchcock, 2010). At the University of Canterbury (UC) the cores were catalogued and cut into workable pieces approximately 100 mm in length. These smaller sections were over-cored to obtain smaller cylinders 40 mm in diameter and ranging from 80 to 100 mm in length, then machined so that their end-faces were flat and parallel in accordance with ISRM standards (Ulusay and Hudson, 2007).

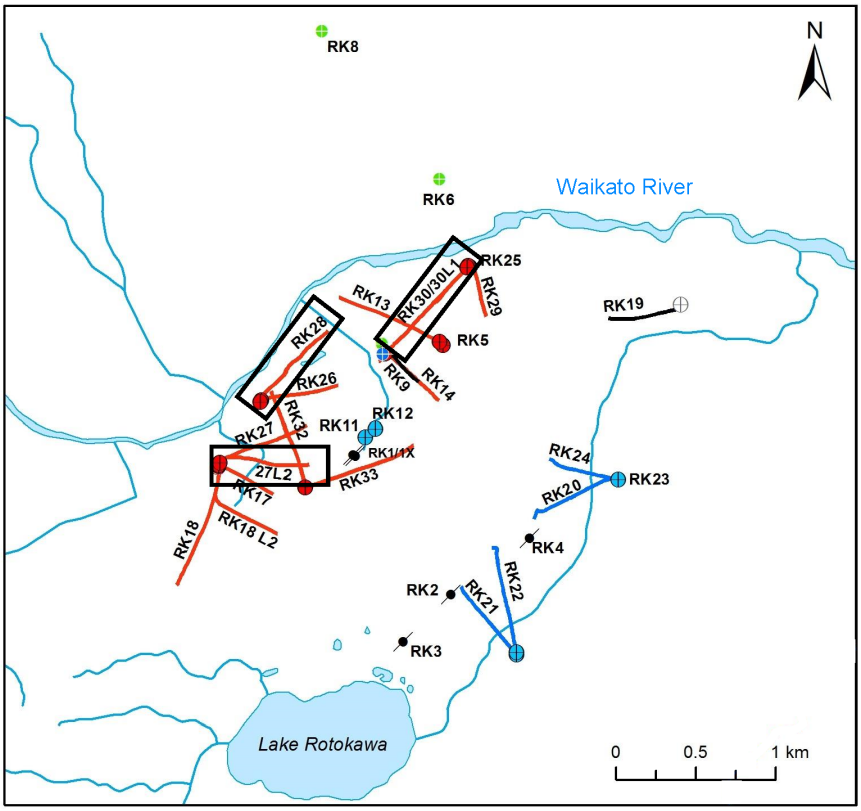

Figure 4.2: Rotokawa Geothermal Field and significant wells. Wells RK27L2. RK28 and RK30 were the source of the core used in this study and are outlined with boxes in the figure.

Table 4.1: Core Depths and orientations for Rotokawa Andesites used in this study

Well Name	Depth of Core (m)	True Vertical Depth (meters below reference level)	Inclination from vertical (degrees)	Azimuth from North (degrees)
RK 28 ST 1	2310-2316	2215-2221	21.94	50.91
RK 27 L2	2120-2126	2001-2007	27.31	88.11
RK 30 L1	2320-2326	2175-2182	20.11	218.47

4.2.2 Rotokawa Andesite Stratigraphy, Petrology and Microfracture Characterization

The Rotokawa Andesite is a series of lavas, pseudo-breccias and breccias. The movement of fluid through the andesite is predominantly along fracture networks (Barton et al., 1995; Hickman et al., 1998; Rae, 2007, Massiot et al., 2012). The andesite overlies basement Miocene greywacke, and is capped by a sequence of

volcaniclastic and sedimentary units; Reporoa Group, Wairakei Ignimbrite, Waiora Formation and Huka Falls Formation (Krupp and Seward, 1987; Rae, 2007).

The Rotokawa Andesite is weakly porphyritic with abundant phenocrysts of plagioclase feldspar and pyroxenes in a fine groundmass of plagioclase microlites and magnetites; occasional tuff and greywacke lithics are also observed (Rae, 2007; Rae et. al, 2010). The andesite is gray to green and occasionally purple in color, depending on alteration within the reservoir; alteration is less intense in the lavas and more intense in the breccia and pseudo-breccia (Ramirez and Hitchcock, 2010). Veins of quartz, calcite, anhydrite and epidote occur, and amygdales within the sample are often filled with chlorite, calcite, hematite, pyrite and chalcedony, often with quartz rims. Alteration is pervasive with the original mineral assemblages typically replaced by secondary hydrothermal alteration species, with some specimens showing very little original mineralogical texture. Plagioclase feldspars have been altered to albite, adularia, occasional calcite and rare pyrite, and ferromagnesian minerals have been replaced by chlorite, quartz, calcite and occasional epidote. Microfractured phenocrysts (Figures 4.3 and 4.4) are abundant and many relict phenocrysts retain original texture are but replaced by secondary mineralization. The alteration chemistry of the samples indicates that this portion of the reservoir is dominated by chlorite/epidote alteration. The degree of alteration is relatively consistent across the core we have sampled with most primary mineralogies replaced by secondary alteration products. Microfracture mineralization indicates that these networks may have been conductive pathways for fluid migration (i.e., the presence of chlorite clays, adularization of plagioclase, calcite and quartz rimming of fractured matrix); we typically observe chlorite, calcite and quartz as alteration mineralogies with occasional epidote centers within the fractures. Backscatter scanning electron microscopy (SEM) was utilized to characterize the microstructure of the specimens (Figure 4.4). At several different magnifications, we see an abundance of microfractures in the samples as well as a clear depiction of the complex alteration mineralogy displayed by the andesite.

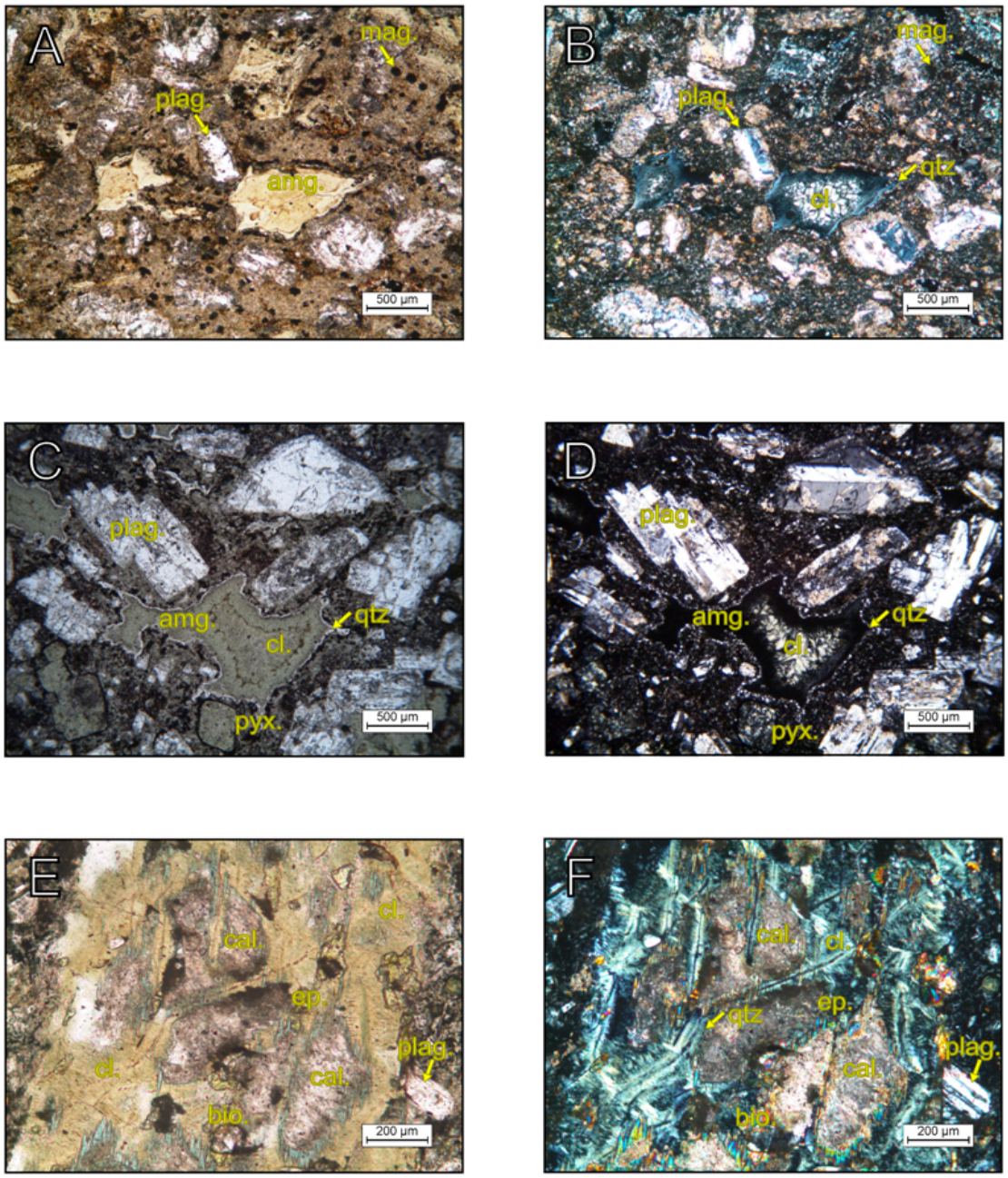

Figure 4.3: Thin section photomicrographs of the Rotokawa Andesite. (A) Plane polarized light of RK28 2310.6C andesitic pseudo-breccia with plagioclase laths (plag.), groundmass is altered plagioclase, abundant magnetite (mag.) and amygdale (amg.). (B) Cross polarized light of RK28 2310.6C clearly shows alteration fabrics of the brecciated andesite with plagioclase (plag.) and amygdales filled with chlorite (cl.) and rimmed by quartz (qtz.). (C) Plane polarized light view of RK27_L2 2121.4A showing andesitic breccia with adularia plagioclase (plag). and amygdale (amg.) filled with chlorite (cl.) quartz (qtz.) highly altered pyroxene (pyx.) in lower portion of image. (D) Cross polarized light view of RK27_L2 2121.4A shows chlorite infill of a large amygdale (amg.) in the centre of the photomicrograph and quartz rim (qtz.), adularia plagioclase (plag.) and highly altered pyroxene (pyx.) (E) Plane polarized light view of RK 30 2322.4A shows highly altered and microfractured plagioclase phenocryst with intense alteration and replacement by chlorite (cl.), epidote (ep.), calcite (cal), possible biotite (bio.) and small adularia plagioclase (plag.) (F) Cross polarized light of RK 30 2322.4A illustrates microfracture network and veining with alteration products of quartz (qtz.), epidote (ep.), biotite (bio.), calcite (cal.) and plagioclase (plag.).

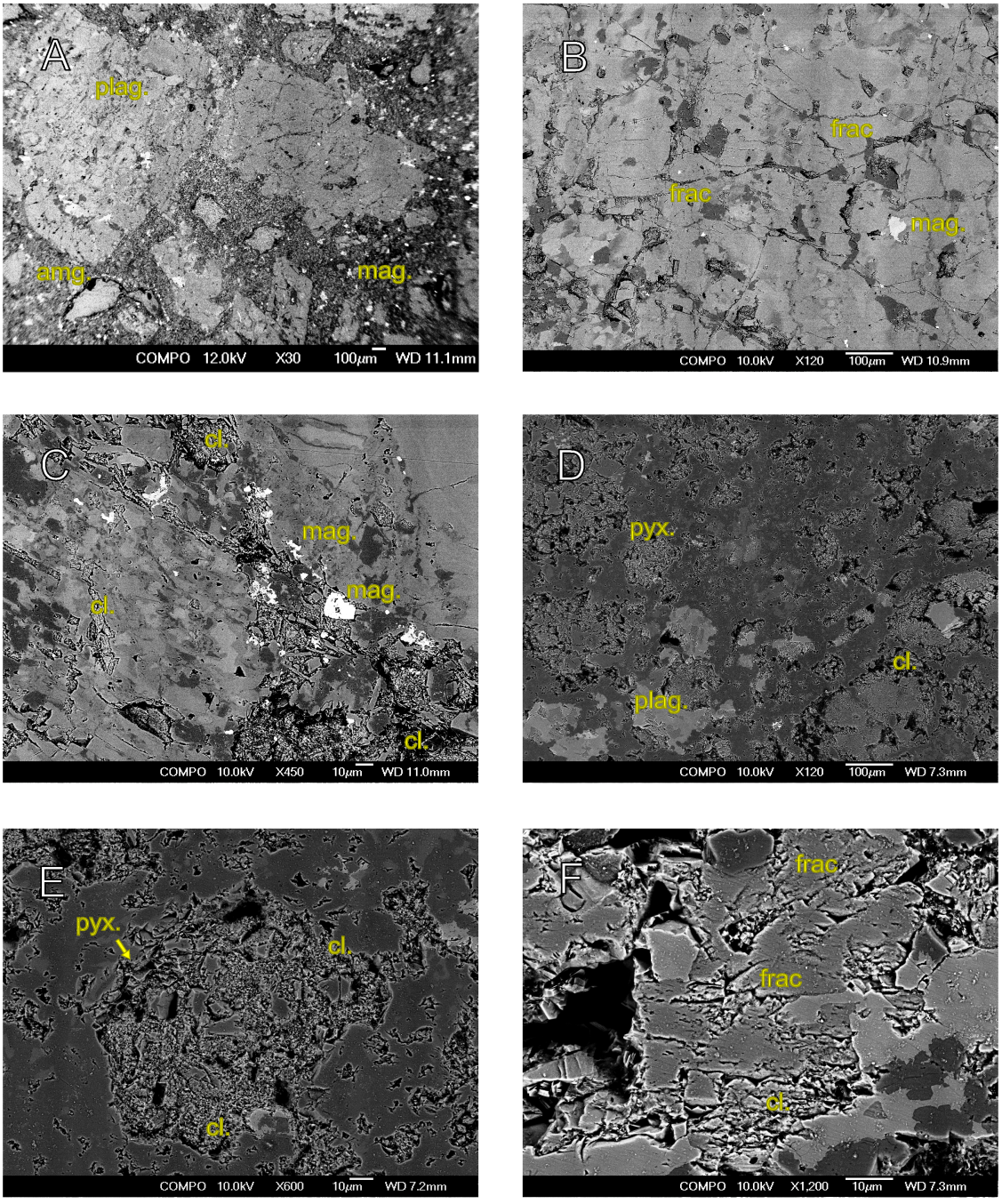

Figure 4.4: Backscattered Scanning Electron Microscope photomicrographs of Rotokawa Andesite samples A-C are from RK 28_2310.6m depth and D-F are from RK 27 2121.1m depth. (A) Andesite with abundant ferromagnesian minerals (mag.) altered amygdale (amg.) and highly scattered magnetites (mag. bright hues) (B) Detail of a fractured plagioclase phenocryst showing the microfractured texture (frac.) and occasional magnetite (mag.) (C) Detail of a fracture in-fill showing chloritization (cl.) and abundant ferromagnesian minerals (mag.). (D) Groundmass of RK_27 sample, pervasive fracturing is not apparent at this magnification but the porous network is quite apparent with pyroxene (pyx.), chlorites (cl.) and plagioclase (plag.). (E) Replacement mineralogy of likely pyroxene phenocryst (pyx.)showing abundant chloritization (cl.) and dissolution textures. (F) Detail of relict pyroxene and abundant chlorite (cl.) with abundant micro-fractures (cl.) apparent in the sample mass.

As discussed previously, strength, porosity, permeability and acoustic velocities can be significantly influenced by microfractures in a sample. Therefore, we deemed it necessary to develop a fundamental understanding of the microfracture densities displayed by the samples. Using reflected light thin section photomicrography, 10 polished thin sections were examined for microfracture densities using the methods suggested by Underwood (1970) and further described by Richter and Simmons (1977), and Wu et al. (2000). In each thin section, an 11 x 11 mm^2 area was selected, which was subdivided into sections of 1 x 1 mm^2. The number of cracks that intersected a grid array of parallel and perpendicular lines that were spaced at 0.1 mm was counted. This allowed calculation of the crack surface area per unit volume according to Equation 4.1:

$$Sv = \frac{\pi}{2} * P_l + (2 - \frac{\pi}{2}) * P_{ll} \tag{4.1}$$

where Sv is the crack surface area per unit volume, P_l is the number of perpendicular lines crossed by crack intersections and P_{ll} is the number of parallel lines crossed by crack intersections. We also characterized the anisotropy of microfracture distribution using Equation 4.2:

$$\Omega_{23} = P_l - P_{ll}/P_l + (4/\pi–1)P_{ll} \tag{4.2}$$

4.2.3 Density and Porosity Measurements

Once the samples were cut and polished as discussed in Section 4.2.1, they were washed with water to remove any debris from preparation then immersed into distilled water under vacuum of about 100 kPa for 24 hours. Samples were taken out of the water, had their surface water removed and weighed. The samples were then placed into a laboratory oven at 105 °C and dried until constant mass was observed. Subsequently they were removed from the oven and held in a dessicator until further characterization was carried out. Sample lengths and diameters were measured to within 0.01 mm. The connected porosity, and dry bulk density of the samples were calculated following the methods recommended by Ulusay and Hudson (2007).

4.2.4 Characterization of Acoustic Velocities and Dynamic Elastic Moduli

Compressional wave (Vp) and shear wave (Vs) velocities and dynamic elastic moduli were measured using a GCTS (Geotechnical Consulting and Testing Systems) Computer Aided Ultrasonic Velocity Testing System (CATS ULT-100) apparatus with axial P- and S-wave piezoelectric crystals. Resonance frequency of the transducers was 900 kHz, pulse acquisition rate was 20 MHz and 108 waveforms were captured for each sample. The velocities were collected under a constant stress of 10 MPa via a Tecnotest servo-controlled 3000 kN loading frame (Figure 4.5). The stress of 10 MPa was used to ensure a consistent waveform across

the specimens and that applied stress was consistent for all measurement cycles. This was determined to be below microcrack closure and opening stress by analyzing the change in axial strain as the sample was loaded to 10 MPa (Eberhardt et al, 1998). We note that there was no change in axial strain and a quiescence of acoustic emissions during the initial loading (Brace et al., 1966; Martin and Chandler, 1994; Lion et al., 2005; Nicksiar and Martin, 2012); this ensured a good quality interpretation of the first arrival time of acoustic pulses. From the acquisition of these data we determined the dynamic Poisson's ratio and Young's Modulus using Equations 4.3 and 4.4 (Guéguen and Palciauskas, 1994), respectively:

$$\nu_d = \frac{Vp^2 - 2Vs^2}{2(Vp^2 - Vs^2)} \tag{4.3}$$

$$E_d = \frac{\varrho * Vs^2 * (3Vp^2 - 4Vs^2)}{Vp^2 - Vs^2} \tag{4.4}$$

where Vp is compressional wave velocity in m/s, Vs is shear wave velocity in m/s, E_d is the Young's modulus in Pa, ν_d is the dynamic Poisson's ratio and ϱ is density in kg/m^3. Our physical and acoustic property characterizations are summarized in Table 4.3. In addition to the determination of the elastic moduli from acoustic measurements, we also utilized the method set forth by Martinez-Martinez et al. (2011) to characterize the spatial attenuation of the compressional wave form anisotropy (Equation 4.5).

$$\alpha s = \frac{20log(\frac{Ae}{Amax})}{L} \tag{4.5}$$

where αs is spatial attenuation in dB/cm, A_e is the maximum amplitude emitted by the piezoelectric crystal, A_{max} is the maximum amplitude recorded of the pulse after passing through the sample and L is the length of the sample in m.

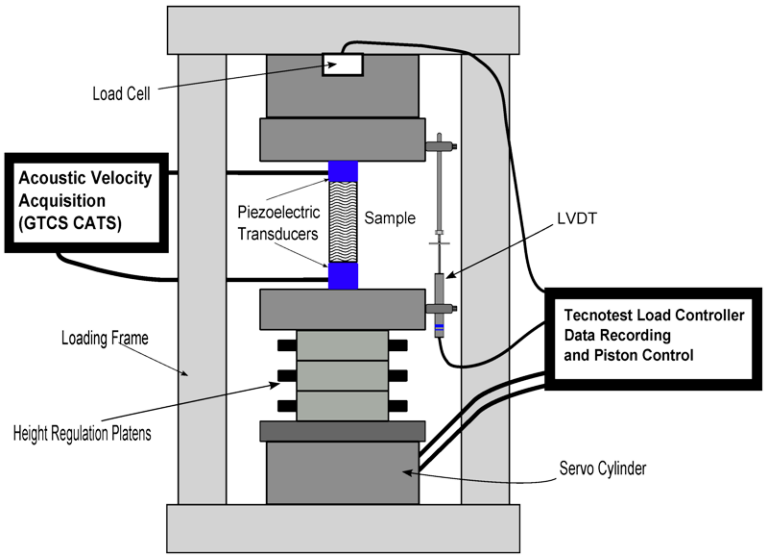

Figure 4.5: Loading Frame set-up for acquisition of acoustic velocities and dynamic elastic moduli at the University of Canterbury (not to scale).

4.2.5 Uniaxial Compressive Strength Testing and Static Elastic Moduli

UCS (Uniaxial Compressive Strength) was determined using a Technotest 3000 kN, servo-controlled loading frame. Specimens were cleaned and fixed with 20 mm Tokyo Sokki Kenkyujo Co. Ltd (TML) strain gauges with a gauge factor of 2.12 (Figure 4.6). Two vertical gauges measured axial strain and two laterally oriented gauges measured radial strain, care was taken to ensure that the strain gauges were perpendicular to their respective axes of deformation. The specimens were deformed at a constant strain rate of 1.0 x 10-5 s^{-1}(controlled by a Linear Variable Differential Transformer, LVDT) at ambient laboratory temperature and humidity conditions. The specimens were also monitored for acoustic emissions (AE) with the Physical Acoustics Corporation MISTRAS AE Node acquisition system. Two Physical Acoustics WSα AE transducers (100-900 kHZ operating frequency) were attached to the samples at the top and base, and hit counts, waveforms, energy and amplitude of the received signals were recorded during sample deformation. AE monitoring was used during deformation as a proxy for microcracking as AE's are generated by the release of energy from a material during the propagation and nucleation of microcracks (Eberhardt et al, 1998; Diederichs et al, 2004). We utilized arbitrary AE energy units (the area under the received waveform signal) for comparison of AE activity across the datasets. Once stress-strain curves were obtained and AE data processed, we calculated the static elastic moduli for each specimen by utilizing Equations 4.6 and 4.7 with the tangent deformation modulus at 50% of the maximum peak stress (Ulusay and Hudson, 2007).

In addition, we selected portions of the stress-strain sequence to identify crack closure, crack initiation, unstable crack propagation and ultimately crack coalescence (Martin, 1993; Eberhardt et al., 1998; Takarli et al., 2008).

$$E_s = (\Delta\sigma_a/\Delta\varepsilon_a) \tag{4.6}$$

$$v_s = -(\Delta\varepsilon_r/\Delta\varepsilon_a) \tag{4.7}$$

where E_s is the static Young's modulus (Pa), v_s is the static Poisson's Ratio, σ_a is axial differential stress (Pa) ε_a is axial strain and ε_r is radial strain.

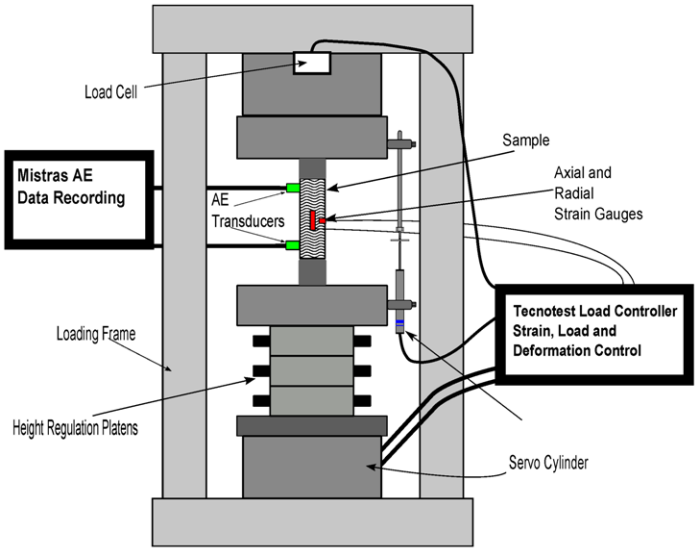

Figure 4.6: Loading frame set-up for Uniaxial Compressive Strength testing with strain gauges and acoustic emission acquisition at University of Canterbury (not to scale).

4.2.6 Permeability Measurements

Gas (argon) permeability measurements were made at the Laboratoire de Déformation des Roches, Université de Strasbourg (France). The 40 mm diameter specimens were over-cored to a diameter of 20 mm and cut and ground flat and parallel to a nominal length of 40 mm. The new samples were then re-evaluated by the triple-weight method to obtain porosity via the Archimedes' method (Ulusay and Hudson, 2007), and oven-dried under vacuum at 40° C until no change in sample mass was observed. The samples were then jacketed with viton sleeves, placed between two steel end-caps and lowered into the pressure vessel (Figure 4.7). A confining pressure of 2 MPa was applied to the sample (provided by distilled water), and permeability

measured using the transient method (or pulse-decay method). For the permeability measurements, an initial differential pore pressure was applied to the sample, the upstream inlet was then closed, and the pore pressure decay monitored over time. The downstream fluid pressure (Pdown) was the ambient atmospheric pressure, and the maximum upstream fluid pressure (Pup) was set so the pressure differential was 0.5 MPa. Permeability was then calculated using Equation 4.8 (after Brace et al., 1968):

$$k_{gas} = \left(\frac{2\eta L}{A}\right)\left(\frac{V_{up}}{P_{up}^2 - P_{down}^2}\right)\left(\frac{\Delta P_{up}}{\Delta t}\right) \tag{4.8}$$

where k_{gas} is the gas permeability, η is the viscosity of the pore fluid, A is the cross-sectional area of the sample, V_{up} is the volume of the upstream pore pressure circuit (approximately 7cm3), P_{up} is the upstream pore pressure, P_{down} is the downstream pore pressure and t is the time. By plotting ΔP_{up} as a function of time, the local slope of the curve is computed to determine the temporal variation of the permeability, k_{gas}. To check whether our data should be corrected for Klinkenberg "slip flow" (Klinkenberg, 1941) we plotted the measured gas permeability as a function of the inverse of the mean pore fluid pressure P_{mean}. For the transient method, since P_{down} is constant, the decay of P_{up} through time corresponds to the decay of the mean pore pressure P_{mean}. We found that, in all cases, the Klinkenberg correction should be applied:

$$k_{true} = k_{gas}(1 + b/P_{mean}) \tag{4.9}$$

Where $k_{true}$is the true permeability, k_{gas} is the gas permeability, b is Klinkenberg slip factor, and $P_{mean}$is the mean pore fluid pressure.

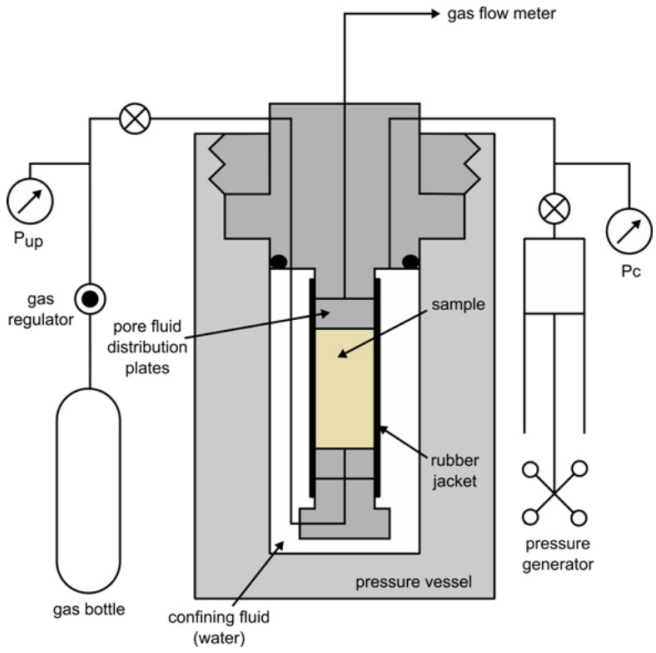

Figure 4.7: Gas permeameter used in permeability measurements at University of Strasbourg (not to scale)

4.3 Results

In the following section we present our data on microstructure (quantitative fracture analysis), macrostructure (bulk density, porosity, acoustic wave velocities and dynamic moduli), strength relations (by UCS testing), and finally fluid transport properties (permeability) of the Rotokawa Andesite.

4.3.1 Quantitative Two Dimensional Microstructural Analysis

We evaluated the microfracture density of 10 specimens as a function of crack density per unit volume (Table 4.2). These samples were selected as a representation of the range of connected porosities observed within the sample set. We found that the crack area per unit volume in our samples ranges from 3.77 to 13.06 mm^2/mm^3. The crack area per unit volume appears to be independent of the alteration and mineralogy of the specimens and, as detailed by the calculated anisotropy factor ($\Omega_{2,3}$), the microcracks are isotropic (Table 4.2).

Table 4.2: Results of quantitative microstructural characterization for Rotokawa Andesite. As discussed in section 4.2.2, crack densities were calculated on thin section samples to ascertain crack areas per unit volume.

Sample Name	Crack density for intercepts parallel to orientation axis $P_{\parallel}$ (mm^{-1})	Crack density for intercepts perpendicular to orientation axis $P_{\perp}$ (mm^{-1})	Crack area per unit volume S_V (mm^2/mm^3)	Anisotropy factor Ω_{23}	Connected Porosity (vol%)
27_21_0B	13.73	13.53	13.06	0.01	14.91
28_10_5A	4.10	4.41	8.33	0.06	7.47
27_20_4_B	1.83	2.06	3.77	0.08	4.37
27_3_3B	4.77	4.77	9.55	0.01	9.81
30_22_4A	2.77	2.62	5.48	0.01	6.49
28_10_9B	3.84	3.90	7.71	0.03	7.42
28_12_1	4.83	4.65	9.59	0.02	7.89
30_21_1B	2.93	2.91	5.85	0.01	7.47
27_21_3A	5.80	5.13	11.31	0.09	16.3
28_10_6C	2.97	2.87	6.38	0.05	5.97

Table 4.3: Compilation of Bulk dry density, Connected porosity, P-wave velocity (Vp), S-wave velocity (Vs), Uniaxial Compressive Strength (UCS) and Dynamic and Static Poisson's Ratio and Young's Moduli for 24 specimens of Rotokawa Andesite selected for destructive testing. Measurements were made at ambient temperature conditions.

Sample Well Number Sample Name	Bulk dry density (g/cm^3)	Connected porosity (vol%)	Vp (m/s)	Vs (m/s)	Spatial Atten. (dB/cm)	UCS (MPa)	Static Young's Modulus (GPa)	Dynamic Young's Modulus (GPa)	Static Poisson's Ratio	Dynamic Poisson's Ratio
RK27_L2_21.5B	2.44	10.72	4005	2443	14.63	85.99	19.9	35.1	0.24	0.20
RK27_L2_21.8A	2.33	13.49	3850	2363	16.47	79.91	25.2	31.2	0.26	0.20
RK27_L2_23.2A	2.56	6.61	4182	2490	22.48	105.26	31.2	38.9	0.19	0.23
RK27_L2_20.4B	2.65	4.37	4556	2752	22.53	211.05	37.7	45.9	0.25	0.21
RK27_L2_21.1C	2.37	13.10	3877	2405	23.60	69.53	21.5	32.5	0.18	0.19
RK27_L2_3.3B	2.45	9.81	3937	2331	23.51	95.78	32.4	29.9	0.13	0.18
RK27_L2_21.0B	2.34	14.91	3752	2337	8.40	60.13	28.1	30.6	0.12	0.17
RK27_L2_21.3A	2.29	16.3	3627	2160	15.13	70.57	30.4	24.6	0.16	0.17
RK_28_10.6C	2.50	5.97	4350	2652	18.27	146.20	43.7	42.4	0.27	0.20
RK_28_10.8C	2.53	6.72	4147	2537	11.67	109.91	27.2	39.1	0.34	0.20
RK_28_10.9B	2.51	7.42	4285	2615	14.67	137.31	32.4	41.5	0.20	0.20
RK_28_13.2A	2.55	6.97	4013	2531	18.53	146.21	38.3	37.2	0.24	0.19
RK_28_10.5A	2.45	7.47	4220	2578	14.83	130.71	27.4	38.8	0.25	0.21
RK28_11.5A	2.51	7.62	4403	2555	10.06	152.76	35.6	37.4	0.27	0.13
RK28_12.1	2.49	7.89	4010	2460	12.23	115.01	29.3	36.2	0.22	0.14
RK_30_20.4A	2.57	5.30	4002	2495	10.39	140.97	33.6	36.9	0.09	0.15
RK_30_21.0A	2.55	6.84	4070	2508	11.17	126.53	26.4	39.8	0.14	0.15
RK_30_21.1B	2.54	7.47	4352	2659	28.75	157.93	25.8	43.2	0.17	0.20
RK_30_21.7B	2.56	6.28	4154	2588	19.91	162.71	28.3	41.1	0.22	0.18
RK_30_22.3B	2.53	7.51	4133	2550	21.72	137.97	31.5	39.2	0.23	0.19
RK_30_22.4A	2.56	6.49	4181	2582	20.27	148.44	34.4	40.7	0.18	0.19
RK_30_22.5B	2.56	6.41	4236	2628	23.43	150.71	33.6	42.1	0.09	0.16
Mean	**2.49**	**8.44**	**4106**	**2510**	**17.39**	**124.62**	**30.6**	**37.5**	**0.20**	**0.18**
Std. Dev.	***0.09***	***3.23***	***221***	***133***	***5.512***	***37.01***	***5.5***	***5.1***	***0.06***	***0.03***

4.3.2 Porosity and Bulk Density

Bulk density decreases as connected porosity increases, as expected for samples of similar composition (Figure 4.8). Bulk dry densities of the samples range from 2.29 to 2.65 g/cm^3, with a mean value of 2.49 g/cm^3. Connected porosities range from 4.37-16.3 (vol%), with a mean value of 8.44 (vol%). While there is some variation in the distribution of pores/vesicles in the samples, we observe that the microcrack density exerts an important control on the porosity and density, as illustrated by the correlation of crack area per unit volume to connected porosity depicted in Figure 4.9.

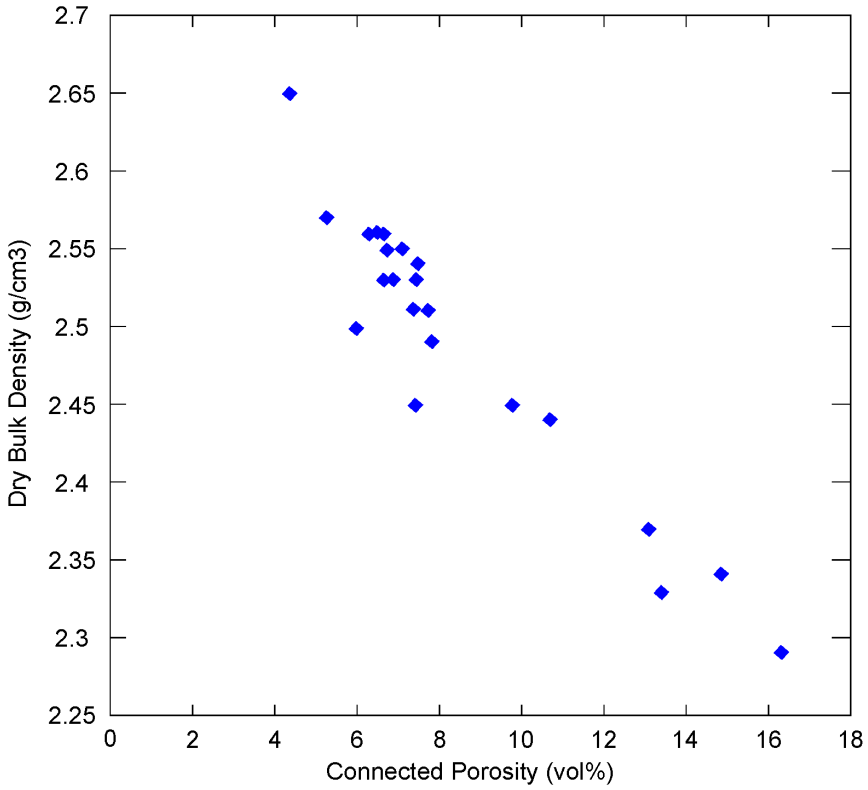

Figure 4.8: Connected porosity versus dry bulk density for Rotokawa Andesite calculated using the weight-method of Ulusay and Hudson (2007).

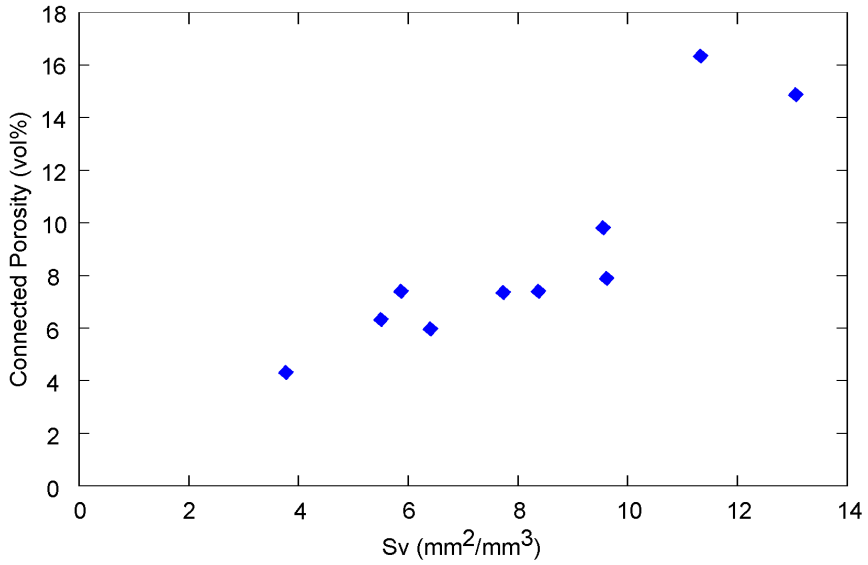

Figure 4.9: Crack area per unit volume (Sv) as determined from reflected light thin sections plotted versus connected porosity for the Rotokawa Andesite.

4.3.3 Ultrasonic wave velocities, dynamic elastic moduli, and spatial attenuation

Measurements made on samples under ambient (pressure and temperature) dry conditions yielded axial P-wave velocities from 3627 to 4556 m/s with a mean value of 4106 m/s, and axial S-wave velocities between 2160 to 2752 m/s with a mean value of 2510 m/s (Table 4.3). Porosity and P-wave velocities show moderate correlation; high porosity correlates to slower acoustic velocities as seen in Figure 4.10. Crack area per unit volume also correlates well with P-wave velocity (Figure 4.11). Axial spatial attenuation for the andesites ranges from 8.39 to 28.74 dB/cm. Figure 4.12 shows the correlation of spatial attenuation and P-wave velocity; we observe that there is no clear trend to spatial attenuation and acoustic velocity. Dynamic Poisson's ratio and dynamic Young's modulus were in the range 0.13-0.23 and 24.6-45.9 GPa, respectively (Table 4.3). Discussion of the empirical data and respective statistical correlations are further elaborated in Section 4.4.2.

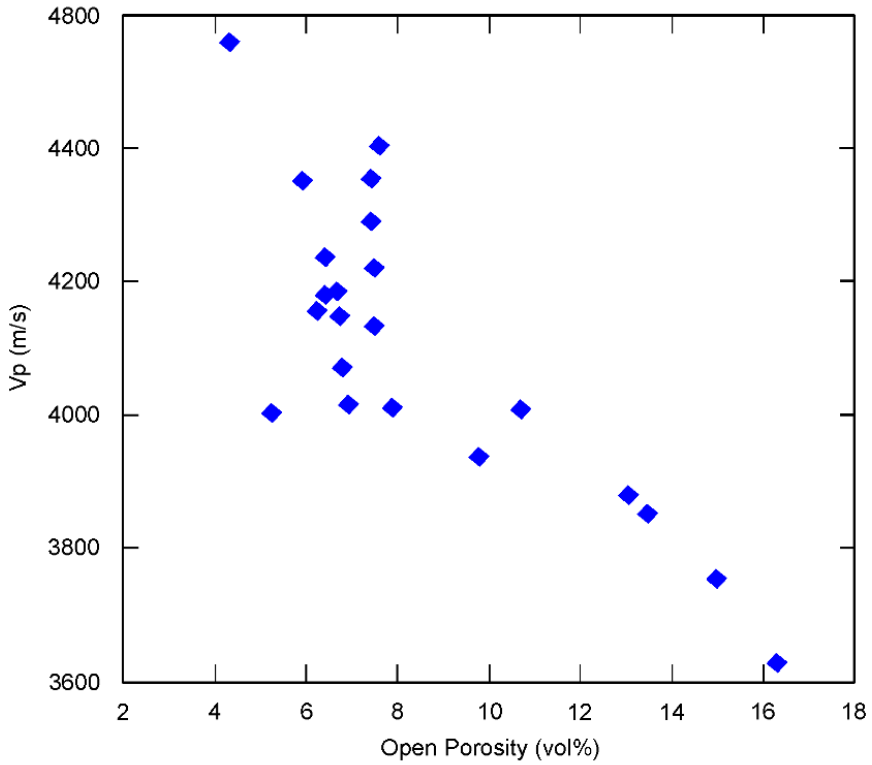

Figure 4.10: Connected porosity (vol%) versus compressional wave velocity (Vp) for the Rotokawa Andesite.

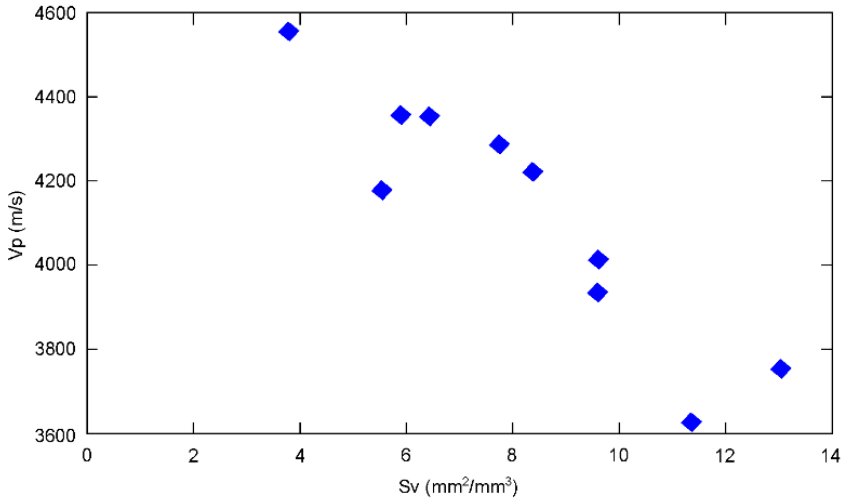

Figure 4.11: Crack area per unit volume (Sv) correlated to compressional wave velocity (Vp) for Rotokawa Andesite.

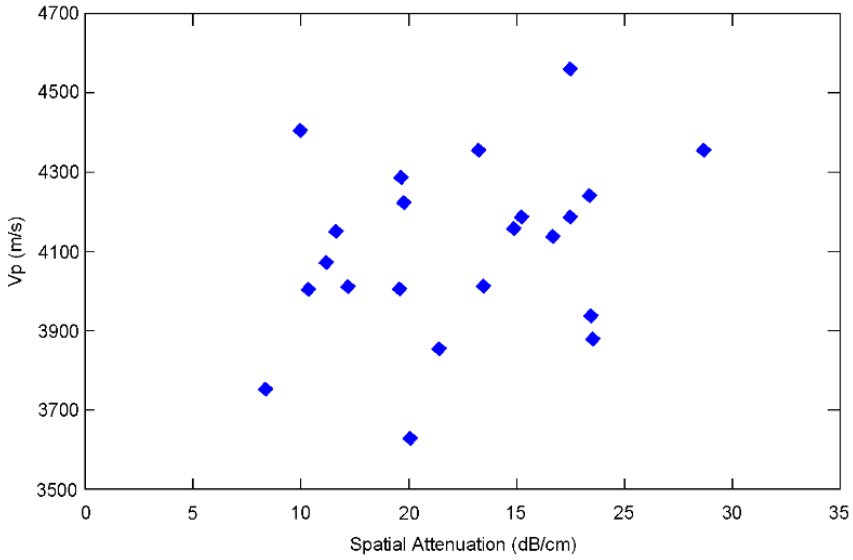

Figure 4.12: Spatial attenuation of axial compressional wave velocity (αs) plotted versus axial compressional wave velocity (Vp) for Rotokawa Andesite.

4.3.4 Uniaxial Compressive Strength and Static Elastic Moduli

In order to characterize the mechanical behavior of the Rotokawa Andesites, the 22 samples given in Table 4.3 were loaded to failure. The dataset shows a large range of UCS (similar to what we observe in the investigation of the other physical properties), from 60 to 211 MPa. The stress-strain behavior of the andesites is very similar across the range of strengths, as shown in Figure 4.13, which best represents the dataset and behavior of the Rotokawa Andesite under uniaxial compression. All specimens in the dataset show brittle behavior as evidenced by the stress-strain relationships and bolstered by analysis of AE activity. An increase of acoustic activity between dilatancy (σ_{cd}) and failure is a benchmark of brittle failure (e.g. Brace and Bombolakis, 1963; Rutter, 1986; Ashby and Sammis, 1990; Heap and Faulkner, 2008) as seen in Figure 4.13. Weaker specimens showed lower overall AE energy output than higher strength specimens. Static Young's moduli showed a range of 19.9-43.7 GPa and static Poisson's ratio from 0.09 to 0.34. A comparison of physical properties to UCS shows that as porosity (Figure 4.14) and crack surface area (Figure 4.15) increase the UCS of the rock decreases, and as axial P-wave velocity increases the strength increases (Figure 4.16).

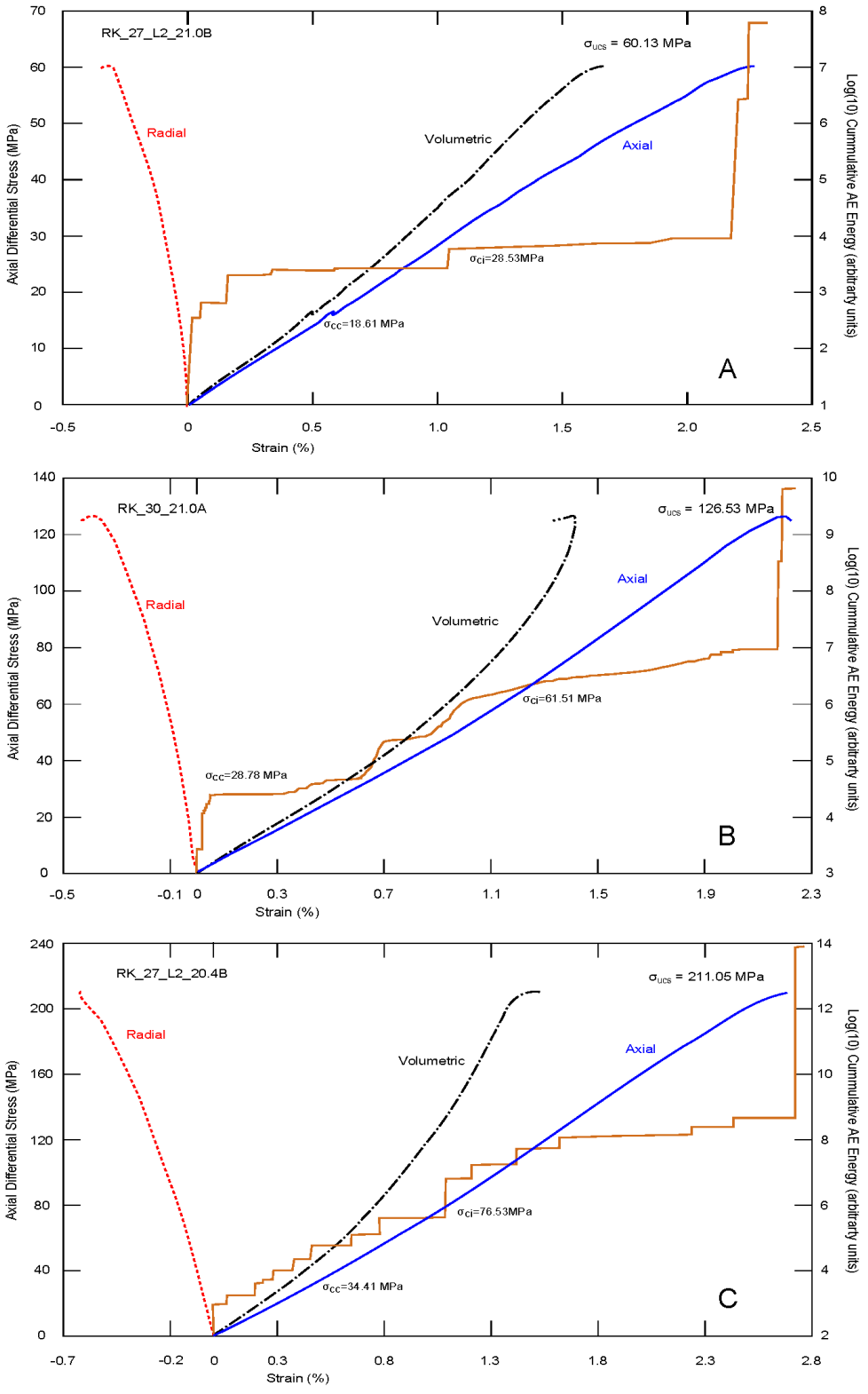

Figure 4.13: Stress-strain behavior of the Rotokawa Andesites when subject to constant strain loading ($1x10^{-5}$/s) and associated arbitrary acoustic emission energy output. All samples in this study showed brittle failure. Samples with low UCS generally developing a single fracture plane (A), samples near the mean UCS values developing several fracture planes (B) and samples with very high UCS showed explosive, catastrophic failure into several large and small pieces with no distinct failure plane (C).

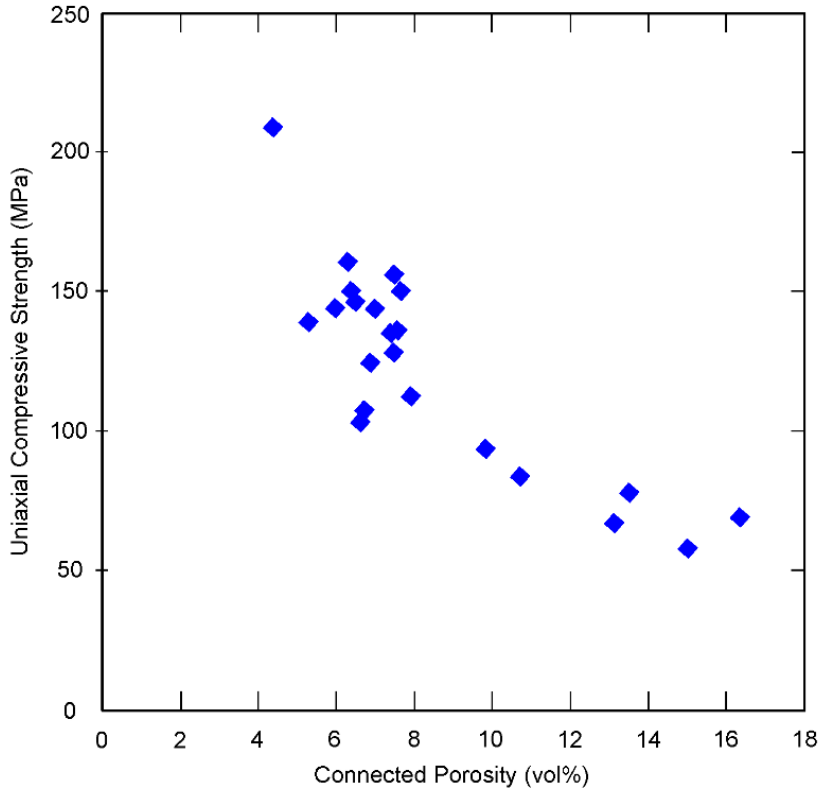

Figure 4.14: Connected porosity (vol%) plotted versus uniaxial compressive strength (MPa) for Rotokawa Andesite at ambient pressures and temperatures.

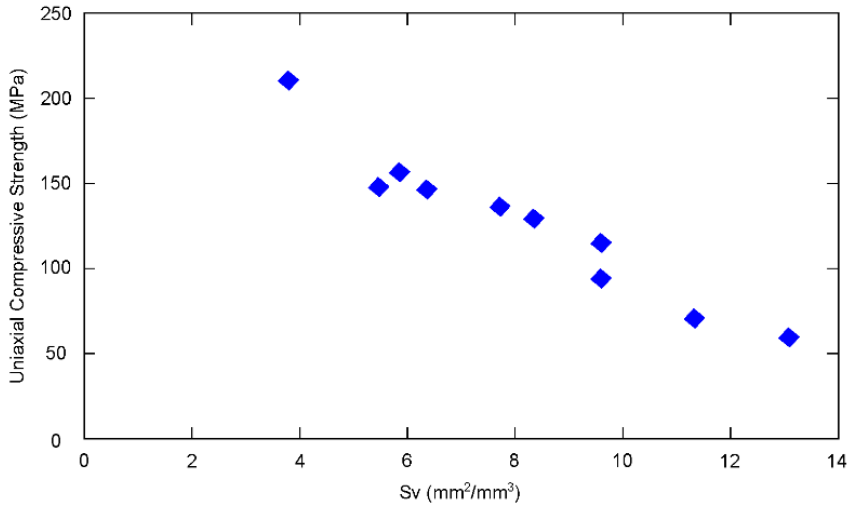

Figure 4.15: Crack area per unit volume (Sv) as measured from reflected light thin sections plotted versus uniaxial compressive strength (UCS) for the Rotokawa Andesite at ambient temperature.

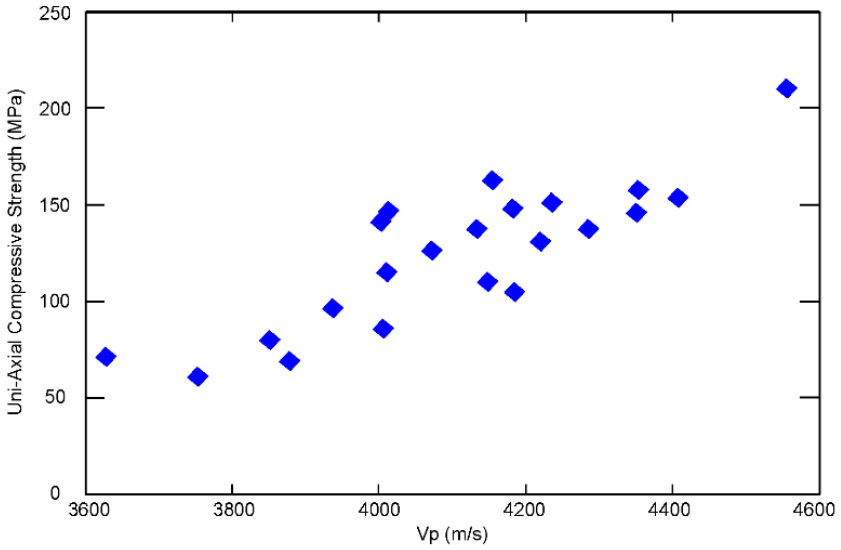

Figure 4.16: Axial P-wave velocity (Vp) as measured at ambient temperatures under an axial load of 10 MPa versus uniaxial compressive strength values for the Rotokawa Andesite at ambient temperature.

4.3.5 Permeability

Our argon permeability measurements show that, for the tested samples, permeability ranges from 9.82 x 10-18 m ^{2} to 1.66 x 10-16 m^2. The results show a trend of increasing permeability with increased porosity (Figure 4.17). We observe that two of the samples contain macrofractures (black stars on Figure 4.17), and have higher permeabilities that deviate from the trend of the dataset.

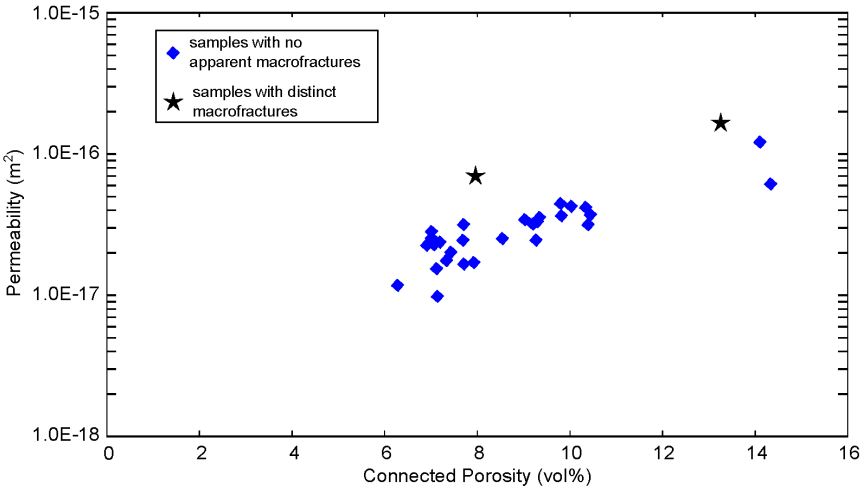

Figure 4.17: Plot of porosity versus permeability for Rotokawa Andesite. A cluster of data is observed near the mean values of porosity with a large range of permeability across the range of 6-8 (vol%) porosity.

4.4 Discussion

4.4.1 Micromechanical interpretation

We have shown that the Rotokawa Andesite contains a pervasive network of isotropic microcracks. Due to their isotropy, we have interpreted that the majority of these microcracks were induced by thermal stressing (Fredrich and Wong, 1986; Reuschlé et al., 2006; Wang et al., 1989; David et al., 1999). Indeed, the Rotokawa Andesite has experienced several cycles of heating and cooling: initial eruption of the andesite, burial in a faulted graben, hydrothermal alteration and eventual exhumation during core recovery (Rae, 2007; Lim et al., 2012). Our microstructural analysis has highlighted that the pervasive microcracking appears independent of lithology, original mineralogy and secondary (hydrothermal alteration) mineralogy.

The intense microcracking in our samples has shown to be a significant factor in all of the physical properties that we have measured. First, microcracking has greatly reduced the propagation velocity of ultrasonic waves through the andesite. We see a clear correlation of crack area per unit volume (Sv) to the observed compressional wave velocities (Figure 4.10), and interpret this to be attenuation of the compressional wave through the cracked intracrystalline and intercrystalline boundaries that are abundant in the andesite. Several authors (Vinciguerra et al., 2005; Keshavarz et al., 2010; Blake et al., 2012) have also shown that the acoustic velocities can be highly attenuated by the presence of microcracks.

Second, the crack surface area and UCS have yielded an excellent correlation (Figure 4.15). As noted by Walsh, (1956 a,b), David et al. (1999), and Chaki et al. (2008), the density of cracks within a specimen is critical in determining the ultimate strength. The development of microcracks during uniaxial compression, and the coalescence of these cracks, leads to the ultimate failure of the sample (Brace et al., 1966; Bieniawski, 1967). In samples that already show relatively high crack densities, less energy is required to coalesce existing cracks and thus, they are inherently weaker specimens (David, et al., 1999; Ferrero and Marini, 2001; Keshavarz et al., 2010). By utilizing AE monitoring during our UCS testing, we observe that fewer events occur during uniaxial compression in weaker samples than those with higher strength (Figure 4.13); there are far more pre-existing cracks in the weaker samples (Hardy, 1981, Eberhardt et al., 1998; Nicksair et al., 2012). Thus, the presence of pre-existing microcracks in the Rotokawa Andesite is shown to exert a strong control on the uniaxial strength of the specimens.

Permeability is one of the most important properties of a geothermal system. In this study, we have seen that porosity (and density) and strength are related to the extent of the microcracking in the andesite. We did not measure crack surface area in the samples used for our permeability measurements (the samples will be used for future studies; calculating crack surface area required destructive thin section preparation).

However, we can, by proxy, assume a correlation between permeability and the extent of the microcracking. Numerous investigations have shown an intrinsic link between reduced acoustic velocities and increased permeability (David et al., 1999, Vinciguerra et al., 2005; Chaki et al., 2008; Nara et al., 2011; Faoro et al., 2013). While we have not measured the relationship of Sv to permeability in our dataset, we show that Sv and Vp are inversely related, and can approximate that those samples with higher crack surface areas will be inherently more permeable.

4.4.2 Empirical Fitting

4.4.2.1 Porosity and UCS

We observe a power-law correlation between sample porosity and UCS (Figure 4.18a), similar to those noted by several authors (e. g. Vernik et al, 1993; Li Li and Aubertin, 2003; Palchick and Hatzor, 2002; Kahraman et al., 2005; Chang et al., 2006; Palchick, 2013) in clastic rock and concrete materials. These authors present empirical fits to the correlation of physical properties versus UCS and show a wide range of correlation within their respective data sets with R^2 values from near 0.6 to as high as 0.95. Tugrul and Zarif (1999) developed a correlation for granitic rocks but at present, no other studies elaborate the role of porosity in direct relation to UCS in hydrothermally altered rocks. Our empirical correlations show that as the porosity of the Rotokawa Andesite increases, the strength of the material is significantly reduced (Figure 4.18a). We propose that our empirical fit (a power-law with a correlation factor of 0.82) can provide useful estimations on the strength of the reservoir rocks. By utilizing values of UCS derived from the correlation of porosity, the minimum strength of the rocks can be applied to such important engineering issues as wellbore stability (Chang et al., 2006; Schöpfer et al., 2009).

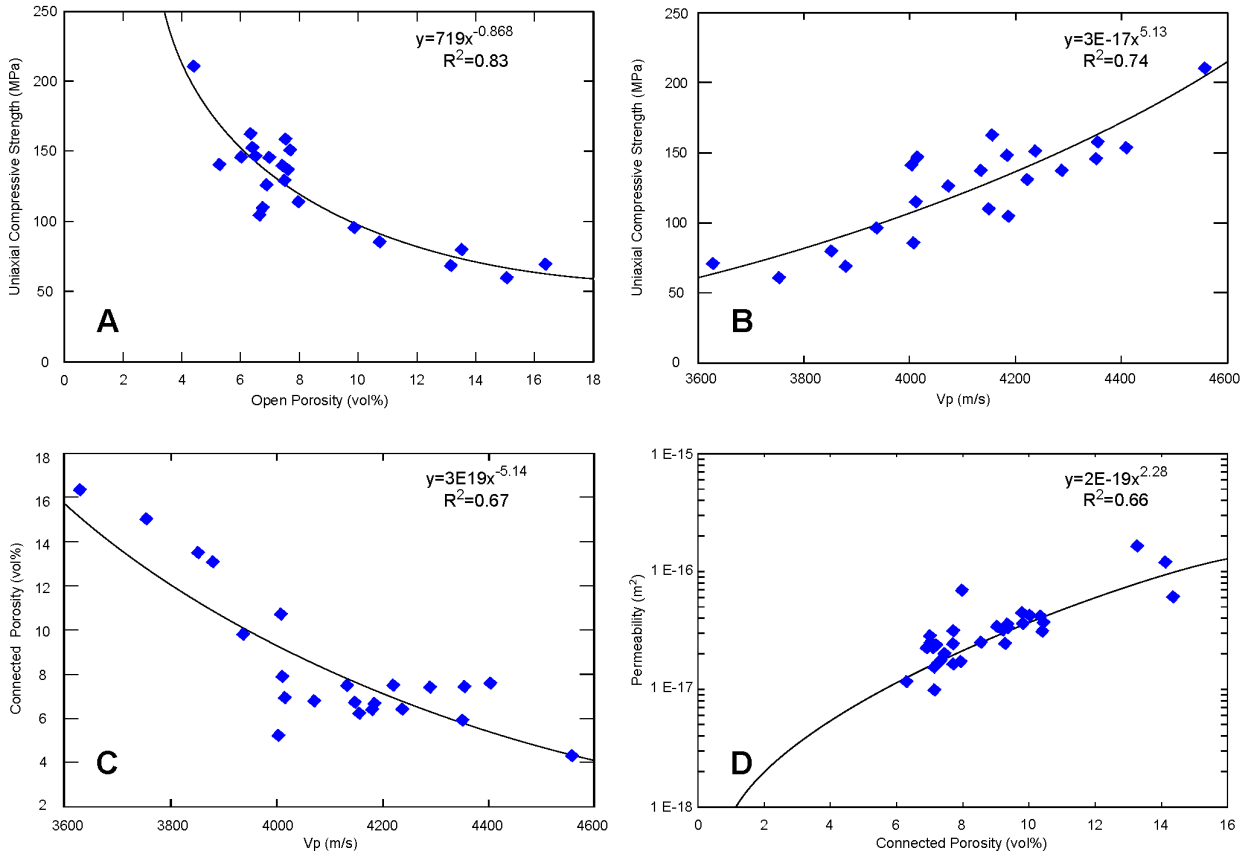

Figure 4.18: Key empirical correlations from our studies of Rotokawa Andesite. (A) Open porosity versus UCS, (B) Compressional wave velocity versus UCS, (C) Compressional wave velocity versus open porosity, (D) Connected porosity versus permeability.

4.4.2.2 Vp and UCS

We observe a power-law correlation between strength and Vp fit with an R^2 value of 0.74 (Figure 4.18b). As noted by Kahraman (2001), the relationship between Vp and UCS is generally non-linear and the higher the strength of the material, the more scattered the data points. In our study, there is an increasing trend of strength with increased Vp but, as previously presented (Figure 4.12), there is a high degree of spatial anisotropy with respect to Vp such that a perfect correlation of strength to acoustic velocity is difficult to obtain. However, Vp is a widely utilized logging tool in borehole geophysics (Chang et al., 2006) and with the correlation that we have observed, a minimum strength criteria can be established from the response of the logging tool. This is an important correlation as geophysical logging is much easier, faster and more efficient than cutting spot cores (as the core for this study was obtained) and so development of empirical correlations to constrain strength such as that seen in Figure 4.18b can help reduce risk and cost associated with geothermal drilling programs.

4.4.2.3 Vp and Porosity

Correlations of Vp and porosity show an increasing trend of porosity with decreased Vp (Figure 4.18c) (also observed by Al-Harthi et al., 1999; Rajabzadeh et al., 2011; Tugrul and Gurpinar, 1997). This can be attributed to both the pore structure distribution within the andesites and the degree of microcracking in the samples. It is clear from microstructural analysis and scanning electron microscopy that the majority of the porosity in the Rotokawa Andesites is composed of fractures and microcracks within the samples. While the microcrack distribution within the samples appear to be isotropic according to our microstructural analysis, (Table 4.2), it is possible that the microcrack networks are not equally distributed throughout the samples as evidenced by spatial attenuation of Vp (Figure 4.10) though the cracks appear to be isotropic.

An explanation for the variation and wide distribution of the data (specifically with regard to those points that fall between 4000-4400 m/s) having similar values of connected porosity is that the crack porosity and natural (vug/vesicle) porosity may interfere with the propagation of the acoustic pulse. The presence of pores can attribute to a scattering of the P-wave (Al-Harthi et al., 1999) and yields the scatter in the data range we present in Figure 4.18c. Further, the application of this relationship can give a very rough approximation for seismic velocities derived from connected porosity. This may be useful during the drilling of additional wells at Rotokawa whereby sample porosity can be measured at the wellsite and yield a rough approximation for P-wave velocities, and as such tie back to our empirical correlations of strength.

4.4.2.4 Porosity and Permeability

There is a clear trend in the Rotokawa Andesites of increasing permeability with increasing porosity, an observation also made by several authors (e.g. Heard and Page, 1982; Géraud, 1994; Stimac et al., 2004; Chaki et al., 2008; Watanabe et al., 2008). Stimac et al. (2004) showed an increasing trend of permeability with porosity in continuous core sourced from the Tiwi Geothermal Field, Philippines, and that pervasive macro-fracturing in the samples is the dominant factor in permeability. Stimac et al. (2008) further argue that geothermal reservoir system permeabilities are dominated by the presence of fractures. We also infer this to be the case in our observations as we see the porosity to be very dependent upon the presence of fractures in the samples (Figure 4.9). Our porosity measurements showed only connected pore space (i.e., pores and cracks), and as such should have a close relationship to sample permeability. The porosity has been shown to be linked to crack surface area (Figure 4.9) and as such, the higher the crack density, the more permeable the sample. However, there are two samples that display distinct macrofractures and lie outside the trend for our dataset (Figure 4.17). These specimens show higher than average permeability for their porosity, which supports the conclusions of Stimac et al. (2008) that macrofractures are critical in

controlling the permeability in the reservoir systems. On the large scale macrofractures are necessary for fluid production from geothermal reservoirs, but the microstructural characteristics of the host rocks cannot be neglected when considering fluid flow, storage capacity and total permeability of the reservoir (Jafari and Babadagli, 2011). However, we note that, at depth, the role of macrofractures quickly diminishes and the microcracks are controlling the permeability (Nara et al., 2011).

We also observe cluster of data points within the 6-8 (vol%) porosity range that show slight variation in permeability (Figure 4.17 and 4.18d). The variation in permeability within similar porosity indicates that the crack networks are not all connected; or we would see a very strong correlation of porosity and crack density to increasing permeability. We observe that our relationship between increasing porosity and permeability is fit by a power-law correlation and is consistent with the Kozeny-Carman relation (Guéguen and Palciauskas, 1994). The dependence of permeability on porosity is a natural assumption that the connected pore space provides pathways for fluid migration. The reality is however not as simple as we see in our non-linear correlation of porosity and permeability. A detailed knowledge of the connected void space geometry and their spatial distribution would be required to build a solid understanding of the sample permeability. The relationship we present in Figure 4.18d fits a power-law correlation which would indicate that the hydraulic radius of the pore space (pore and cracks) are similar in size but that the higher the concentration of cracks, the higher the permeability we observe (Bourbié and Zinszner, 1985). To take this one step further, the variation in permeability for similar values of porosity can be linked to the alignment and connectivity of the microfractures in the samples. The more tortuous the pathway for fluid migration, the lower the permeability we would observe. Similarly, there are occasional macrofractures in the samples that deviate from the rest of the dataset (black stars, Figure 4.17) and these macrofractures greatly increase permeability at a confining pressure of 2 MPa. It is possible then that the variation in permeability for samples of similar porosity is attributed to a preferential linkage of microcracks, resulting in less tortuous pathways. The correlation that we present can provide a close approximation for the permeability of the samples based on simple porosity measurements. The empirical correlation is then provided as useful for an approximation of permeability without going through the rigors of geometrical permeability modeling, which we present in the next section.

4.4.3 Application of micromechanical and geometrical permeability models

Extracting empirical relationships between laboratory-derived rock properties is certainly useful, however, the parameters are not easily related to independently measurable quantities (i.e., they lack a physical basis). Micromechanical (e.g., the wing-crack model of Ashby and Sammis, 1990) and geometrical permeability models (e.g., the Kozeny-Carman relation; Guéguen and Palciauskas, 1994) can be better-constrained as

the parameters used in such models have a clear physical meaning. In this section we attempt both sliding wing-crack modeling and Kozeny-Carman permeability modeling to investigate the microstructural controls on deformation and fluid flow, respectively.

4.4.3.1 Micromechanical Modeling

Micromechanical modelling can provide useful insights in the mechanics of compressive failure in brittle rock (Wong and Baud, 2012). Since the rocks of this study contain high microcrack densities, we will use the sliding wing-crack model of Ashby and Sammis (1990). This model idealises the rock microstructure as an elastic continuum embedded with inclined (45°) microcracks (of length 2c). These microcracks act as stress concentrators for the initiation of "wing" cracks when the frictional resistance of the closed crack is overcome and the stress at the tip of the crack exceeds the critical stress intensity factor (K_{IC}). The cracks can then propagate in the direction of the maximum principal stress. Eventually the cracks coalesce, resulting in the failure of the elastic medium. In the case of uniaxial compression, Zhu et al. (2011) derived an analytical approximation to estimate UCS:

$$UCS_p = \left(\frac{1.346}{\sqrt{1+\mu^2}-\mu}\right)\left(\frac{K_{IC}}{\sqrt{\pi c}}\right) D_0^{-0.256} \tag{4.10}$$

Where μ is the friction coefficient of the sliding crack and D_0 is an initial damage parameter. D_0 is a function of the angle of the initial microcrack with respect to the maximum principal stress and the initial number of sliding cracks per unit area (Ashby and Sammis, 1990). The analytical solution (that assumes an initial crack angle of 45°) presented above contains five parameters. We have, through experimental data and observations, a good handle on three of the parameters. First, we have measured the UCS of 22 samples (Table 4.3). Second, μ rarely deviates from 0.6-0.7 (Byerlee, 1978). Third, c can be determined from optical microscopy. One issue is that we do not have a laboratory-determined value for K_{IC}. WhileK_{IC} of andesite has been previously measured to be about 1.5 MPa·m$^{0.5}$ (Ouchterlony, 1990; Obara et al., 1992; Tutluoglu and Keles, 2011; Nara et al., 2012), there is no guarantee that this value is representative of the hydrothermally-altered Rotokawa Andesite. For this reason, we have chosen a slightly lower K_{IC} of 1.0 MPa·m$^{0.5}$ for our analysis.

Using our UCS data, we can solve Equation 4.10 to assign a value of D_0 to each experiment (using μ = 0.6; K_{IC} = 1.0; c = 0.001 m). The goal of such analysis is, assuming that the other parameters remain roughly constant between different samples/cores, to see if it is possible to estimate D_0 using an easily measured physical property, such as Vp. Our analysis shows that D_0 ranges from 0.0019 to 0.26 for the 22

measured samples (with average of 0.039). D_0 is plotted against the crack area per unit volume (Sv) and Vp in Figure 4.19b. In all cases, D_0 is higher as Sv increases (Figure 4.19A). While this may appear logical (D_0 is a function of the initial crack density), it serves as an encouraging proof of concept. Interestingly, the increase in D_0 with crack density is not linear; D_0 increases more rapidly beyond 10 mm^{-1} (Figure 4.19A).

Unfortunately, the relationship between D_0 and Vp is quite clouded (Figure 4.19B) and probably represents variable vesicle density (the model assumes that vesicles do not play a role in failure in compression) and hydrothermal alteration (K_{IC} is constant). The conclusion of this pilot analysis is that the variability within the Rotokawa Andesite is potentially too large to permit meaningful microstructural wing-crack modelling, but greater success could be achieved with laboratory-determined values for K_{IC}. Therefore, if micromechanical modelling is to be deployed as a feasible method to predict the strength of Rotokawa Andesite reservoir rocks, the samples/cores should be grouped by their alteration, and K_{IC} measured for each alteration group.

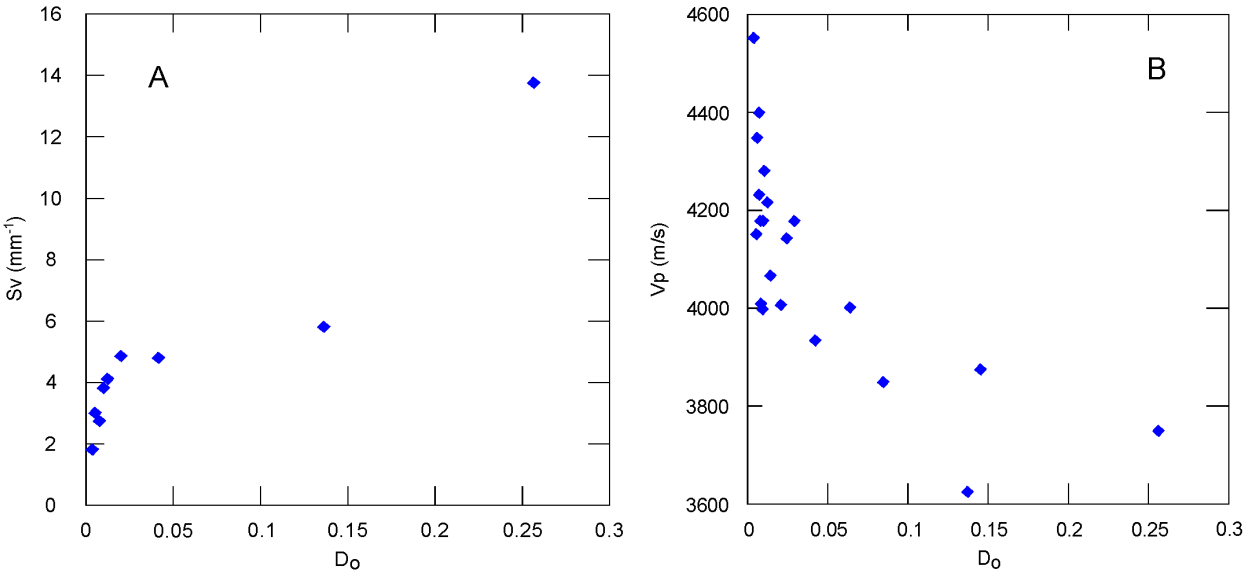

Figure 4.19: Results of Micromechanical modeling for Rotokawa Andesite (A) Initial damage parameter D_0 versus measured crack density, Sv (mm^{-1}). (B) Prediction of compressional wave velocity as a function of initial damage parameter D_0.

4.4.3.2 Permeability Modeling

Kozeny-Carman models are those that use the notion of a hydraulic radius (see Guéguen and Palciauskas, 1994). Forms of the Kozeny-Carman relation have previously been used in the study of volcanic rocks (e.g., Saar and Manga, 1999; Costa, 2006; Bernard et al., 2007), while others have used a heavily simplified version (e.g., Rust et al., 2003; Mueller et al., 2005). The Kozeny-Carman relation is of the form:

$$k_{kc} = \frac{\phi(r_H)^2}{b\tau^2} \tag{4.11}$$

Where k_{kc} is the permeability, ϕ is the connected porosity, b is a geometrical factor, τ is the tortuosity of the equivalent channel (i.e., the ratio of its actual to nominal length; tortuosity has been previously estimated through measurements of electrical conductivity), and r_H is the hydraulic radius (i.e., the volume of pores divided by the surface of the pores; specific surface area has been previously estimated with Brunauer-Emmett-Teller (BET) absorption techniques). The power law exponent for our data (excluding those samples with macrofractures) is about 2 (Figure 4.18) and is therefore consistent with the Kozeny-Carman model (Bourbié and Zinszner, 1985; Doyen, 1988). Since the entire dataset can be described by a single power law exponent, we conclude that, within our limited range of connected porosities, there is no dramatic shift in pore space connectivity or tortuosity, as was the case for Fontainebleau sandstone at a porosity of 9% (Bourbié and Zinszner, 1985) and andesite samples from Volcán de Colima at a porosity of about 11% (Heap et al., submitted to JGR). Extrapolating to porosities outside this range may be treacherous, especially to lower porosities where we may expect to encounter a switch to a higher power law exponent. However, within the dataset, the model predicts an increase in permeability by a factor of 1.5 for an increase in porosity of 1 (vol%) (an increase not uncommon for rock following a thermal stressing episode, see, for example Chaki et al., 2008).

4.4.4 Application of Results to Geothermal Exploration and Exploitation

The relationships between porosity, acoustic wave velocities, strength and permeability can be valuable in understanding fluid flow regimes in a geothermal reservoir. Our results indicate strong correlations of these parameters, similar to those observed by Stimac et al. (2004; 2008). The data we have obtained are from cores sourced from three production wells, which were very expensive to obtain, time consuming and potentially risky (Finger and Blankenship, 2010; Hole, 2013). It may be possible, using the microstructural and empirical correlations that we present that our data may be applied to new wells that are drilled in geothermal environments and help refine if our correlations hold true at the reservoir scale. The physical parameters, such as porosity and ultrasonic wave velocities, are obtainable through the use of down-hole geophysical logging suites. The empirical correlations provided in Section 4.4.2, and our models in Section 4.4.3, can then be used to predict more difficult to obtain properties such as strength and permeability from the logging tool responses. Such correlations and calibrations are quite common in the hydrocarbon industry especially during exploration drilling and it is considered that through the utilization of our dataset greater understanding can be developed of the Rotokawa reservoir.

4.5 Conclusions

1. Our study provides a comprehensive evaluation of the physical and mechanical properties of the Rotokawa Andesite through a multi-disciplinary approach. We have evaluated the Rotokawa Andesite from the microstructural to macroscopic scale and have presented robust datasets that permit the correlation and comparison of important physical properties to geothermal exploitation. Our study provides a comprehensive understanding of how the relationships of microstructural texture influence key physical properties such as strength and permeability, which are essential for the optimal utilization of a geothermal resource.

2. We have shown that the microstructure of the Rotokawa Andesite is the predominant controlling factor for physical properties and mechanical properties and is largely independent of the alteration mineralogy. Guided by a systematic understanding of the rock on the microscale we show that empirical correlations of strength and porosity can be developed and applied to field scale engineering problems. Correlations of physical parameters such as density, porosity and ultrasonic velocities to more complex properties such as strength and permeability can be paramount in exploitation of geothermal reservoirs. By utilizing geophysical logging tools after the drilling of wells to ascertain properties such as porosity, our dataset provides useful means to address complex reservoir problems.

3. We further boost our empirical correlations by applying classical physical models based on sound physical theory to predict both UCS and permeability through understanding of the microstructure. We have applied these models with some degree of success, but these models are best-suited for homogeneous, isotropic materials. Further work to constrain these models should include laboratory investigations of fracture toughness (K_{IC}) and the factors that influence this variable. However, our fit for the damage criterion D_0 is acceptable and builds the foundations for future understanding and may permit the construction of similar better-constrained models.

4. The study comprises a large dataset in the goal to further push the knowledge that can be sourced from a geothermal environment such as the Rotokawa Andesite. The properties that we have evaluated are very difficult to constrain without direct information from rocks sourced from the reservoir. Geothermal reservoirs are complex and harsh environments from which the recovery of intact core can present a significant and financially risky challenge.The results that we present here may help us to understand this complex reservoir environment by their application to field-scale engineering and geological issues.

5. Through our analyses, we have investigated several readily quantifiable and measurable physical properties of the Rotokawa Andesite. However, the dataset is not exhaustive. Further studies need to be carried out to replicate near-reservoir conditions in the laboratory, and should focus on permeability at high confining pressures and temperatures similar to those found in the reservoir. Additionally, strength measurements should be conducted under similar high-temperature environments, utilizing similar fluids to those in the reservoir.

4.6 Acknowledgements

The authors wish to thank Mighty River Power Company Ltd. for a generous grant for Paul Siratovich, which allowed collaboration with Mike Heap and Thierry Reuschlé. We also wish to thank the Rotokawa Joint Venture, a joint venture between the Tauhara North No. 2 Trust and Mighty River Power Company Ltd. for the core material used in this study. The staff of the Department of Geological Sciences at the University of Canterbury were invaluable in assisting in all aspects of this research. The Brian Mason Trust also provided for the transportation and delivery of the core to UC. The authors of this study also acknowledge a Hubert Curien Partnership (PHC) Dumont d'Urville grant (grant number 31950RK) which has assisted the France-New Zealand collaboration for this and future projects.

4.7 References

Al-Harthi, A.A., Al-Amri, R.M., Shehata, W.M., 1999. The porosity and engineering properties of vesicular basalt in Saudi Arabia. Eng. Geol. 54, 313–320.

Ashby, M.F., Sammis, C.G., 1990. The Damage Mechanics of Brittle Solids in Compression. Pure Appl. Geophys. 133, 489–521.

Barton, C.A., Zoback, M.D., Moos, D., 1995. Fluid flow along potentially active faults in crystalline rock. Geology 23, 383–383.

Bernard, M.-L., Zamora, M., Géraud, Y., Boudon, G., 2007. Transport properties of pyroclastic rocks from Montagne Pelée volcano (Martinique, Lesser Antilles). J. Geophys. Res. 112, B05205.

Bibby, H.M., Caldwell, T.G., Davey, F., Webb, T., 1995. Geophysical evidence on the structure of the Taupo Volcanic Zone and its hydrothermal circulation. J. Volcanol. Geotherm. Res. 68, 29–58.

Bieniawski, Z.T., 1967. Mechanism of Brittle Fracture of Rock Part II - Experimental Studies. Int. J. Rock Mech. Min. Sci. 4, 407–423.

Blake, O.O., Faulkner, D.R., Rietbrock, a., 2012. The Effect of Varying Damage History in Crystalline Rocks on the P- and S-Wave Velocity under Hydrostatic Confining Pressure. Pure Appl. Geophys. 170, 493–505.

Bloomberg, S., Rissmann, C., Mazot, A., Oze, C., Horton, T., Kennedy, B., Werner, C., Christenson, B., Pawson, J., 2012. Soil Gas Flux Exploration At The Rotokawa Geothermal Field And White Island , New Zealand, in: Proceedings, Thirty Sixth Workshop on Geothermal Reservoir Engineering. p. 11.

Bourbie, T., Zinszner, B., 1985. Hydraulic and acoustic properties as a function of porosity in Fontainebleau sandstone. J. Geophys. Res. 90, 11524–11532.

Brace, W.F. and Bombolakis, E.G., 1963. A note on brittle crack growth in compression. J. Geophys. Res. 68, 3709–3713.

Brace, W.F., Paulding, B., Scholz, C., 1966. Dilatancy in the fracture of crystalline rocks. J. Geophys. Res. 71, 3939–3953.

Brace, W.F., Walsh, J.B., Frangos, W.T., 1968. Permeability of granite under high pressure. J. Geophys. Res. 73, 2225–2236.

Byerlee, J.D., 1978. Friction of rocks. Pure Appl. Geophys. 116, 615–626.

Chaki, S., Takarli, M., Agbodjan, W.P., 2008. Influence of thermal damage on physical properties of a granite rock: Porosity, permeability and ultrasonic wave evolutions. Constr. Build. Mater. 22, 1456–1461.

Chang, C., Zoback, M.D., Khaksar, A., 2006. Empirical relations between rock strength and physical properties in sedimentary rocks. J. Pet. Sci. Eng. 51, 223–237.

Cole, J.W., 1990. Structural control and origin of volcanism in the Taupo volcanic zone, New Zealand. Bull. Volcanol. 52, 445–459.

Collar, R.J., Browne, P.R.L., 1985. Hydrothermal Eruptions at The Rotokawa Geothermal Field, Taupo Volcanic Zone, New Zealand, in: Proceedings 7th NZ Geothermal Workshop. p. 5.

Costa, A., 2006. Permeability-porosity relationship: A reexamination of the Kozeny-Carman equation based on a fractal pore-space geometry assumption. Geophys. Res. Lett. 33, L02318.

David, C., Menendez, B., Darot, M., 1999. Influence of stress-induced and thermal cracking on physical properties and microstructure of La Peyratte granite. Int. J. Rock Mech. Min. Sci. 36, 433–448.

Diamantis, K., Gartzos, E., Migiros, G., 2009. Study on uniaxial compressive strength, point load strength index, dynamic and physical properties of serpentinites from Central Greece: Test results and empirical relations. Eng. Geol. 108, 199–207.

Diederichs, M.., Kaiser, P.., Eberhardt, E., 2004. Damage initiation and propagation in hard rock during tunnelling and the influence of near-face stress rotation. Int. J. Rock Mech. Min. Sci. 41, 785–812.

DiPippo, R., 2008. Geothermal Power Plants: Principles, Applications, Case Studies and Environmental Imapc, 2nd ed. Elsevier Ltd, Oxford, UK.

Doyen, P.M., 1988. Permeability, conductivity, and pore geometry of sandstone. J. Geophys. Res. 93, 7729–7740.

Eberhardt, E., Stead, D., Stimpson, B., Read, R.S., 1998. Identifying crack initiation and propagation thresholds in brittle rock. Can. Geotech. J. 35, 222–233.

Faoro, I., Vinciguerra, S., Marone, C., Elsworth, D., Schubnel, a., 2013. Linking permeability to crack density evolution in thermally stressed rocks under cyclic loading. Geophys. Res. Lett. 40, 2590–2595.

Ferrero, A.M., Marini, P., 2001. Experimental Studies on the Mechanical Behaviour of two Thermal Cracked Marbles. Rock Mech. Rock Eng. 34, 57–66.

Finger, J., Blankenship, D., 2010. Handbook of Best Practices for Geothermal Drilling. Sandia National Laboratories, Albuquerque.

Fredrich, J.T., Wong, T., 1986. Micromechanics of Thermally Induced Cracking in Three Crustal Rocks. J. Geophys. Res. 91, 12743–12764.

Géraud, Y., 1994. Variations of connected porosity and inferred permeability in a thermally cracked granite. Geophys. Res. Lett. 21, 979–982.

Grant, M.A., Bixley, P.F., 2011. Geothermal Reservoir Engineering, 2nd ed. Elsevier Science Ltd, Oxford, UK.

Guéguen, Y., Schubnel, a., 2003. Elastic wave velocities and permeability of cracked rocks. Tectonophysics 370, 163–176.

Guéguen, Y. and Palciauskas, V., 1994. Introduction to the Physics of Rocks. Princeton University Press, Princeton, New Jersey.

Gupta, H., Roy, S., 2006. Geothermal Energy: An Alternative Resource for the 21st Century, First. ed. Elsevier B.V., Oxford, UK.

Hardy, H., 1981. Applications of acoustic emission techniques to rock and rock structures: a state of the art review, in: In: Drnevich, G. (Ed) Acoustic Emission in Geotechnical Engineering Practice. ASTM STP 750. pp. 4–92.

Heap, M.J., Faulkner, D.R., 2008. Quantifying the evolution of static elastic properties as crystalline rock approaches failure. Int. J. Rock Mech. Min. Sci. 45, 564–573.

Heap, M.J., Mollo, S., Vinciguerra, S., Lavallée, Y., Hess, K., Dingwell, D.B., Baud, P., Iezzi, G., 2013. Thermal weakening of the carbonate basement under Mt . Etna volcano (Italy): Implications for volcano instability. J. Volcanol. Geotherm. Res. 250, 42–60.

Heap, M.J., Vinciguerra, S., Meredith, P.G., 2009. The evolution of elastic moduli with increasing crack damage during cyclic stressing of a basalt from Mt. Etna volcano. Tectonophysics 471, 153–160.

Heap. M.J., Lavallee, Y., Petrakova, L., Baud, P., Reushcle, T., Varley, N.R., Dingwell, D.B., 2014. Microstructural controls on the physical and mechanical properties of edifice-forming andesites at Volcán de Colima, Mexico. J. Geophys. Res. Submitted.

Heard, H.C., Page, L., 1982. Elastic Moduli , Thermal Expansion , and Inferred Permeability of Two Granites to 350øC and 55 Megapascals. J. Geophys. Res. 87, 9340–9348.

Hedenquist, J.W., Mroczek, E.K., Giggenback, W.F., 1988. Geochemistry of the Rotokawa geothermal system: Summary of data, interpretation and appraisal for energy development., in: Chemistry Division DSIR Technical Note 88/6, September. p. 63.

Hickman, S., Zoback, M., Benoit, R., 1998. Tectonic controls on reser- voir permeability in the Dixie Valley, Nevada, geothermal field, in: Proceedings Twenty-Third Workshop on Geothermal Reservoir Engineering, Stanford Univeristy, California, January 26-28.

Hole, H.M., 2013. Geothermal Drilling- Keep it simple. Proc. 35th New Zeal. Geotherm. Work. Rotorua, New Zealand, Novemb. 17-20.

Horie, T., Muto, T., 2010. The Worlds Largest single cylinder Geothermal Power Generation Unit - Nga Awa Purua Geothermal Power Station, New Zealand, in: GRC Transactions Vol. 34. pp. 1039–1044.

Jafari, A., Babadagli, T., 2011. Effective fracture network permeability of geothermal reservoirs. Geothermics 40, 25–38.

Jaya, M.S., Shapiro, S. a., Kristinsdóttir, L.H., Bruhn, D., Milsch, H., Spangenberg, E., 2010. Temperature dependence of seismic properties in geothermal rocks at reservoir conditions. Geothermics 39, 115–123.

Ju, Y., Asce, A.M., Yang, Y., Peng, R., Mao, L., 2013. Effects of Pore Structures on Static Mechanical Properties of Sandstone. J. Geotech. Geoenvironmental Eng. 139, 1745–1755.

Kahraman, S., 2001. Evaluation of simple methods for assessing the uniaxial compressive strength of rock. Int. J. Rock Mech. Min. Sci. 38, 981–994.

Kahraman, S., Gunaydin, O., Fener, M., 2005. The effect of porosity on the relation between uniaxial compressive strength and point load index. Int. J. Rock Mech. Min. Sci. 42, 584–589.

Keshavarz, M., Pellet, F.L., Loret, B., 2010. Damage and Changes in Mechanical Properties of a Gabbro Thermally Loaded up to 1,000°C. Pure Appl. Geophys. 167, 1511–1523.

Klinkenberg, L.J., 1941. The permeability of porous media to luquids and gases. Am. Pet. Institute, Drill. Prod. Pract. 200–213.

Kristinsdóttir, L.H., Flóvenz, Ó.G., Árnason, K., Bruhn, D., Milsch, H., Spangenberg, E., Kulenkampff, J., 2010. Electrical conductivity and P-wave velocity in rock samples from high-temperature Icelandic geothermal fields. Geothermics 39, 94–105.

Krupp, R.E., Seward, T.M., 1987. The Rotokawa geothermal system, New Zealand; an active epithermal gold-depositing environment. Econ. Geol. 82, 1109–1129.

Legmann, H., Sullivan, P., 2003. The 30 MW Rotokawa I geothermal project five years of operation, in: International Geothermal Conference, Reykjavik, Sept. pp. 26–31.

Li, L., Aubertin, M., 2003. A general relationship between porosity and uniaxial strength of engineering materials. Can. J. Civ. Eng. 30, 644–658.

Lim, S.S., Martin, C.D., Åkesson, U., 2012. In-situ stress and microcracking in granite cores with depth. Eng. Geol. 147-148, 1–13.

Lion, M., Skoczylas, F., Ledésert, B., 2005. Effects of heating on the hydraulic and poroelastic properties of bourgogne limestone. Int. J. Rock Mech. Min. Sci. 42, 508–520.

Luping, T., 1986. A study of the quantitative relationship between strength and pore-size distribution of proous materials. Cem. Concr. Res. 16, 87–96.

Lutz, S.J., Hickman, S., Davatzes, N., Zemach, E., Drakos, P., 2010. Rock Mechanical Testing and Petrologic Analysis in Support of Well Stimulation Activities at the Desert Peak Geothermal Field, Nevada, in: Proceedings, Thirty-Fifth Workshop on Geothermal Reservoir Engineering. Stanford University, Stanford, California, February 1-3, p. 11.

Martin, C.D., 1993. The Strength of Massive Lac du Bonnet Granite Around Underground Openings. University of Manitoba.

Martin, C.D., Chandler, N.A., 1994. The progressive fracture of Lac du Bonnet granite. Int. J. Rock Mech. Min. Sci. 31, 643–659.

Martínez-Martínez, J., Benavente, D., García-del-Cura, M. a., 2011. Spatial attenuation: The most sensitive ultrasonic parameter for detecting petrographic features and decay processes in carbonate rocks. Eng. Geol. 119, 84–95.

Massiot, C., Mcnamara, D., Lewis, B., Price, L., Bignall, G., 2012. Statistical Corrections of Fracture Sampling Bias in Boreholes from Acoustic Televiewer Logs, in: New Zealand Geothermal Workshop Proceedings.

Mueller, S., Melnik, O., Spieler, O., 2005. Permeability and degassing of dome lavas undergoing rapid decompression: An experimental determination. Bull. Volcanol. 67, 526–538.

Nara, Y., Meredith, P.G., Yoneda, T., Kaneko, K., 2011. Influence of macro-fractures and micro-fractures on permeability and elastic wave velocities in basalt at elevated pressure. Tectonophysics 503, 52–59.

Nara, Y., Morimoto, K., Hiroyoshi, N., Yoneda, T., Kaneko, K., Benson, P.M., 2012. Influence of relative humidity on fracture toughness of rock: Implications for subcritical crack growth. Int. J. Solids Struct. 49, 2471–2481.

Nicksiar, M., Martin, C.D., 2012. Evaluation of Methods for Determining Crack Initiation in Compression Tests on Low-Porosity Rocks. Rock Mech. Rock Eng. 45, 607–617.

Obara, Y., Sakaguchi, K., Nakayama, T., Sugawara, K., 1992. Anisotropy effect on fracture toughness of rocks. Int. J. Rock Mech. Min. Sci. Geomech. Abstr. 30, 137.

Ouchterlony, F., 1990. Fracture toughness testing of rock with core based specimens. Eng. Fract. Mech. 35, 351–366.

Palchik, V., 2013. Is there Link between the Type of the Volumetric Strain Curve and Elastic Constants, Porosity, Stress and Strain Characteristics? Rock Mech. Rock Eng. 46, 315–326.

Palchik, V., Hatzor, Y.H., 2002. Crack damage stress as a composite function of porosity and elastic matrix stiffness in dolomites and limestones. Eng. Geol. 63, 233–245.

Pereira, J.-M., Arson, C., 2013. Retention and permeability properties of damaged porous rocks. Comput. Geotech. 48, 272–282.

Pola, A., Crosta, G., Fusi, N., Barberini, V., Norini, G., 2012. Influence of alteration on physical properties of volcanic rocks. Tectonophysics 566-567, 67–86.

Quinao, J., Sirad-azwar, L., Clearwater, J., Hoepfinger, V., Le Brun, M., Bardsley, C., 2013. Analyses and Modeling of Reservoir Pressure Changes to Interpret the Rotokawa Geothermal Field Response to Nga Awa Purua Power Station Operation, in: Proceedings 38th Workshop on Geothermal Reservoir Engineering. Stanford University, Stanford, California, February 11-13, p. 10.

Rae, A., 2007. Rotokawa Geology and Geophysics. GNS Science Consultancy Report 2008/83.

Rae, A.J., McCoy-West, A.J., Ramirez, L.E., Alcaraz, S.A., 2009. Geology of Production Well RK28 , Rotokawa Geothermal Field, GNS Science Consultancy Report 2009/253.

Rae, A.J., McCoy-West, A.J., Ramirez, L.E., McNamara, D., 2010. Geology of Production Wells RK30L1 and RK30L2 Rotokawa Geothermal Field, GNS Science Consultancy Report 2010/02.

Rajabzadeh, M. a., Moosavinasab, Z., Rakhshandehroo, G., 2011. Effects of Rock Classes and Porosity on the Relation between Uniaxial Compressive Strength and Some Rock Properties for Carbonate Rocks. Rock Mech. Rock Eng. 45, 113–122.

Ramirez, L.E., Hitchcock, D., 2010. Geology of Production Well RK27L2 , Rotokawa Geothermal Field, GNS Science Consultancy Report 2010/100.

Reuschlé, T., Gbaguidi Haore, S., Darot, M., 2006. The effect of heating on the microstructural evolution of La Peyratte granite deduced from acoustic velocity measurements. Earth Planet. Sci. Lett. 243, 692–700.

Richter, D., Simmons, G., 1977. Microcracks in crustal igneous rocks: microscopy, in: Heacock, J.G., Keller, G.V., Oliver, J.E., Simmons, G. (Ed.), The Earth's Crust. American Geophysical Union, Washington, DC, pp. 149–180.

Rowland, J. V., Sibson, R.H., 2004. Structural controls on hydrothermal flow in a segmented rift system, Taupo Volcanic Zone, New Zealand. Geofluids 4, 259–283.

Rowland, J. V., Wilson, C.J.N., Gravley, D.M., 2010. Spatial and temporal variations in magma-assisted rifting, Taupo Volcanic Zone, New Zealand. J. Volcanol. Geotherm. Res. 190, 89–108.

Rust, A.C., Manga, M., Cashman, K. V, 2003. Determining Flow type , shear rate and shear stress in magmas from bubble shapes and orientations. J. Volcanol. Geotherm. Res. 122, 111–132.

Rutter, E.H., 1986. On the nomenclature of mode of failure transitions in rocks. Tectonophysics 122, 381–387.

Saar, M.O., Manga, M., 1999. Permeability-porosity relationship in vesicular basalts. Geophys. Res. Lett. 26, 111–114.

Schöpfer, M.P.J., Abe, S., Childs, C., Walsh, J.J., 2009. The impact of porosity and crack density on the elasticity, strength and friction of cohesive granular materials: Insights from DEM modelling. Int. J. Rock Mech. Min. Sci. 46, 250–261.

Sewell, S.M., Cumming, W.B., Azwar, L., Bardsley, C., 2012. Integrated MT and Natural State Temperature Interpretation for a Conceptual Model Supporting Reservoir Numerical Modelling and Well Targeting at the Rotokawa Geothermal Field, New Zealand, in: Proceedings: Thirty-Seventh Workshop on Geothermal Reservoir Engineering. Stanford University, Stanford California, p. 8.

Smith, R., Sammonds, P.R., Kilburn, C.R.J., 2009. Fracturing of volcanic systems: Experimental insights into pre-eruptive conditions. Earth Planet. Sci. Lett. 280, 211–219.

Sousa, L.M.O., Suárez del Río, L.M., Calleja, L., Ruiz de Argandoña, V.G., Rey, A.R., 2005. Influence of microfractures and porosity on the physico-mechanical properties and weathering of ornamental granites. Eng. Geol. 77, 153–168.

Stanchits, S., Vinciguerra, S., Dresen, G., 2006. Ultrasonic Velocities, Acoustic Emission Characteristics and Crack Damage of Basalt and Granite. Pure Appl. Geophys. 163, 975–994.

Stimac, J. A., Powell, T.S., Golla, G.U., 2004. Porosity and permeability of the Tiwi geothermal field, Philippines, based on continuous and spot core measurements. Geothermics 33, 87–107.

Stimac, J., Nordquist, G., Suminar, A., Sirad-Azwar, L., 2008. An overview of the Awibengkok geothermal system, Indonesia. Geothermics 37, 300–331.

Takarli, M., Prince, W., Siddique, R., 2008. Damage in granite under heating/cooling cycles and water freeze thaw condition. Int. J. Rock Mech. Min. Sci. 45, 1164–1175.

Tugrul, A., Zarif, I.H., 1999. Correlation of mineralogical and textural characteristics with engineering properties of selected granitic rocks from Turkey. Eng. Geol. 51, 303–317.

Tugrul, A., Gurpinar, O., 1997. The effect of chemical weathering on the engineering properties of Eocene basalts in northeastern Turkey. Environ. Eng. Geosci. 3, 225–234.

Tutluoglu, L., Keles, C., 2011. Mode I fracture toughness determination with straight notched disk bending method. Int. J. Rock Mech. Min. Sci. 48, 1248–1261.

Ulusay, R. and Hudson, J., 2007. The Complete ISRM Suggested Methods for Rock Characterization, Testing and Monitoring: 1974-2006, 1974th–2006th ed. Elsevier, Antalya, Turkey.

Underwood, E.E., 1970. Quantitative Stereology for Microstructural Analysis, in: Quantitative Stereology. Addison-Wesley Pub. Co., Reading, Massachusets, p. 274.

Vernik, L., Bruno, M., Bovberg, C., 1993. Empirical relations between compressive strength and porosity of siliciclastic rocks. Int. J. Rock Mech. Min. Sci. Geomech. Abstr. 30, 677–680.

Vinciguerra, S., Trovato, C., Meredith, P., Benson, P., 2005. Relating seismic velocities, thermal cracking and permeability in Mt. Etna and Iceland basalts. Int. J. Rock Mech. Min. Sci. 42, 900–910.

Walsh, J.B., 1965a. The Effect of Cracks on the Compressibility of Rock. J. Geophys. Res. 70.

Walsh, J.B., 1965b. The Effect of Cracks in Rocks on Poisson's Ratio. J. Geophys. Res. 70, 5249–5257.

Wang, H.F., Bonner, B.P., Carlson, S.R., Kowallis, B.J., Heard, H.C., 1989. Thermal Stress Cracking in Granite. J. Geophys. Res. 94, 1745.

Watanabe, T., Shimizu, Y., Noguchi, S., Nakada, S., 2008. Permeability measurements on rock samples from Unzen Scientific Drilling Project Drill Hole 4 (USDP-4). J. Volcanol. Geotherm. Res. 175, 82–90.

Wilson, C.J.N., Houghton, B.F., Mcwilliams, M.O., Lanphere, M.A., Weaver, S.D., Briggs, R.M., 1995. Volcanic and structural evolution of Taupo Volcanic Zone , New Zealand: a review. J. Volcanol. Geotherm. Res. 68, 1–28.

Wong, T.F., Baud, P., 2012. The brittle-ductile transition in porous rock: A review. J. Struct. Geol. 44, 25–53.

Wu, X.Y., Baud, P., Wong, T., 2000. Micromechanics of compressive failure and spatial evolution of anisotropic damage in Darley Dale sandstone. Int. J. Rock Mech. Min. Sci. 37, 143–160.

Zhu, W., Baud, P., Vinciguerra, S., Wong, T., 2011. Micromechanics of brittle faulting and cataclastic flow in Alban Hills tuff. J. Geophys. Res. 116, 1–23.

Chapter 5

Thermoelastic Properties of the Rotokawa Andesite

P.A. Siratovich[a], Y. Lavallée[b], F. von Aulock[b], J. Cole[a], B. Kennedy, M. Villeneuve[a]

[a]Department of Geological Sciences, University of Canterbury, Private Bag 4800, Christchurch 8140, New Zealand

[b]Department of Earth, Ocean and Ecological Sciences, School of Environmental Sciences, University of Liverpool, United Kingdom

To be submitted to the *Journal of Volcanology and Geothermal Research.*

Abstract

Thermal properties of geothermal reservoir rocks are essential to constraining important engineering concerns such as wellbore stability, reservoir forecasting and stimulation procedures. To better constrain these properties in the reservoir, thermal property measurements were carried out on samples recovered from the Rotokowa Andesite geothermal reservoir, located in the Taupo Volcanic Zone, New Zealand. In particular, measurements of linear thermal expansion, thermogravimetric analysis, and differential scanning calorimetry were measured utilizing varied experimental heating rates of 2, 5 and 20 K/min. The property analyses were carried out to determine if heating rates influenced the measurement of thermal properties, specifically thermal expansion coefficients and strain rate in the samples. Our results indicate that thermal expansion is not heating rate dependent within the range investigated though the strain rate is significantly dependent on heating rate, with higher strain rates observed in conjunction with higher heating rates. We also investigated whether microcracking or decrepitation of fluid inclusions may be exacerbated by high heating rates, but showed no rate dependence. We incorporated results of tensile strength testing on the Rotokawa Andesite

to apply our thermal property measurements to a thermal stress model. By using a one dimensional stress model, we built a failure criterion for the Rotokawa Andesite when subject to thermal stressing and resultant thermal stress. The importance of this study is to further understand the critical heating and cooling rates at which thermal stress causes cracking within the Rotokawa reservoir. Thermal stress cracking in the Rotokawa reservoir can be used to enhance permeability but can also affect wellbore stability, so constraining these conditions can be beneficial to resource utilization.

Keywords: thermal expansion coefficient, geothermal, thermal stress, thermomechanical analysis, simultaneous thermal analysis

5.1 Introduction

A sound knowledge of how rocks respond to induced or natural thermal gradients is essential to predicting the onset of thermal cracking which can lead to degradation of strength and an increase in permeability. Detailed studies on the conditions that constrain the onset of thermal cracking in a geothermal reservoir is essential for the optimal utilization of the resource, wellbore stability considerations, reservoir forecasting and stimulation procedures (Zoback et al., 2003). To further this understanding in a geothermal reservoir, it is necessary to quantify the thermal properties of the reservoir rocks. The Rotokawa Andesite is the main geothermal reservoir rock at the Rotokawa geothermal field and served as the source material for this study.

The optimization of a high-enthalpy geothermal energy project is highly dependent on the natural permeability of the system (Grant and Bixley, 2011). However, the perturbation of the natural state of the reservoir by drilling and extraction of heat and fluids changes the dynamics of the reservoir with respect to pressure and temperature (Ghassemi and Zhang, 2004). With change in temperature, the host rocks of the reservoir are subject to thermal gradients which can subsequently cause thermal cracking. Such thermal gradients can arise from drilling fluids interacting with hot reservoir rocks, drawdown of reservoir fluids leading to cooling, and the injection of spent reservoir fluids for pressure maintenance and to enhance permeability by thermally induced cracks. These cracks may lead to the increase of permeability of the well over both short and long time scales (Axelsson and Thorhallsson, 2009; Grant et al., 2013). The introduction of cold fluids has been well documented to re-open and enhance already existing fractures and to also induce the formation of new fractures (Kitao et al., 1990; Flores-Armenta and Tovar-Aguado, 2008; Axelsson and Thórhallsson, 2009).

There is a direct correlation between the development of thermal cracks in rocks and heating and cooling (Simmons and Cooper, 1978; Finnie et al., 1979, Homande-Etienne and Troalen, 1984, David et al., 1999).

The effect of thermal cracking on rocks can attenuate acoustic velocities (Vinciguerra et al., 2005; Fortin et al., 2011; Heap et al., 2013a), increase porosity (Bauer and Handin, 1983; David et al., 1999; Chaki et al., 2008), increase permeability as a result of microcracking (Heard and Page, 1982; Darot et al., 1992, Fortin et al., 2011, Nara et al., 2011; Faoro et al., 2013), degrade strength (Balme et al., 2004; Keshavarz et al., 2010, Patel et al., 2013; Heap et al., 2013b), and have a significant influence on thermal expansion coefficients (Cooper and Simmons, 1977; Lo and Wai, 1982; Lin, 2002).

Thermal cracking in rock is attributed to several processes: the mis-matched thermal expansion of minerals, heterogeneous heating rates, anisotropic thermal diffusion of mineral species, and the bursting of fluid inclusions (e.g. Cooper and Simmons, 1977; Wong and Brace, 1979; Lo and Wai, 1982, Keshavarz et al., 2010). Lin (2002) identified that the decrepitation of fluid inclusions from quartz crystals generated microcracks in samples of Inanda Granite. This work complemented the earlier conclusions presented by Hall and Bodnar (1989) that correlated acoustic emissions (AE) to cracks induced by the decrepitation of fluid inclusions from Westerly Granite.

Several authors have described the effect of porosity on thermal expansion coefficients. Richter and Simmons (1974) published one of the classical papers on thermal expansion and concluded that thermal expansion can be predicted at low heating rates by the mineral components of the rocks and that above 2^{o}C/min thermal cracks form in specimens that affect the whole rock thermal expansion coefficient. Additionally, they showed that microcrack porosity has an inverse effect on the thermal expansion coefficients. In a subsequent study, Cooper and Simmons (1977) showed that with increasing temperature the severity of thermal cracking increases. They also showed that the presence of cracks can provide void space into which mineral species can expand, accommodating differential expansion.

Cooper and Simmons (1977) defined the coefficient of thermal expansion in any direction as:

$$\alpha_{ij} = \delta\epsilon_{ij}/\delta T \tag{5.1}$$

Where $\delta\epsilon$ is change in strain, δT is change in temperature and α_{ij} is the coefficient of linear thermal expansion.

This was derived to a third- order polynomial whose solution is defined as:

$$\alpha = \frac{1}{L} * (\frac{dL}{dT}) \tag{5.2}$$

where L=the reference length of the sample at temperature T_0, dL= the difference in length of the sample at temperature T_1 and $dT = T_1 - T_0$.

The solution then provides the basis for which linear thermal expansion can be derived at any given temperature from analysis of the change in sample length based on the reference length of the sample.

The role of thermal expansion in thermoelastic stress is classically given by Timoshenku and Goodier (1970) such that thermal stress can be simplified and calculated by the following relation:

$$\sigma_t = \frac{\alpha E \Delta T}{(1-\nu)} \tag{5.3}$$

where σ_t=tensile thermal stress (MPa) α = linear thermal expansion coefficient, E =Young's modulus (GPa), ΔT= temperature differential, ν = Poisson's Ratio. By utilizing this formula, we can derive the instantaneous stress that a plane will experience as a result of an induced temperature differential. From this, we can approximate the amount of mechanical stress that can be manifest on a rock body by thermal stress.

In this paper, we quantified the thermal properties of the Rotokawa Andesite from thermomechanical analysis (TMA), differential scanning calorimetry (DSC), thermogravimetric analysis (TG), porosity and density studies, and develop an understanding of the constraints by which thermal stress may be manifest on rocks of the Rotokawa Andesite. The collected data are used in conjunction with previous studies of physical properties of the andesite to build models to predict the thermal expansion. These data are then applied to the classical model of thermoelastic stress (Timoshenku and Goodier, 1970) to investigate potential responses of the Rotokawa Andesite to induced thermal gradients.

5.2 Materials and Methods

5.2.1 Source Material: Rotokawa Andesite

The Rotokawa geothermal field is located in the Taupo Volcanic Zone, North Island, New Zealand (Figure 5.1a) and provides the working fluid used within two commercial-scale power plants. The geothermal resource is hosted in andesite lavas and breccias of the Rotokawa Andesite. This reservoir fluids are typically two-phase with reservoir temperatures of 225-330^{o}C with observed reservoir pressures of 150-250 bar(g) (Quinao et al., 2013).

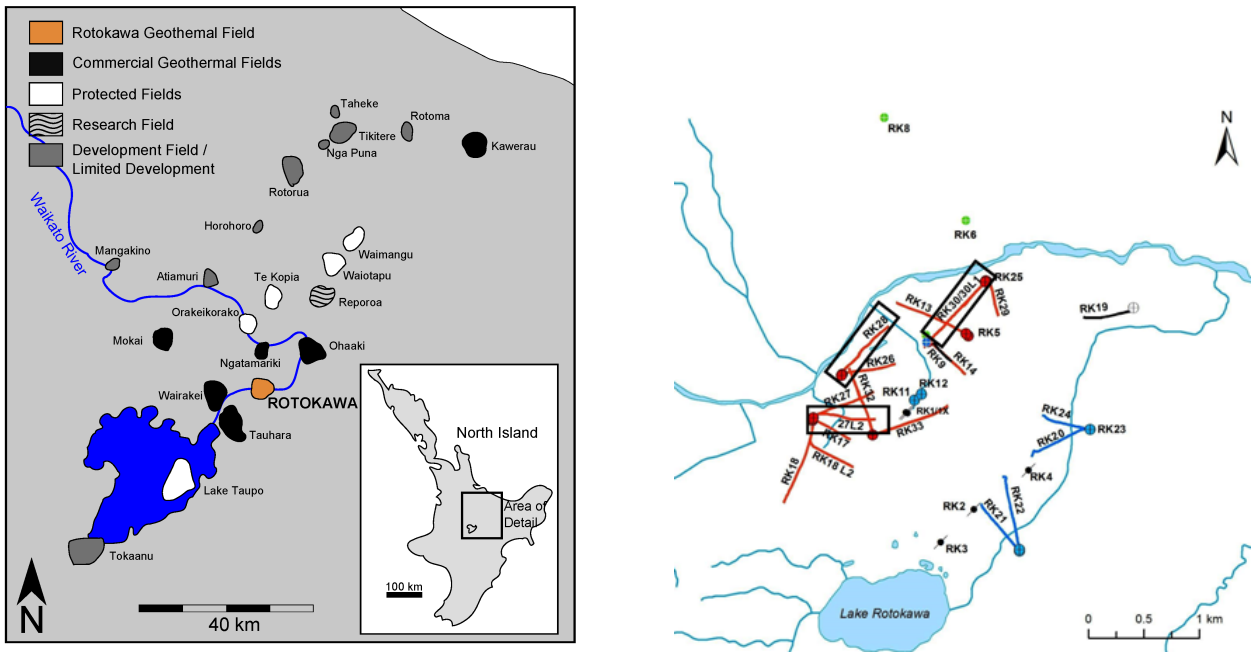

Figure 5.1: (A) Taupo Volcanic Zone and location of Rotokawa Geothermal Field, Central North Island, New Zealand (Adapted from Sewell et al., 2012). (B) Wells of The Rotokawa Geothermal Field. Wells highlighted with boxes are the source of core used in this study.

Spot cores of Rotokawa Andesite were taken during the drilling of the three production wells seen in Figure 5.1b: RK28, RK30 and RK27L2 (a well from which two bores were drilled from one surface location). The Rotokawa Andesite consists of brecciated porphyritic andesite lava with a primary mineralogy of plagioclase phenocrysts and pyroxenes set in a fine-grained groundmass. Some phenocrysts are weakly flow oriented and show evidence of brittle mechanical deformation such that many are pervasively cracked or shattered. The Rotokawa Andesite is also intensely hydrothermally altered and includes an assemblage of secondary minerals such as: calcite, adularia, chlorite, quartz, epidote, hematite, leucoxene, and pyrite. The plagioclase phenocrysts are relatively in-tact but partial replacement of quartz and calcite is apparent. Occasional amydgdales are present, typically filled with chlorite and rimmed with quartz and calcite (See Chapter 4 of this volume and Rae et al., 2009; 2010; Ramirez and Hitchcock, 2010).

5.2.2 Sample Preparation

Original cores of Rotokawa Andesite (from the same depths and orientations as detailed in Chapter 4) were cut into blocks and relevant core orientations noted as X, Y and Z; with the Z direction being along the

length of the wellbore and X, Y perpendicular to the orientation of the well. Density, and porosity were determined using the triple weight method (Ulusay and Hudson, 2007).

At the University of Liverpool (UL) a series of samples were prepared for thermomechanical analysis (TMA) by drilling cylinders of 6 mm diameter and 5 mm in length cut from the core blocks. The samples were then washed in an ultrasonic bath for 2 minutes and dried in a laboratory oven at 105^{o}C until constant mass was recorded and held in a dessicator prior to testing. A representative series of these samples were then analyzed for porosity and density properties using and Accu-Pyc helium pycnometer.

Samples were also selected for simultaneous thermal analysis (STA) that were milled into discs from off-cuts of the specimens used for TMA. These were ground to discs approximately 1mm in thickness. The samples were similarly washed in an ultrasonic bath for 2 minutes, oven dried at 105^{o}C, weighed and held in a dessicator until testing.

5.2.3 Thermophysical Measurements

Linear thermal expansion (TE) and strain were measured at UL using a Netzch TMA 402 F1 Hyperion Thermomechanical Analyzer (TMA). Multiple heating, cooling and load cycles are possible with the device of up to 1200^{o}C and sample loads ranging from 3mN to 3N. A high precision inductive linear displacement transducer (LVDT) measures the change in length of the sample with a resolution of 0.125 nm.

An illustrated schematic of the TMA is seen in Figure 5.2.

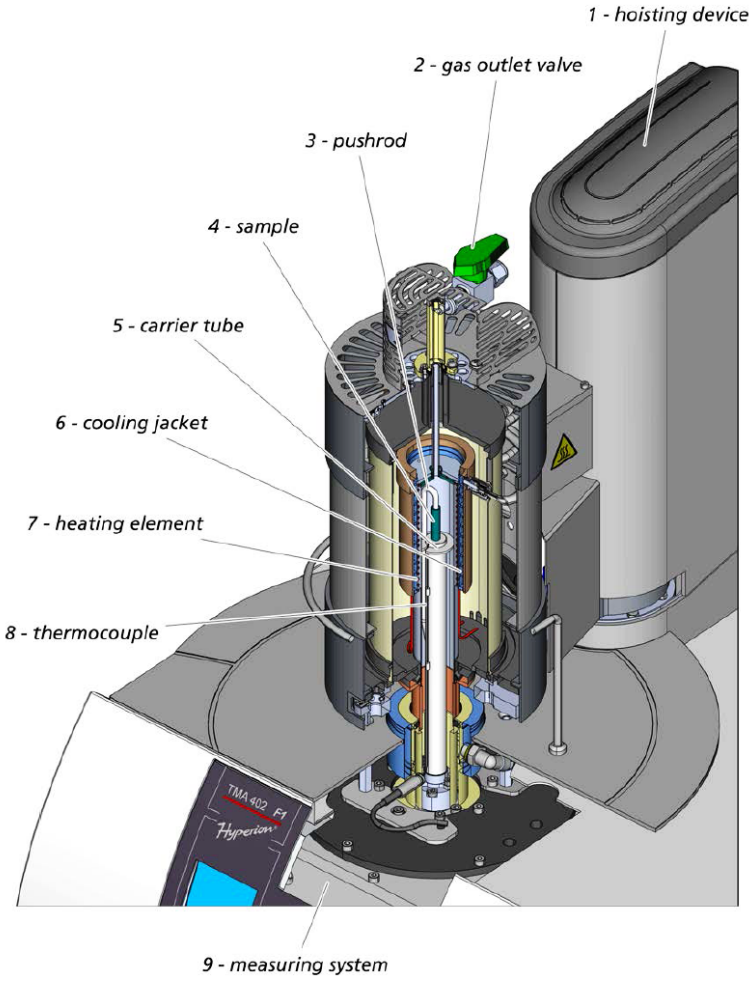

Figure 5.2: Schematic of NETZSCH TMA 402 F1 Hyperion (modified from NETZSCH, 2012a)

In order to quantify the thermal expansion coefficients, a known standard of alumina (Al_2O_3) of the same geometry as the samples to be analyzed is utilized. The alumina standard is then used as a baseline for determining the thermo-mechanical behavior of the unknown samples as system components are also subject to thermal expansion during testing. Samples were placed into the sample chamber, loaded with desired force, and heating and cooling cycle started. The data from the TMA is collected by a PC interface and the Netzch Instrument Cockpit software. The results of the analysis were loaded into the Netzch Proteus software and the user can analyze the results of the experiment including determination of thermal expansion coefficients, change in sample length, strain, strain rates, etc.

From a starting temperature of 25^{o}C, we utilized heating and cooling rates of 2, 5, and 20^{o}K/min respectively to achieve a target temperature of 350^{o}C. The samples were held in place by a constant load of 100 mN throughout testing. The atmosphere inside the sample chamber was Argon gas provided by a constant flow of 20ml/min. All samples were held at the target temperature of 350^{o}C for a period of 30

minutes to allow the sample and apparatus to achieve thermal equilibrium before beginning cooling cycle (Figure 5.3). Once the cycle was completed, data on thermal expansion coefficients, sample length change (if any permanent strain was manifest), and strain rates were subsequently analyzed.

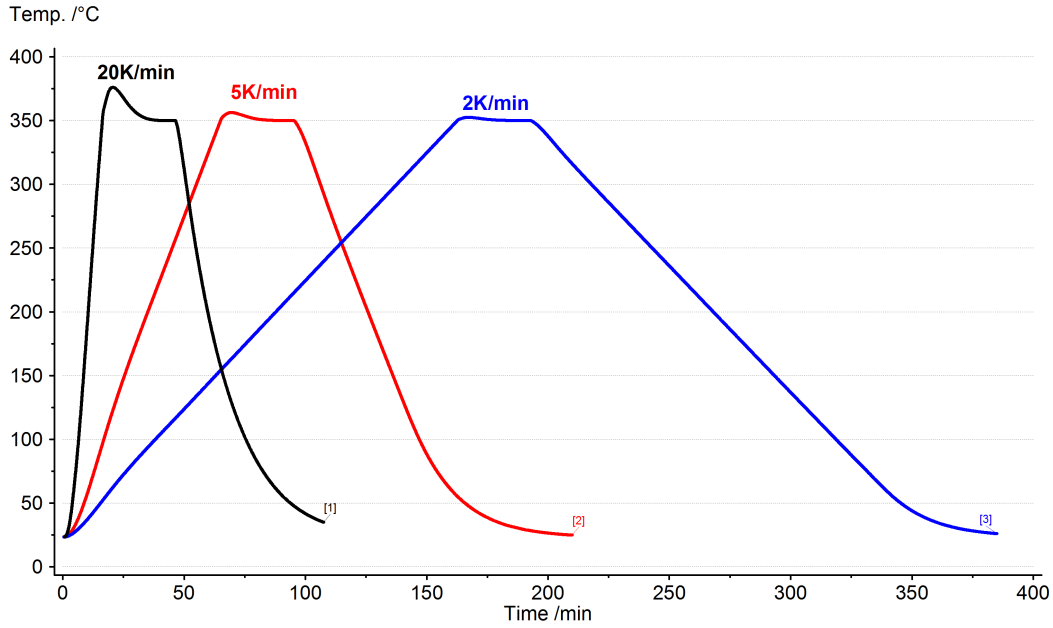

Figure 5.3: Heating and Cooling Profiles Used in TMA. [1] 20k/min, [2] 5kmin, [3] 2k/min.

5.2.4 Measurements Using Simultaneous Thermal Analysis

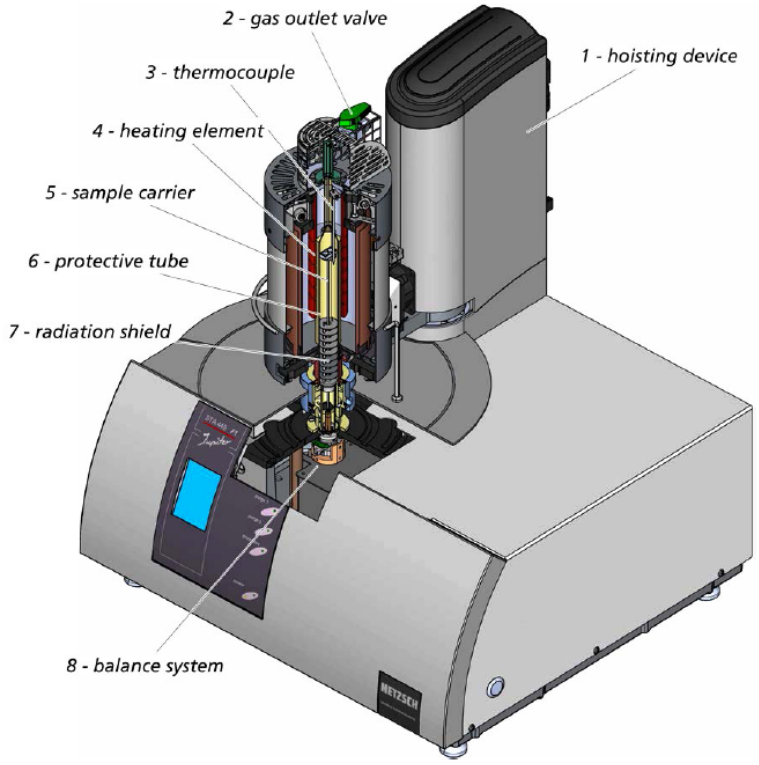

Figure 5.4: NETZSCH STA 449 F1 Jupiter system components (modified from NETZSCH, 2012b)

Measurements of thermogravimetric analysis (TG), differential scanning calorimetry (DSC) and specific heat capacity (Cp) were carried out using a Netzsch STA 449 F1 Jupiter analyzer (Figure 5.4). The STA measures the aforementioned properties by using a high-precision analytical balance to measure gravimetric changes and utilizes resistivity changes between sample and reference for calorimetric measurements. The sample is placed in a Platinum-Rhodium crucible, weighed and placed on the sample carrier. A starting temperature of 30^{o}C, was chosen and we utilized heating and cooling rates of 2, 5, and 20^{o}K/min to target temperatures of 350^{o}C and 900^{o}C respectively. The atmosphere inside the STA was also that of Argon gas using a flow rate of 20 ml/min. We also compared the results of our data to that of a reference material: a sapphire (Al_2O_3) disc that exhibits constant mass during TG measurements and no significant thermodynamic changes during calorimetry testing (DSC/Cp). The data collection system is similar to that of the TMA and data is collected continuously during measurements.

5.3 Results and Discussion

5.3.1 Thermal Expansion Data

Values of linear thermal expansion coefficients (α) were calculated for different heating, cooling and temperature steps utilizing Equation 5.2 and the displacement/temperature curves as presented in Figure 5.5. Generally there is little systematic variation in alpaha values at the three different rates or when heating and cooling are compared. However alpha does vary according to the temperature range over which it is measured (Table 4.1).

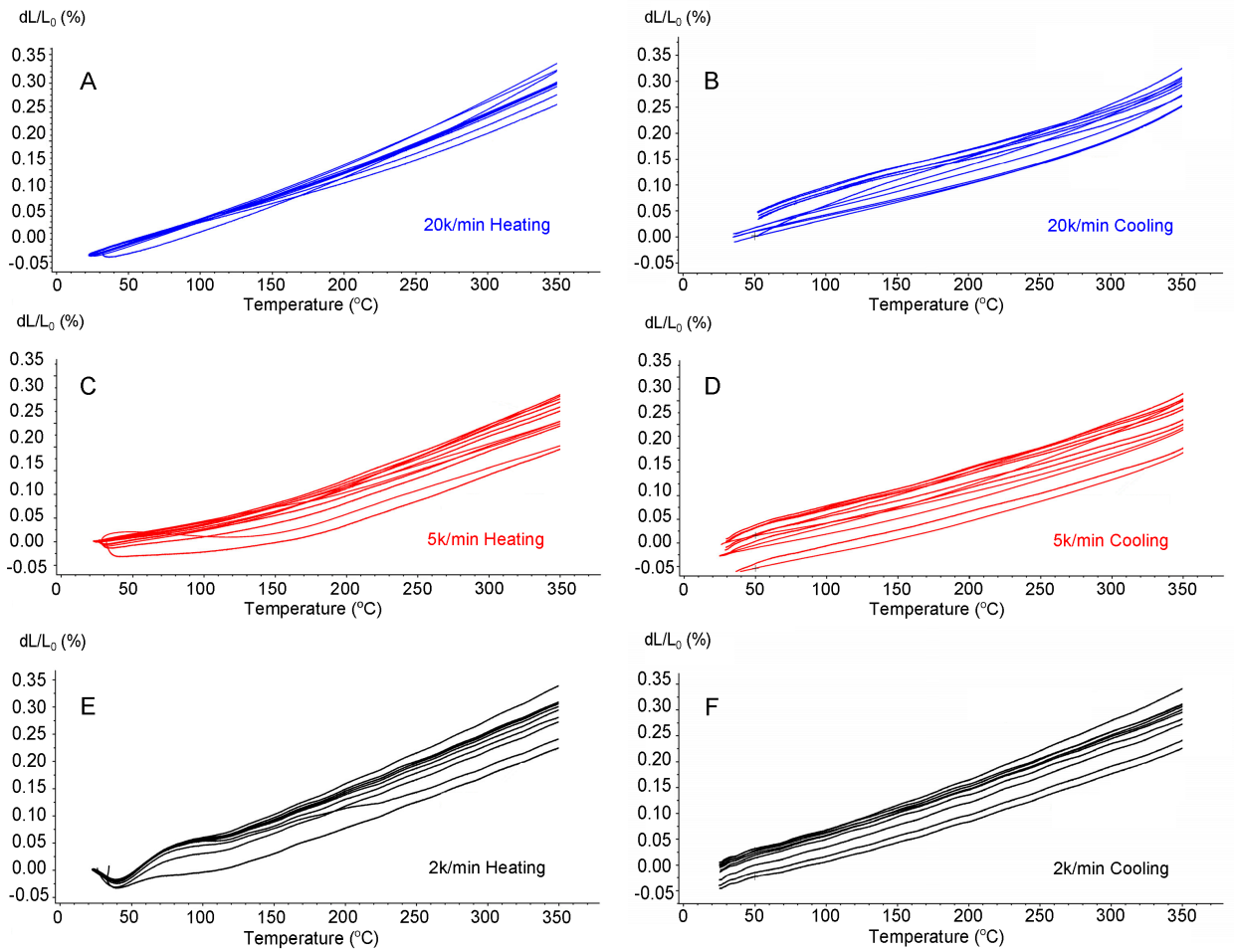

Figure 5.5: Linear displacement curves for Rotokawa Andesite (dL/L_0) during linear thermal expansion testing grouped by heating and cooling rates. (A) 20 K/min heating (B) 20 K/min cooling (C) 5 K/min heating (D) 5 K/min cooling (E) 2 K/min heating (F) 2 K/min cooling.

Table 5.1: Linear thermal expansion coefficient values for Rotokawa Andesite by measured temperature interval.

Temperature Interval (ºC)	**Min. Alpha** (10^{-6}/K)	**Max. Alpha** (10^{-6}/K)	**Mean Alpha** (10^{-6}/K)	**Std. Deviation** (10^{-6}/K)
50-100	3.56	13.25	7.76	2.45
100-150	3.99	9.82	7.46	1.06
150-200	5.95	11.28	8.60	1.28
200-250	6.03	12.65	9.35	1.37
250-300	7.47	13.35	10.19	1.18
300-350	9.25	14.05	11.21	1.15
50-350	4.84	14.10	9.09	1.41

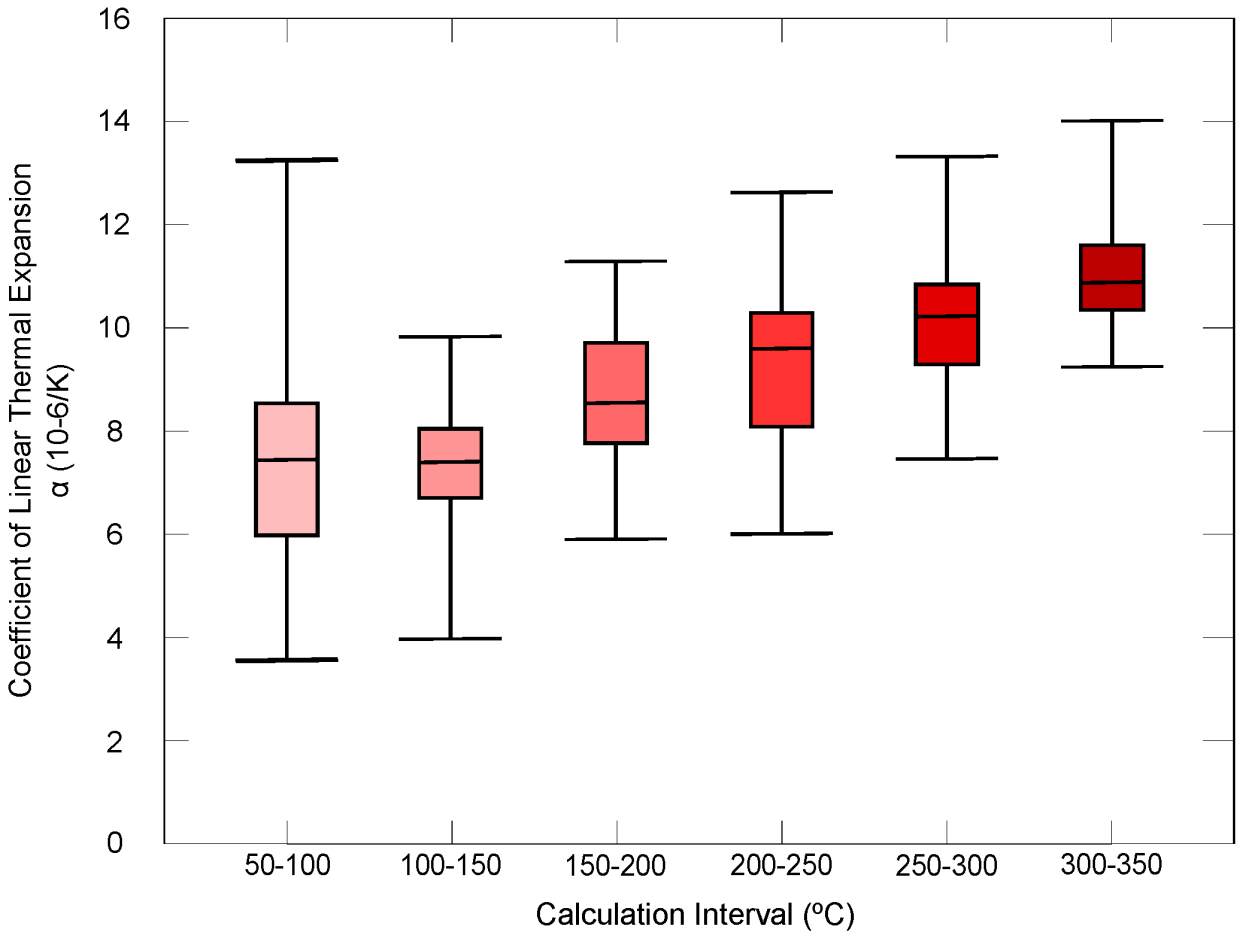

Figure 5.6: Coefficients of thermal expansion of Rotokawa Andesite grouped by temperature steps of measurement. The error bars represent the minimum and maximum values of each temperature step. The ends of the boxes are the 1st and 3rd quartile medians of the dataset and the black lines in the middle of the box are the mean values of the measurement interval.

There is an overall upward trend in the values of thermal expansion as calculated at different temperature steps (Figure 5.6). We see that at 50-100ºC the average value of α is $7.76 * 10^{-6}$/K while at 300-350ºC the value has increased by 44% to $11.21 * 10^{-6}$/K. It has also been observed by several other authors that as the

measured temperature interval increases, so do the values of thermal expansion (e.g. Richter and Simmons, 1977; Lo and Wai, 1982; Lin, 2002). We also calculated the thermal expansion coefficients for the entire dataset from the highest to lowest temperature of 50-350^{o}C to assist in building a stress model presented in Section 5.3.5. The values we observed range from $4.84 * 10^{-6}$/K to $14.1 * 10^{-6}$/K with a mean value of $9.09 * 10^{-6}$/K. Of note is the wide range of alpha values observed in the 50-100^{o}C interval. This can be attributed to a differential heating of the apparatus, sample and sample holder early in the heating cycle and that steady heat flux is established by the next temperature step, resulting in more consistent data.

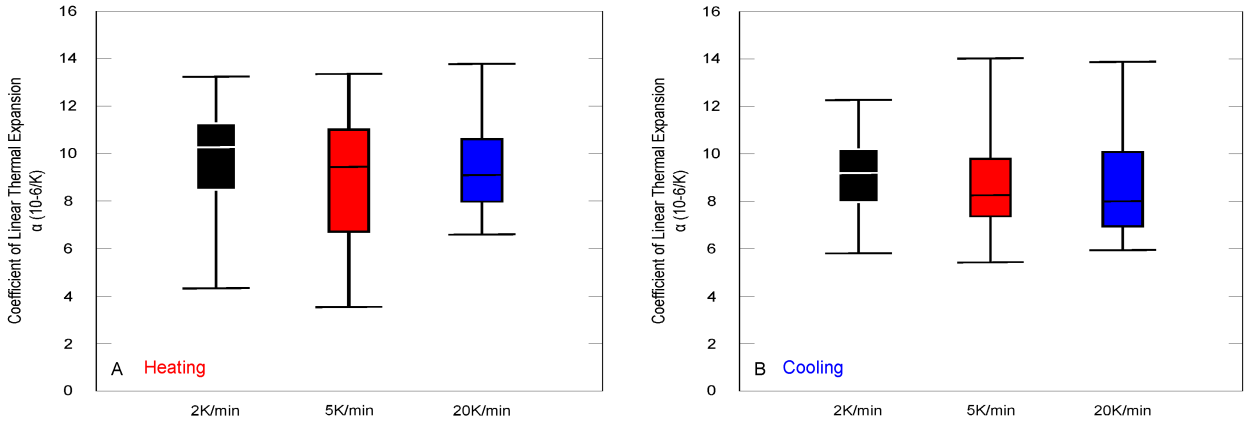

Figure 5.7: Coefficient of linear thermal expansion ranges for the Rotokawa Andesite. (A) Range of thermal expansion coefficients during heating by heating rate. (B) Range of thermal expansion coefficients during cooling cycle by cooling rate.

Figure 5.7a and 5.7b shows the ranges of calculated linear thermal expansion during heating and cooling grouped by heating rate. The thermal expansion coefficient ranges are very similar across the heating rates used of 2, 5 and 20K/min. There is little variation in the dataset for both heating and cooling cycles. We do observe that the minimum measured α value at 20 K/min heating is significantly larger than those observed at 2 and 5 K/min. There is also little variation in the dataset between heating and cooling cycles. However, mean values for cooling are systematically lower than for heating but again well within the range of experimental runs. Additionally, the range of thermal expansion values that we measured during cooling is much smaller which may be attributed to a more consistent heat flow during cooling than that of heating and is simply a function of the measurement methodology we have chosen. Some of the variation observed might be due to the early stages of heating where there is a slight hysteresis in the system (as evidenced by the heating curves in Figure 5.5) and that the values reported account for this behavior. It is worth considering that the Rotokawa Andesite has a complex thermal and chemical history and that the variation in observed α values as a function of rate may be due to sample variability

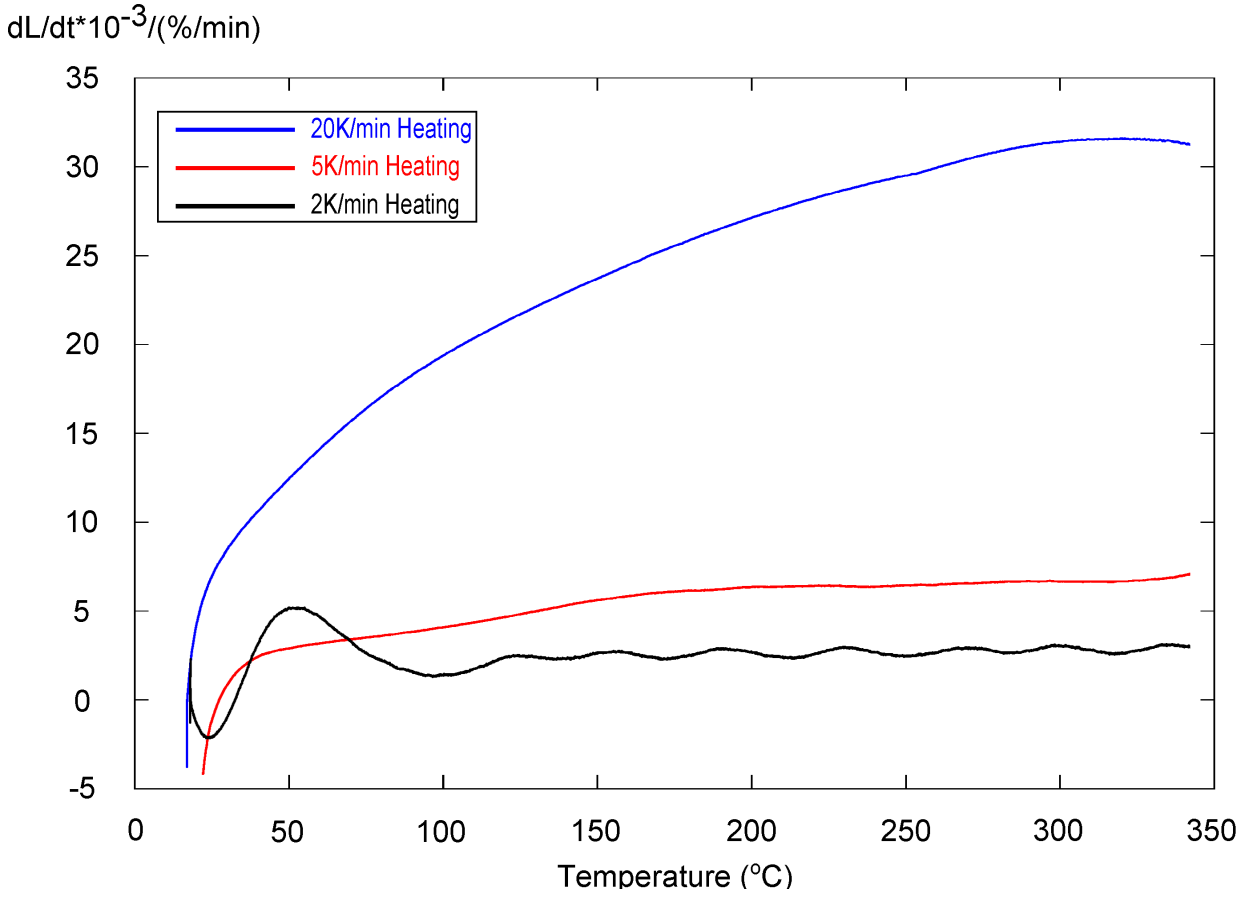

Figure 5.8: Strain rates as a function of heating rate.

In the interest of thermal strain and resulting stress, we also plot our results as the strain rate for the samples under the three heating regimens previously discussed. These data are detailed in Figure 5.8 as the derivative of the change in length during heating. We show that the strain rate is inherently higher with a faster heating rate with the largest increase in strain rate between 20-100^{o}C. We see no evidence that there is a manifestation of critical strain (macroscopic cracking) during the thermal expansion testing. The onset of a macroscopic crack would likely be recorded by the high-precision LVDT. We must consider however that it is possible microcracking occured that went undetected, as we had no acoustic emission recording capability which may have indicated such events.

To further this discussion, we look to the example of Yong and Wang (1980) where different heating rates of 0.4-12.5^{o} C/min were used to initiate microcracking in samples of Westerly Granite. They concluded that regardless of the rate of heating, no cracking was observed until a specific threshold temperature was reached (70^{o} C). This was supported by a lack of acoustic emissions during the cycling until the temperature threshold was crossed. However, once the threshold was reached, the rate did significantly influence the propagation of thermal cracks with higher rates yielding more cracking. Lin (2002) showed, permanent strain from cracking

was observed as a change in the ultimate sample geometry after testing. We did not observe any significant deviations in the linear displacement curves as permanent strain in our samples. From this we can assume that microcracking was unlikely in our tests on the Rotokawa Andesite regardless of the heating rate. By comparison with Young and Wang (1980) and Lin (2002) it is probably that a threshold temperature for cracking was not reached in our samples.

5.3.2 Simultaneous Thermal Analysis

Our data indicate that the Rotokawa Andesite experiences the largest thermomechanical changes above 500^{o}C. This is shown in Figure 5.9 as the sample deviates away from the sapphire standard reference curve. The TG curve in Figure 5.9a shows that there is no shift in sample mass at the temperatures at which we conducted our linear thermal expansion measurements (30-350^{o}C). However, the samples begin to experience mass loss above 450^{o}C and consistently lose mass to 900^{o}C such that samples lose between 2.8-5.2 wt% over the testing interval. The mass losses observed during the heating phase are accompanied by significant endothermic reactions that are observed by differential scanning calorimetry (DSC) as seen in Figure 5.9b. The mass loss and endothermic reactions are likely be the result of one or more of the following processes: dehydration, decarbonation, release of other volatiles and glass transitions (e.g. Neuhoff and Wang, 2007; Mollo et al., 2012; Heap et al., 2013 a,b).

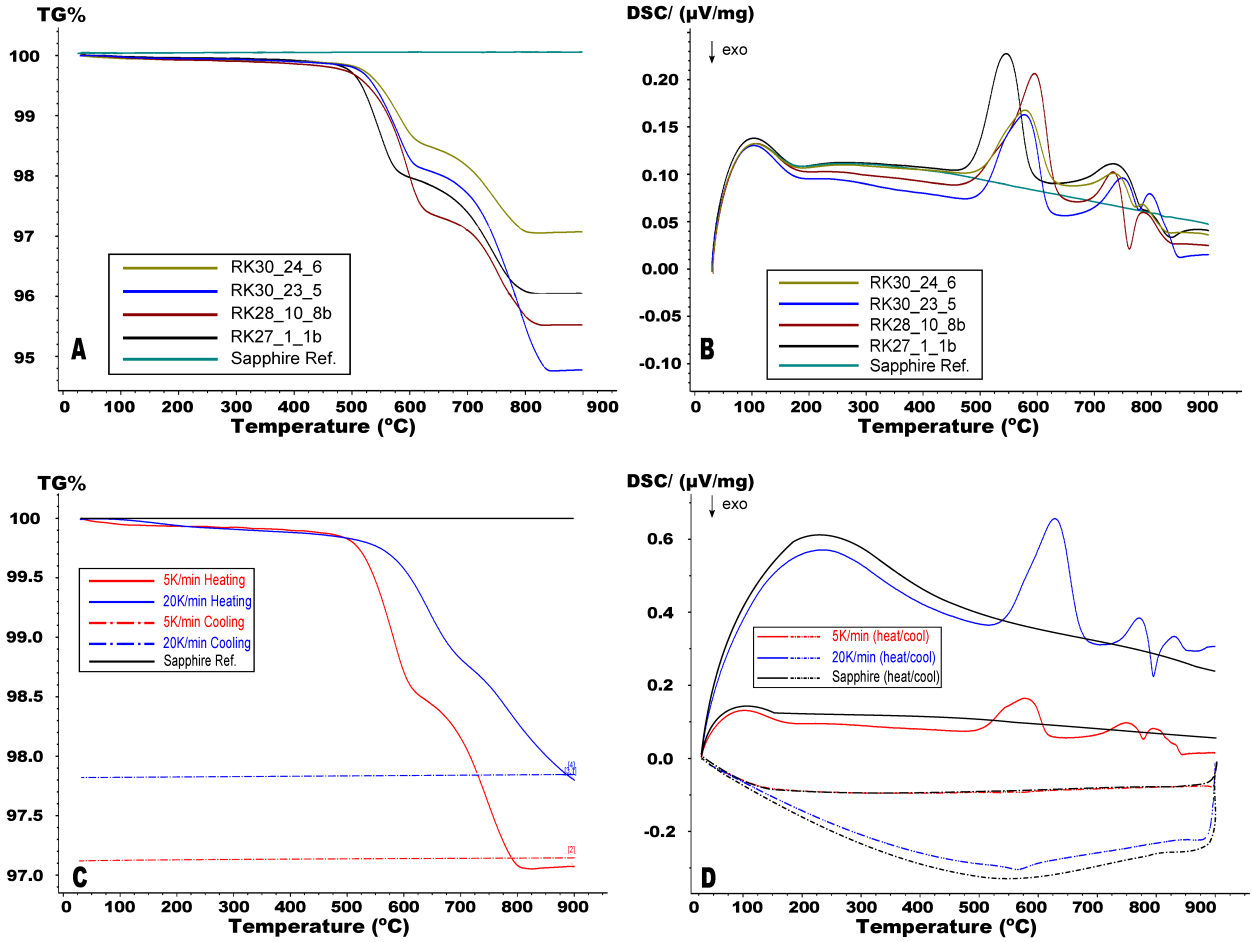

Figure 5.9: Results of Simultaneous Thermal Analysis for Rotokawa Andesites. (A) Summary of thermogravimetric (TG) analyses by well with sapphire reference curve . (B) Summary of differential scanning calorimetry (DSC) results by well with sappphire reference curve. (C) Dependence of heating rate on TG (D) Dependence of heating rate on DSC see text for further explanation.

By combining the TG and DSC measurements, the most significant changes occur in the Rotokawa Andesite between 550^{o}C and 900^{o}C. These changes are manifest as the endothermic peaks seen in both Figures 5.9b and 5.9d. The lack of large deviation away from the sapphire curve below 450^{o}C is consistent with the lack of thermal cracking and lack of large abrupt changes in thermal expansion behavior (Figure 5.5) These results are somewhat surprising considering several constituent minerals of the Rotokawa Andesite (e.g. adularia, silica, chlorite, biotite, calcite) are considered sensitive to temperature changes (Fleming and Fawcett, 1976; de Caritat et al., 1993; Neuhoff and Wang, 2007) and any thermo-chemical change during our expansion testing would significantly affect the results.

There is a small peak and reversal of the calorimetric (DSC) curve at the beginning of testing from 20^{o}C to near 150^{o}C at 5 K/min heating, and a similar variation from 20^{o}C to near 500^{o}C at 20 K/min (Figures 5.9b and 5.9d). These peaks could have been thermo-chemical processes that went undetected by

analysis of the TG curves. However, the sapphire standard shows a similar behavior. This indicates that the endothermic deviation is a result of our testing methodology and not thermo-chemical proccesses in the sample.

Figure 5.9c illustrates TG change by varied heating rate. Our data show that slower heating rates enact mass loss and chemical reactions in the sample at slightly lower temperatures, but the magnitude of these changes are less than those with higher heat flow. Similarly, the rate of heating on the DSC measurements was found to enact earlier endothermic reactions but of a lesser magnitude of those at a higher heating rate. It is also important to note that during the cooling phase of both TG and DSC analysis, no significant reactions occurred as evidenced by the cooling curves in Figures 5.9c and 5.9d; this was comfirmed by comparison to the sapphire standards which exhibited similar behavior.

As previously discussed, devolatization of mineral phases and the bursting of fluid inclusions during heating (and possibly cooling) are processes that have been attributed to the formation of microfractures in samples (Lin, 2002; Keshavarz et al., 2010). However, in our TG and DSC experiments there is no evidence that these processes are occurring below 450^{o}C. Above 450^{o}C significant reactions and weight loss indicate that these processes may be ocurring. We would anticipate that bursting of fluid inclusions would generate a change in TG from vaporization of the fluids entrained in the samples and that the process would also influence the enthalpy of the system, and this would be made clear by the DSC curve.

The exact endothermic reactions could be a combination of several thermo-chemical processes but their exact nature and processes are outside the scope of this research. We are most interested in the processes at the lower heating phases (30-350^{o}C) and as such, we do not see evidence for thermo-chemical reactions taking place within our range of measurement that would significantly affect our results.

5.3.3 Kaiser Effect

The Kaiser 'temperature-memory' effect has been described by several authors (e.g. Yong and Wang, 1980; Lavrov, 2005; Heap et al., 2013a) in rocks and engineering materials. The Kaiser effect is a constraint that materials should not be subject to damage (either thermal or mechanical) that do not exceed a previous threshold to which the material has already been subjected. In the case of the Rotokawa Andesite, the rocks we have studied have been subject to several iterations of thermal and mechanical stressing; eruption as an andesitic lava/breccia (thermal stress), burial and deposition (mechanical stress), host rock to a hydrothermal system (thermal stress) and subsequent removal as core (thermal and mechanical stressing).

In our experiments, we could be constrained by the Kaiser effect. We see no evidence of thermal cracking in our thermomechanical testing regardless of heating rate, as also observed by Yong and Wang (1980)

albeit at much lower temperatures. Additionally, we see no damage to samples during simultaneous thermal analysis also independent of heating rate. Therefore we have to conclude that though previous studies on Westerly Granite and similar rocks (Richter and Simmons, 1974; Simmons and Cooper, 1978; David et al., 1999; Lin 2002) have observed the onset of thermal cracking at temperatures much lower than our study, their source materials were not subjected to the high-temperature, hydrothermal conditions found in the Rotokata reservoir. As such, we consider that the thermogravimetric and calorimetric changes near 450^{o}C could possibly be evidence of the previous temperature threshold at which thermal damage may be observed in the Rotokawa Andesite.

5.3.4 Relating Thermal Expansion to Porosity

Cooper and Simmons (1977) demonstrated that porosity within a rock can serve as void space in which minerals can expand during heating, which accounts for measured thermal expansion values being lower than modeled values based on mineral contents. They explained that the pore space allows differential mineral expansion to be compensated in the porous space (predominantly cracks) resulting in the low values. We are also interested in the role of porosity and its effect on the thermal expansion of the Rotokawa Andesite. By utilizing specimens that comprise the wide range of porosity of our dataset we have attempted to find a correlation of porosity to thermal expansion behavior.

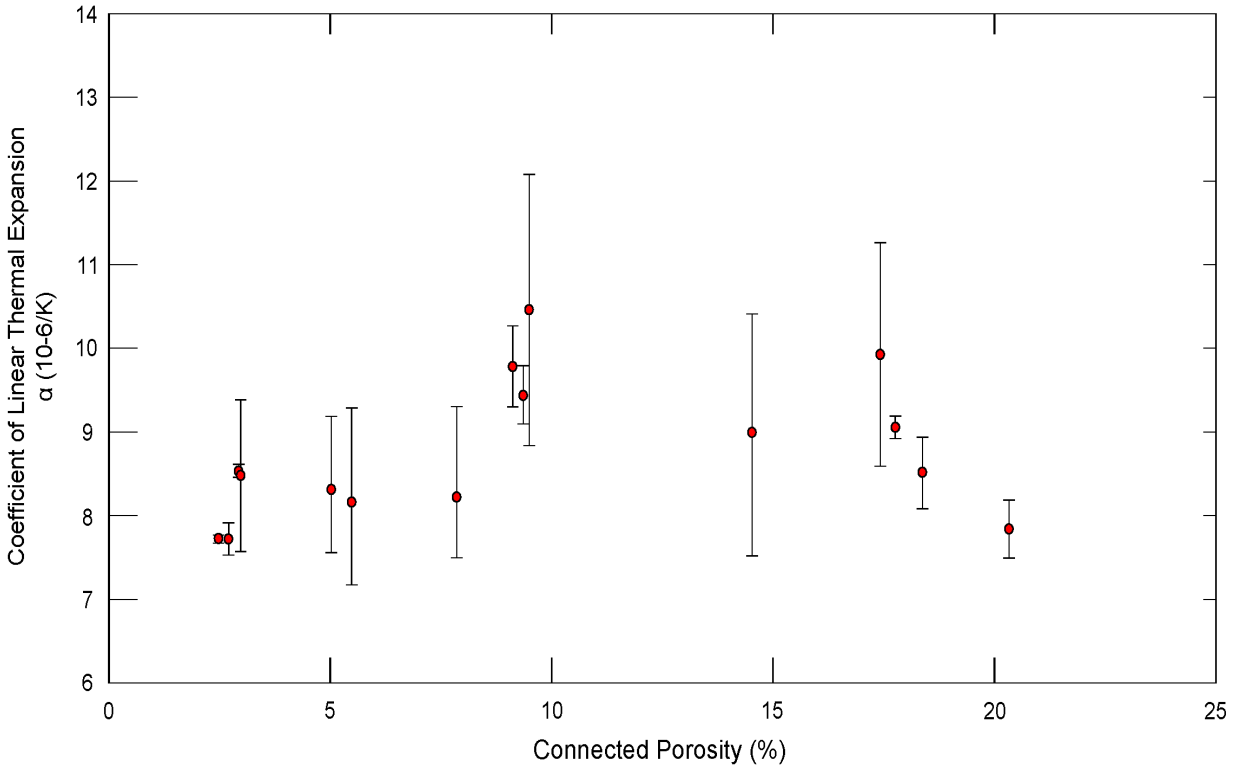

Figure 5.10: Plot of porosity versus coefficient of linear thermal expansion for Rotokawa Andesite. The error bars represent minimum and maximum values of TE by porosity with circles representing the mean values.

We show that there is no direct correlation of the thermal expansion behavior to porosity in the Rotokawa Andesite (Figure 5.10). The range of thermal expansion varies considerably across the values of porosity and as such we observe that similar values of thermal expansion are observed at approximately 5 (vol%) porosity as we do at 20 (vol%) porosity. This may be attributed to the anisotropic petrologic fabric of the Rotokawa Andesite whereby the expansion properties of the rocks are controlled purely by mineralogy and not by fabric. This is not necessarily contradictory to the findings of Cooper and Simmons (1977) as their samples consisted of relatively isotropic fine-grained granites, gabbros and felsite while the Rotokawa Andesite is severely hydrothermally altered and the mineralogy and textures are very different to those used by Cooper and Simmons. However, we cannot discount that porosity may play a small role in our thermal expansion measurements for accommodation of differential mineral expansion.

Accordingly, modeling of thermal expansion from physically measured properties can allow us to interpret whether the Rotokawa Andesite may follow classical behavior of thermal expansivity. As such we apply a classical physical model of thermal expansion from porosity as presented for rocks by Palciauskas and Domenico, (1982) and more recently has expanded by work in materials science engineering by Zeng et al. (2012).

The first of the models that we apply is that presented by Palciauskas and Domenico, (1982) such that thermal expansion coefficients can be predicted as:

$$\alpha_d = \alpha_s(1-\phi)^{1/3} \tag{5.4}$$

where α_d is the thermal expansion coefficient of a porous material, $\alpha_s$is the thermal expansion coefficient of the solid phase of the material and ϕ is the porous volume of the total material. To fit this model, we utilized the minimum, average and mean values of thermal expansion coefficients observed within our dataset to serve as the solid phase thermal expansion coefficient.

Further we attempt to constrain our model using that presented by Zeng et al. (2012) where thermal expansion is derived for cement pastes using the relationship:

$$\alpha_d = \alpha_c(1-\phi)^{2.38} \tag{5.5}$$

where α_d is the thermal expansion coefficient of a porous material, $\alpha_c$is the thermal expansion coefficient of the studied material where ϕ= 0 by linear regression. We utilize the highest observed value of our dataset to serve as α_c. The results of the application of these models are shown in Figure 5.11.

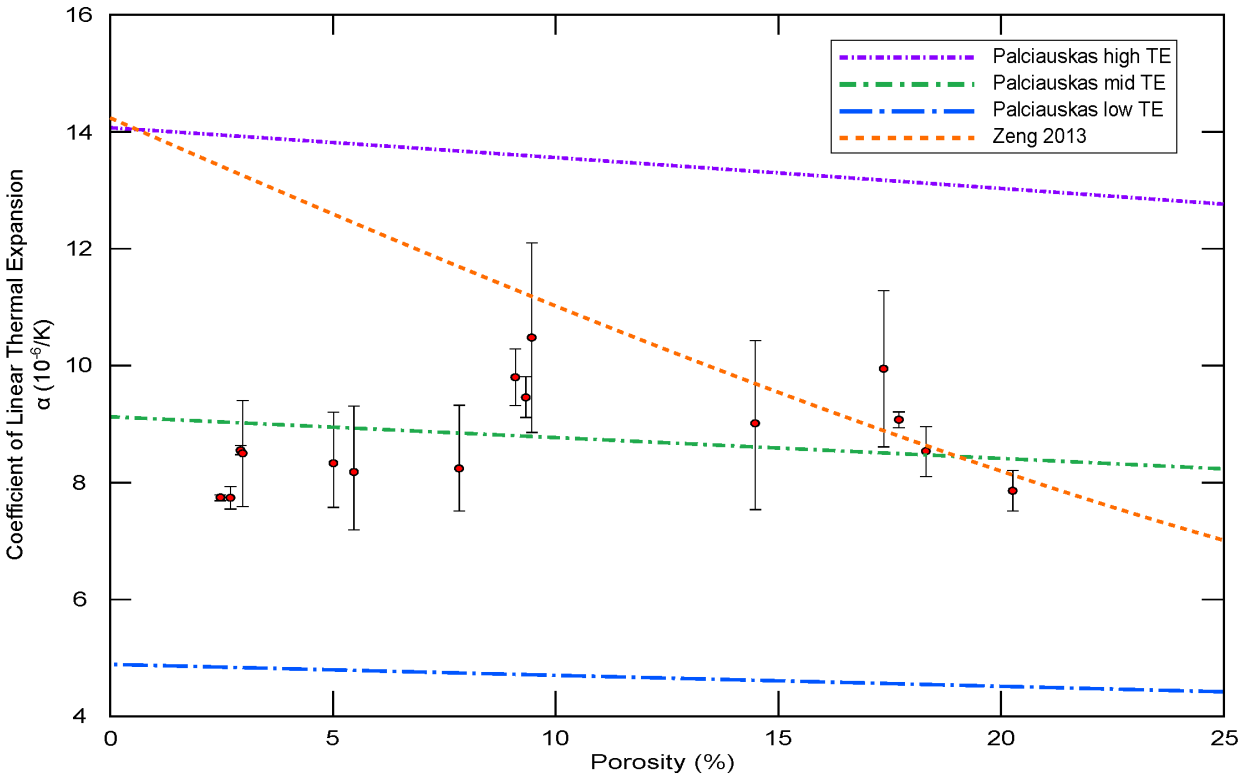

Figure 5.11: Thermal expansion as a function of porosity of the Rotokawa Andesite using the models of Palciauskas and Domenico, (1982) and Zeng et al., (2012).

The best fit for the data is achieved using the Palicauskas mid-TE model which uses the mid-range value of thermal expansion for the solid phase of the material. However, this does not give us an adequate fit to our experimental data to conclude that this model should be sufficient for the Rotokawa Andesite. The models that we have attempted to fit to our thermal expansion data show an increase of thermal expansion with decreasing porosity, a trend that we do not explicitly observe. Further, the model of Zeng et al., (2012) does not provide any sort of logical fit to our dataset. The experimental dataset that we present is clearly unconstrained by porosity and the attempt to fit to these models further reinforces this conclusion. The models of Zeng et al., (2012) and Palciauskas and Domenico (1982) are built assuming isotropic pore distribution within the samples, which we do not readily observe in the Rotokawa Andesite. The linear thermal expansion behavior of the Rotokawa Andesite could be constrained by mineralogy and petrological investigations and modeling but further analytical work would be needed to build, constrain and confirm such models.

5.3.5 Utilizing Thermal Experimental Data to Create A Tensile Stress Model

Table 5.2: Physical Properties of Rotokawa Andesite

	Porosity (%)	Vp (m/s)	Vs (m/s)	Es	vs	$\sigma_{tensile}$	α at dt 300^{o}C
Mean	8.44	4106	2510	30.6	0.20	15.4	9.08e-6
Minimum	5.3	3381	2140	19.9	0.09	9.9	4.84e-6
Maximum	20.4	4506	2722	43.7	0.34	24.1	1.41e-5

The practical application of thermal expansion data can be utilized to constrain thermo-elastic stress conditions that result from temperature gradients imposed on rock and other materials. By using our experimental data on the thermal properties of the Rotokawa Andesite coupled with previous studies that we have carried out to constrain physical properties (See Siratovich et al, 2012 and Chapter 4), we can build models to predict how the andesite will behave under thermal stress. As such, we consider the classical theory of thermoelasticity (from Timoshenko and Goodier, 1970) applied to an isotropic unconfined cylinder of Rotokawa Andesite to be:

$$\sigma_t = \frac{2\alpha E \Delta T}{(1-\nu)} * (I_l) \tag{5.6}$$

where σ_t=thermal stress on a plane (MPa), α = linear thermal expansion coefficient, E =Young's modulus (GPa), ΔT= temperature differential, ν = Poisson's Ratio, and I_l= an influence value of thermal diffusion, radius and time given by Timoshenko and Goodier, (1970). By utilizing our mean thermal expansion data and the results of previous investigations of physical properties of the Rotokawa Andesite (Table 5.2), we apply the following conditions to the model such that $E = 30,600$ MPa, ΔT= temperature differential, $\nu = 0.20$ (values from measurements detailed in Chapter 4), I_l=0.235 and α =minimum, maximum and mean values of linear thermal expansion measured using a temperature differential of 300^{o}C (as given by Equation 5.2 in Section 5.1). We then propose that a temperature differential is instantaneously imposed on the rock and the Young's modulus and Poisson ratio are kept constant such that the only physical variable is the thermal expansion coefficient. Figure 5.12 shows the results of this linear model. The model indicates that the higher the thermal expansion coefficient, the higher the stress experienced as a result of an instantaneous temperature change. The results of this analysis are interesting from two separate perspectives: 1) the tensile stress that would be imparted on a sample during our thermomechanical testing is well below the tensile strength of the rock and our heating rates could not generate a high enough dT to cause such failure and 2) we have established a failure criterion for the Rotokawa Andesite in tension by utilizing our thermomechanical and physical property measurements.

The first of these results applies directly to our thermal expansion measurements. The highest heating rate that we achieved was 20 K/min as previously discussed, thus the instantaneous temperature differential a specimen would see is far below the minimum temperature differential to create tensile failure as seen in Figure 5.12. There was no point during the testing which the sample could have experienced a greater than 40^{o}C instant temperature change. Thus, it is highly unlikely that we have manifested any sort of tensile failure in our samples during thermal property testing.

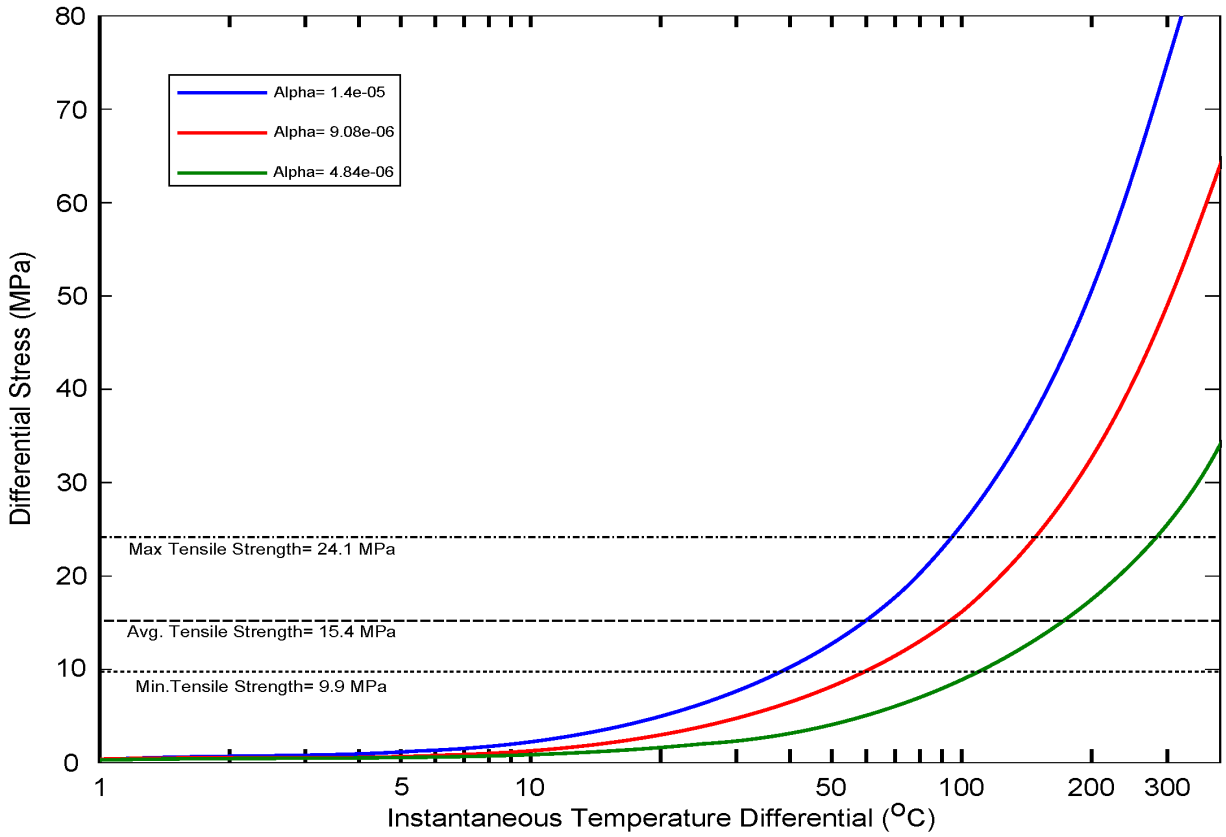

Figure 5.12: Tensile stress model for Rotokawa Andesite. Thermoelastic stress is modeled as a function of an instantaneous temperature differential applied to an unconstrained cylinder of Rotokawa Andesite.

The second result of this model is more applicable to a geothermal environment where it may be desirable to create tensile fractures at the wellbore face to enhance permeability of the reservoir rock. This can be achieved by the introduction of cold fluid to the face of the wellbore that in turn imparts the tensile stress which results in development and potential propagation of a tensile fracture. The model imparts an instantaneous temperature differential to create tensile failure based on our experimental tests on indirect tensile strength. We expect that the mean value of thermal expansion would provide for the most accurate behavior of Rotokawa Andesite under a thermal load. As such if we assume that the minimum tensile strength we have observed in our studies is the strength of the weakest rock in the reservoir, we would anticipate

tensile fracture in these rocks to occur at temperature differential of 60^{o}C. Similarly, if we assume a very low thermal expansion of the rocks the same failure would require a differential of 121^{o}C. These instantaneous temperature differentials could be expected in the Rotokawa Reservoir during a thermal sitmulation, and give support to field data for thermal cracking to be partially responsible for enhanced permeability.

5.4 Conclusions

1. The Rotokawa Andesite displays a very similar thermal expansion behavior regardless of the rate of heating. This is further constrained by a distinct lack of cracking during thermal testing experiments as we have observed no discernible permanent strain in the samples. The lack of a rate dependence on the development of thermal cracking furthers the findings of Yong and Wang (1980) that regardless of heating rate, temperature thresholds control the onset of thermal cracking.

2. Our TG and DSC results show that within the experimental range of our thermal expansion experiments (less than 450^{o}C) fluid inclusions do not decrepitate and mineral phases do not de-volitize and this is consistent with the lack of thermal cracking. The nature of the reactions that take place above 450^{o}C require more data to deliver a solid understanding and could be the focus of further research.

3. Linear thermal expansion coefficients of the Rotokawa Andesite are not dependent on the porosity of the dataset. We have attempted to apply classical models of thermal expansion derived from porosity measurements and find that our data simply do not follow the traditional models built from isotropic, heterogeneous materials. Further work on the mineralogy and petrological fabric of the Rotokawa Andesite may yield data to apply models of expansion based on the mineral components.

4. Utilizing our previous studies on the physical properties and the findings of this study we have constrained a model of thermoelastic tensile stress that can be applied to the Rotokawa Andesite. This model presents the simplified conditions under which tensile failure may be expected in the Rotokawa Andesite as a result of thermal stress. The results of this model may be used to further predict the failure criteria where tensile fractures may be expected in a borehole which is essential to predictions of borehole stability and in planning of thermal stimulation procedures.

5.5 Acknowledgements

The authors wish to thank Mighty River Power Company Ltd. for funding to support this research. We also thank the Rotokawa Joint Venture (a joint venture of the Tauhara North No. 2 Trust and Mighty River Power Company Ltd.) for providing the core used in our investigations. Funding for P. Siratovich was provided by a generous grant from Mighty River Power Company Ltd. Y. Lavallée and F. von Aulock acknowledge support from the European Research Council for the Starter Grant on Strain Localisation in Magmas (SLiM, nbr. 306488). B. Kennedy was partially funded by a Marsden Fast Start (09-UO-017C).

5.6 References

Axelsson, G., Thórhallsson, S., 2009. Review of Well stimulation Operations in Iceland. Geotherm. Resour. Counc. Trans. 33, 795–800.

Balme, M., Rocchi, V., Jones, C., Sammonds, P., Meredith, P., Boon, S., 2004. Fracture toughness measurements on igneous rocks using a high-pressure, high-temperature rock fracture mechanics cell. J. Volcanol. Geotherm. Res. 132, 159–172.

Bauer, S.J., Handin, J., 1983. Thermal Expansion and Cracking of Three Confined, Water-Saturated Igneous Rocks to 800C. Int. J. Rock Mech. Min. Sci. Geomech. Abstr. 20, A171–A171.

Chaki, S., Takarli, M., Agbodjan, W.P., 2008. Influence of thermal damage on physical properties of a granite rock: Porosity, permeability and ultrasonic wave evolutions. Constr. Build. Mater. 22, 1456–1461.

Cooper, H.W., Simmons, G., 1977. The Effect of Cracks on the Thermal Expansion of Rocks. Earth Planet. Sci. Lett. 36, 404–412.

Darot, M, Gueguen, Y., Baratin, M.-L., 1992. Permeability of Thermally Cracked Granite. Geophys. Res. Lett. 19, 869–872.

David, C., Menendez, B., Darot, M., 1999. Influence of stress-induced and thermal cracking on physical properties and microstructure of La Peyratte granite. Int. J. Rock Mech. Min. Sci. 36, 433–448.

de Caritat, P., Hutcheon, I., Walshe, J.L., 1993. Chlorite geothermometry: a review. Clays Clay Miner. 41, 219–239.

Faoro, I., Vinciguerra, S., Marone, C., Elsworth, D., Schubnel, a., 2013. Linking permeability to crack density evolution in thermally stressed rocks under cyclic loading. Geophys. Res. Lett. 40, 2590–2595.

Finnie, I., Cooper, G.A., Berlie, J., 1979. Fracture Propagation in Rock by Transient Cooling. Int. J. Rock Mech. Min. Sci. Geomech. Abstr. 16, 51.

Fleming, P.D., Fawcett, J.J., 1976. MgO-FeO-AlrOs-SiOrH2O at 2 kbar Upper stability of chlorite * quartz in the system water pressure. Am. Mineral. 61, 1175–1193.

Flores-Armenta, M., Tovar-Aguado, R., 2008. Thermal Fracturing of Well H-40 , Los Humeros Geothermal Field. Geotherm. Resour. Counc. Trans. 32, 8–11.

Fortin, J., Stanchits, S., Vinciguerra, S., Guéguen, Y., 2011. Influence of thermal and mechanical cracks on permeability and elastic wave velocities in a basalt from Mt. Etna volcano subjected to elevated pressure. Tectonophysics 503, 60–74.

Ghassemi, A., Zhang, Q., 2004. Poro-thermoelastic mechanisms in wellbore stability and reservoir stimulation, In: Proceedings, Twenty-Ninth Workshop on Geothermal Reservoir Engineering. Stanford University, Stanford, California, January 26-28, 2004, p. 7.

Grant, M.A., Bixley, P.F., 2011. Geothermal Reservoir Engineering, 2nd ed. Elsevier Science Ltd, Oxford, UK.

Grant, M.A., Clearwater, J., Quinao, J., Bixley, P.F., Le Brun, M., 2013. Thermal Stimulation of Geothermal Wells: A Review of Field Data, In: Proceedings, Thirty-Eighth Workshop on Geothermal Reservoir Engineering. Stanford University, Stanford, California. p. 7.

Hall, D.L., Bodnar, R.J., 1989. Comparison of fluid inclusion decrepitation and acoustic emission profiles of Westerly granite and Sioux quartzite. Tectonophysics 168, 283–296.

Heap, M.J., Lavallée, Y., Laumann, a., Hess, K.-U., Meredith, P.G., Dingwell, D.B., Huismann, S., Weise, F., 2013. The influence of thermal-stressing (up to 1000°C) on the physical, mechanical, and chemical properties of siliceous-aggregate, high-strength concrete. Constr. Build. Mater. 42, 248–265.

Heap, M J, Mollo, S., Vinciguerra, S., Lavallée, Y., Hess, K., Dingwell, D.B., Baud, P., Iezzi, G., 2013. Thermal weakening of the carbonate basement under Mt . Etna volcano (Italy): Implications for volcano instability. J. Volcanol. Geotherm. Res. 250, 42–60.

Heard, H.C., Page, L., 1982. Elastic Moduli , Thermal Expansion , and Inferred Permeability of Two Granites to 350øC and 55 Megapascals. J. Geophys. Res. 87, 9340–9348.

Homand-Etienne, F, Troalen, J.P., 1984. Behaviour of Granites and Limestones Subjected to Slow and Homogeneous Temperature Changes. Eng. Geol. 20, 219–233.

Keshavarz, M., Pellet, F.L., Loret, B., 2010. Damage and Changes in Mechanical Properties of a Gabbro Thermally Loaded up to 1,000°C. Pure Appl. Geophys. 167, 1511–1523.

Kitao, K., Ariki, K., Hatakeyama, K., Wakita, K., 1990. Well Stimulation Using Cold-Water Injection Experiments in the Sumikawa Geothermal Field, Akita Perfecture, Japan. Geotherm. Resour. Counc. Trans. 14, 1219–1224.

Lavrov, A., 2005. Fracture-induced Physical Phenomena and Memory Effects in Rocks: A Review. Strain 41, 135–149.

Lin, W., 2002. Permanent strain of thermal expansion and thermally induced microcracking in Inada granite. J. Geophys. Res. 107, 2215.

Lo, K.Y., Wai, R.S.C., 1982. Thermal expansion, diffusivity, and cracking of rock cores from Darlington, Ontario. Can. Geotech. J. 19, 154–166.

Mollo, S., Heap, M.J., Iezzi, G., Hess, K.-U., Scarlato, P., Dingwell, D.B., 2012. Volcanic edifice weakening via decarbonation: A self-limiting process? Geophys. Res. Lett. 39, Vol. 39, 15, L15307

Nara, Y., Meredith, P.G., Yoneda, T., Kaneko, K., 2011. Influence of macro-fractures and micro-fractures on permeability and elastic wave velocities in basalt at elevated pressure. Tectonophysics 503, 52–59.

NETZSCH, GmBH., 2012a. Operating Instructions Thermomechanical Analysis TMA 402 F1/F2 Hyperion. Selb, Germany.

NETZSCH, GmBH., 2012b. Operating Instructions Simultaneous TG-DTA/DSC Apparatus STA 449 F1 Jupiter. Selb, Germany.

Neuhoff, P.S., Wang, J., 2007. Isothermal measurement of heats of hydration in zeolites by simultaneous thermogravimetry and differential scanning calorimetry. Clays Clay Miner. 55, 239–252.

Palciauskas, V. V., Domenico, P. A., 1982. Characterization of drained and undrained response of thermally loaded repository rocks. Water Resour. Res. 18, 281–290.

Patel, A., Manga, M., Carey, R.J., Degruyter, W., 2013. Effects of thermal quenching on mechanical properties of pyroclasts. J. Volcanol. Geotherm. Res. 258, 24–30.

Quinao, J., Sirad-azwar, L., Clearwater, J., Hoepfinger, V., Le Brun, M., Bardsley, C., 2013. Analyses and Modeling of Reservoir Pressure Changes to Interpret the Rotokawa Geothermal Field Response to Nga Awa Purua Power Station Operation, In: Proceedings 38th Workshop on Geothermal Reservoir Engineering. Stanford University, Stanford, California, February 11-13, p. 10.

Rae, A.J., McCoy-West, A.J., Ramirez, L.E., Alcaraz, S.A., 2009. Geology of Production Well RK28 , Rotokawa Geothermal Field, GNS Science Consultancy Report 2009/253.

Rae, A.J., McCoy-West, A.J., Ramirez, L.E., McNamara, D., 2010. Geology of Production Wells RK30L1 and RK30L2 Rotokawa Geothermal Field, GNS Science Consultancy Report 2010/02.

Ramirez, L.E., Hitchcock, D., 2010. Geology of Production Well RK27L2 , Rotokawa Geothermal Field, GNS Science Consultancy Report 2010/100.

Richter, D., Simmons, G., 1974. Thermal expansion behavior of igneous rocks. Int. J. Rock Mech. Min. Sci. Geomech. Abstr. 11, 403–411.

Sewell, S.M., Cumming, W.B., Azwar, L., Bardsley, C., 2012. Integrated MT and Natural State Temperature Interpretation for a Conceptual Model Supporting Reservoir Numerical Modelling and Well Targeting at the Rotokawa Geothermal Field, New Zealand, In: Proceedings: Thirty-Seventh Workshop on Geothermal Reservoir Engineering. Stanford University, Stanford California, p. 8.

Simmons, G., Cooper, H.W., 1978. Thermal Cycling Cracks in Three Igneous Rocks. Int. J. Rock Mech. Min. Sci. Geomech. Abstr. 15, 145–148.

Siratovich, P., Davidson, J., Villeneuve, M., Gravley, D., Kennedy, B., Cole, J., Wyering, L., Price, L., 2012. Physical And Mechanical Properties Of The Rotokawa Andesite From Production Wells RK 27 _ L2 , RK 28 And RK 30, In: Proccedings New Zealand Geothermal Workshop 19-21 November. p. 7.

Timoshenko, S.P., Goodier, J.N., 1970. Theory of Elasticity, 3rd ed. McGraw-Hill, New York, NY.

Ulusay, R. and Hudson, J., 2007. The Complete ISRM Suggested Methods for Rock Characterization, Testing and Monitoring: 1974-2006, 1974th–2006th ed. Elsevier, Antalya, Turkey.

Vinciguerra, S., Trovato, C., Meredith, P., Benson, P., 2005. Relating seismic velocities, thermal cracking and permeability in Mt. Etna and Iceland basalts. Int. J. Rock Mech. Min. Sci. 42, 900–910.

Wong, T.F., Brace, W.F., 1979. Thermal Expansion of Rocks: Some Measurements at High Pressure. Tectonophysics 57, 95–117.

Yong, C. and Wang, C.Y., 1980. Thermally Induced Acoustic Emission in Westerly Granite. Geophys. Res. Lett. 7, 1089–92.

Zeng, Q., Li, K., Fen-Chong, T., Dangla, P., 2012. Effect of porosity on thermal expansion coefficient of cement pastes and mortars. Constr. Build. Mater. 28, 468–475.

Zoback, M.D., Barton, C.A., Brudy, M., Castillo, D., Finkbeiner, T., Grollimund, B., Moos, D., Peska, P., Ward, C., Wiprut, D., 2003. Determination of stress orientation and magnitude in deep wells. Int. J. Rock Mech. Min. Sci. 40, 1049–1076.

Chapter 6

Experimental Thermal Stimulation of the Rotokawa Andesite

P.A. Siratovich[a], M. Heap[b], J. Cole[a], M. Villeneuve[a], T. Reuschlé[b], K. Swanson[a], B. Kennedy[a], D. Gravley[a]

[a]Department of Geological Sciences, University of Canterbury, Private Bag 4800, Christchurch 8140, New Zealand

[b]Laboratoire de Déformation des Roches, Équipe de Géophysique Expérimentale, Institut de Physique de Globe de Strasbourg (UMR 7516 CNRS, Université de Strasbourg/EOST), 5 rue René Descartes, 67084 Strasbourg cedex, France.

To be Submitted to *Geophysical Research Letters*.

Abstract

Permeability enhancement by cold water injection in geothermal wells has proven to be an effective stimulation technique in many active geothermal fields. We report the results of laboratory experiments designed to replicate thermal stimulation of core sourced from a geothermal reservoir by heating rocks to 325^{o}C at 20 MPa pressure and quenching these rocks rapidly to 20^{o}C while maintaining a pressure of 20 MPa. We show that permeability is increased by an order of magnitude over original pre-treatment values. Ultrasonic velocities also reflect a significant change after stimulation testing. We utilize scanning electron microscopy to evaluate the microstructural change to our samples and supplement our physical property investigations. The results imply that thermal stimulation can be successfully repeated in the laboratory and is coupled with both thermal and chemical components and we discuss the implications this may have for future application of geothermal well stimulation.

Keywords: thermal stimulation, permeability, geothermal, scanning electron microscope, chemical alteration

6.1 Introduction

Thermal stimulation of geothermal wells is a technique that is used to enhance near-wellbore permeability in wells that are underperforming (Kitao et al., 1990; Flores-Armenta and Tovar-Aguado, 2008) and is a known phenomenon in wells that are used for long-term reinjection of spent reservoir fluids (Grant et al., 2013). This process can be done immediately after wells are drilled to enhance the fluid handling capabilities of the wells or can be carried out long after the wells have been utilized and may be experiencing a decline in productivity or injectivity.

Cracking can occur in the wells that can be linked to tectonic stress in the reservoir environment, coupled with thermoelastic stress that results from injection of fluids that are cooler than the reservoir formations. These fluids may be waste streams from power-plants that can range in temperature from 40-180^{o}C or can be from nearby fresh water sources where it is necessary to maximize the thermal gradient applied to the reservoir formations. Both injection streams are of a lower temperature than those found in the reservoir and thus a differential thermal stress is created. However, thermal cracking cannot be exclusively identified as the single clear physical mechanism that creates permeability enhancement. The thermal stresses have been postulated to create new fractures, re-open existing sealed fractures and dialate open fractures by contraction of the surrounding rock through cooling. It has been suggested that stimulation may also be achieved without thermal cracking by cleaning out debris from open fractures that have been plugged during drilling and completion operations (Axelsson and Thórhallsson, 2009), or chemically by dissolving fracture filling minerals and enhancing permeability of existing fractures (Flores et al., 2005; Pasikki et al., 2010).

The subject of thermally induced cracks in the laboratory is not a new field of research and has been proven to influence many important physical properties. Specifically applicable to geothermal development are investigations of permeability increase, strength degradation and acoustic velocity attenuation (e.g. Darot et al., 1992; David et al., 1999; Vinciguerra et al., 2005; Nara et al., 2011) . The majority of studies on this area of interest has been carried out on granites and other isotropic media. Milsch et al., (2008) presented an excellent study on long-term, low flow rate studies of rocks similar to the geothermal system at Groß-Schönebeck coupled with permeability measurements. However, there is a distinct lack of information on geothermal core and thermal cracking in the laboratory under fully water saturated conditions, coupled with high thermal gradients and rapid fluid flow-rates.

We have conduced experiments to constrain the processes that may result in permeability enhancement in a geothermal reservoir environment, and have carried out a series of tests on core sourced directly from an active geothermal reservoir. We have characterized important physical properties before subjecting the cores to high-temperature thermal stimulation tests using a specially designed “geothermal stimulation

device" (Figure 6.1a). The results of our investigation and implications for geothermal stimulations are then discussed.

6.2 Experimental Procedures

We have utilized core sourced from the Rotokawa Andesite, the reservoir lithology of the high-temperature, high-enthalpy geothermal reservoir at the Rotokawa geothermal field located in the Taupo Volcanic Zone, North Island, New Zealand. Five samples of Rotokawa Andesite were cut into cores 20 mm diameter by 40 mm length, and characterized for porosity, density, permeability, and acoustic wave velocities.

Porosity and bulk density of the samples were determined using the triple-weight water saturation method (Ulusay and Hudson, 2007). Permeability was determined at the Laboratoire de Déformation des Roches (LDR, Université de Strasbourg) using a gas permeameter with argon gas as the pore-pressure media and distilled water as the confining media (see Heap et al., 2013 for further description). All samples needed Klinkenberg slip correction applied to determine true permeability (Klinkenberg, 1941). Ultrasonic wave velocities were measured at the University of Canterbury using a GCTS CATLS ULT-100 (Geotechnical Consulting and Testing Systems Computer Aided Ultrasonic Velocity Testing System) with axial P- and S-wave piezoelectric transducer crystals with a resonance frequency of 900 kHz. The acoustic measurements were conducted under a force of 1.5 kN provided by a Tecnotest servo-controlled loading frame to ensure consistent contact of the transducers and repeatability of the axial load applied to the samples. The ultrasonic velocities and measured densities were then utilized to calculate the dynamic Young's modulus (E_d) and Poisson's ratio (v_d) (Guéguen and Palciauskas, 1994).

The samples were then subjected to thermal stressing under confined, high temperature, water saturated conditions. They were heated at 2^{o}C/min to a target temperature of 325^{o}C, and held for two hours. The system was then quenched using 20^{o}C water at a flow rate of 145 ml/min to a final temperature of 20^{o}C while maintaining a system pressure of 20 MPa. The peak quenching rate is greater than 27^{o}C/min in the initial portion of the cooling cycle and averages 10.9^{o}C/min from 325^{o}C to 100^{o}C and further declines to 2^{o}C/min from 100^{o}C to 20^{o}C as evidenced in Figure 6.1b. Acoustic emissions were monitored during the sample cycle using the Mistras AE (acoustic emission) acquisition system using a Physical Acoustics D9215 high temperature sensor with frequency range set to 100-500 kHz. The thermal stimulation system schematic, pressure, temperature and acoustic output during a thermal cycle of Rotokawa Andesite are presented in Figure 6.1 with Figure 6.1b detailing an example of a thermal stimulation cycle in the device.

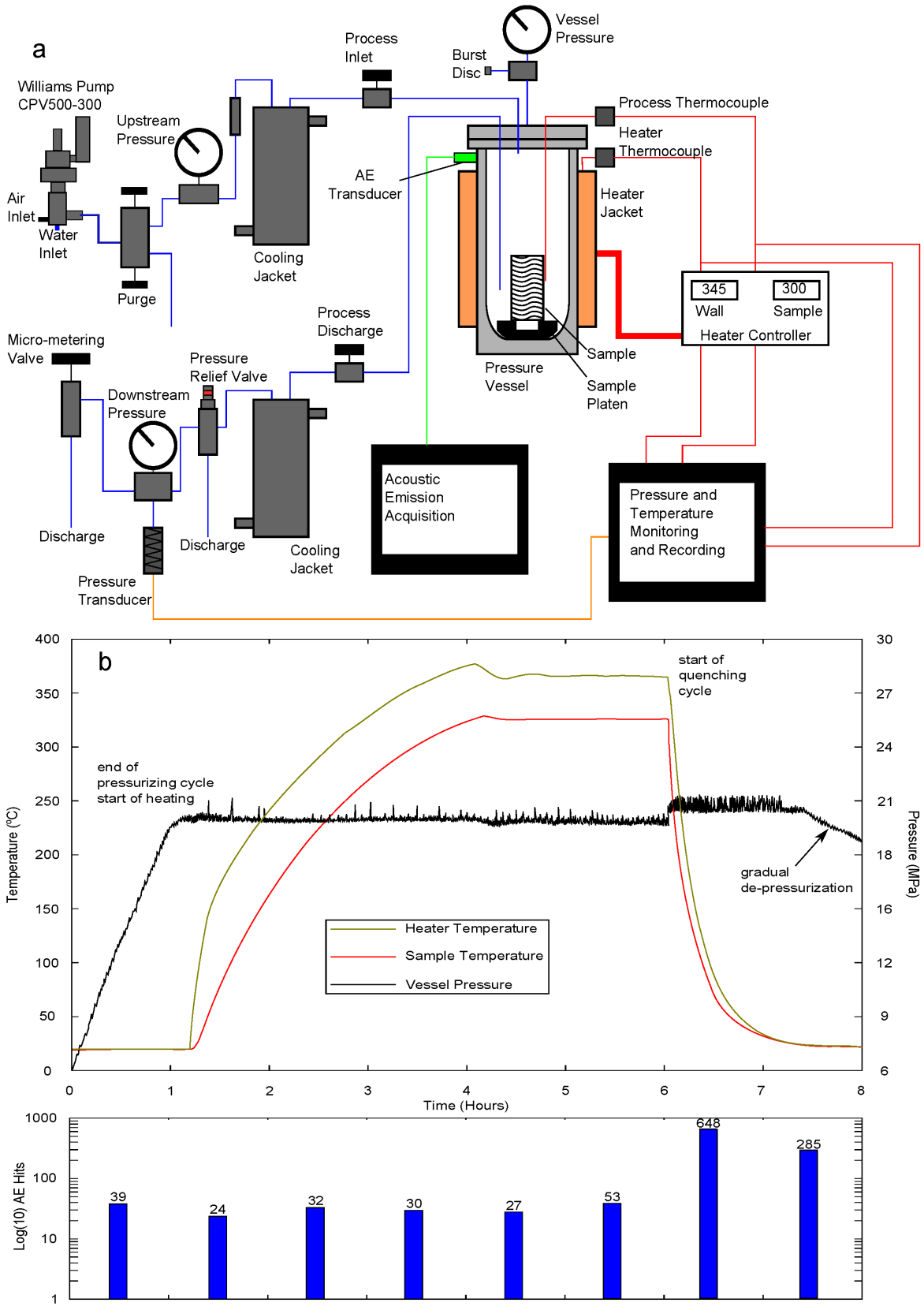

Figure 6.1: (a) Thermal treatment apparatus (b) Pressure, temperature and acoustic emission profile for thermal treatment cycle of sample 27-3.7a.

6.3 Results

Figure 6.2 details the key physical parameters that we measured to gain an understanding of how thermal quenching after heating may influence the properties of the Rotokawa Andesites. Porosity shows an average increase of 0.7 (vol%) with a range of 0.5-1.0 (vol%) change in porosity across the dataset (Figure 6.2a). This is coupled with a marked increase in permeability for all samples, where we observe that the mean value of permeability has increased from $2.9 * 10^{-17}$m^2 to $2.3 * 10^{-16}$ m^2 across all samples, such that the stimulated values are an average of 7.8 times more permeable. This is neither a trivial nor insignificant shift and shows that we have achieved an increase in permeability for the Rotokawa Andesite following our stimulation methodology. Accordingly, we see a marked decrease in our acoustic wave velocities with average compressional wave attenuation of 540 m/s and shear wave velocities showing average attenuation of 96 m/s. The reduction in these velocities show that we have created cracking in the samples as the acoustic properties are very sensitive to the presence of cracks in the material (Stanchits et al., 2006). Figure 6.2b shows the graphical representation of the acoustic attenuation where both Vp and Vs are significantly reduced following thermal treatment which is a direct indication of an increase in microfracture densities (Anderson et al., 1974; Stanchits et al., 2003). Coupled with measurements of bulk density and attenuated acoustic velocities we subsequently show a significant decrease in the dynamic Young's modulus and Poisson's ratio (Figure 6.2c) after thermal stimulation testing.

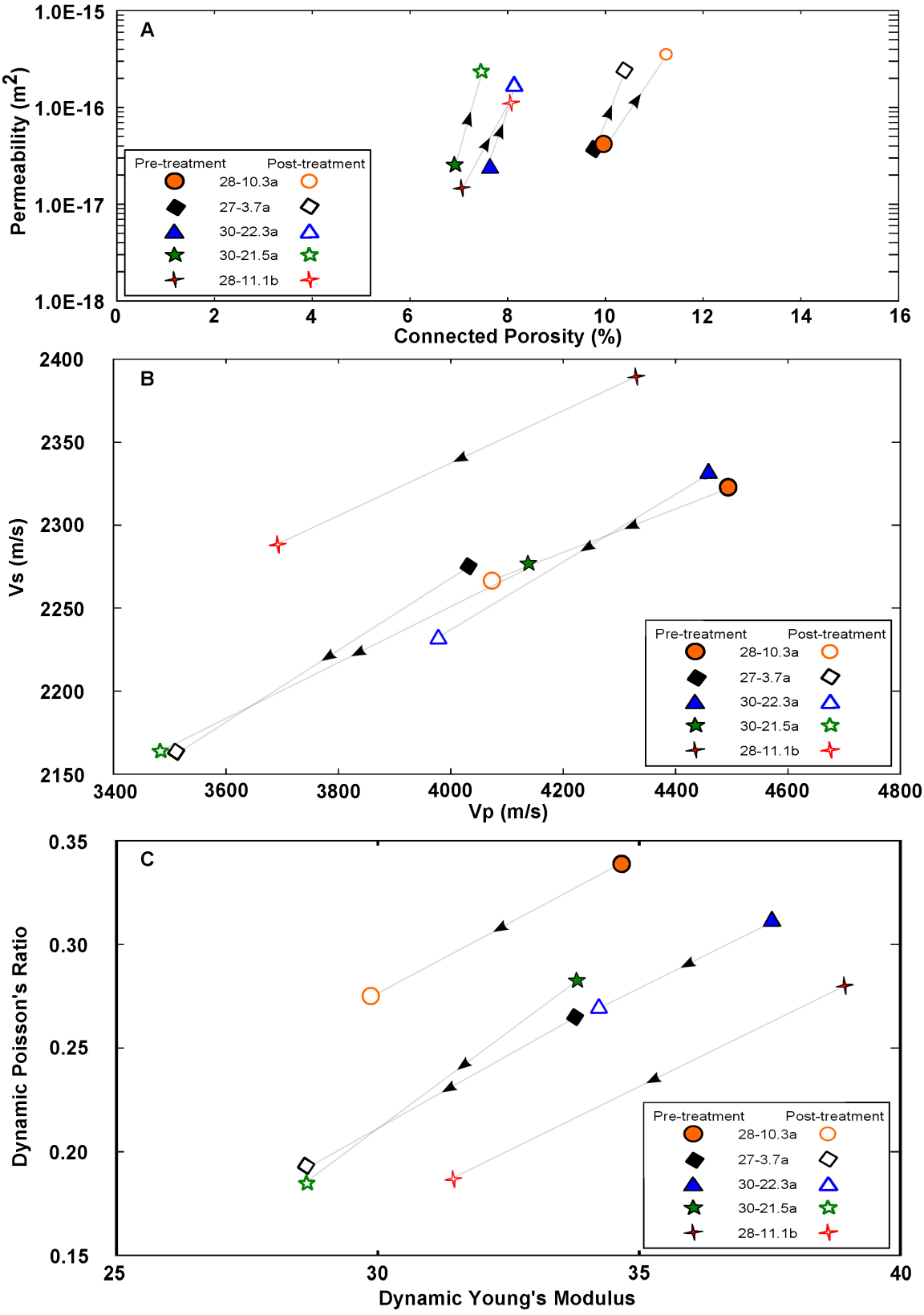

Figure 6.2: Pre-treatment and post-tretment comparisons of physical properties of Rotokawa Andesite (a) Porosity and permeability. (b) Compressional wave velocities (Vp) and shear wave velocities (Vs). (c) Dynamic Young's modulus and Poisson's ratio.

To support our macroscopic property investigations indicating that fracturing has occurred in the samples, we utilized backscattered scanning electron microscopy on the sample surfaces. An examination of pre-test (Figure 6.3 a and c) and post-test (Figure 6.3 b and d) scans shows that the microstructure of the samples has changed as a result of the thermal stimulation procedure. The stimulation process appears to force a dissolution of the sample structure with a preference for the matrix while phenocrysts retain some original fabric but are also largely altered. This is further supported by Figure 6.4 where the sample was in contact with the platen at the base of the sample chamber and no alteration is observed where water has not been in contact.

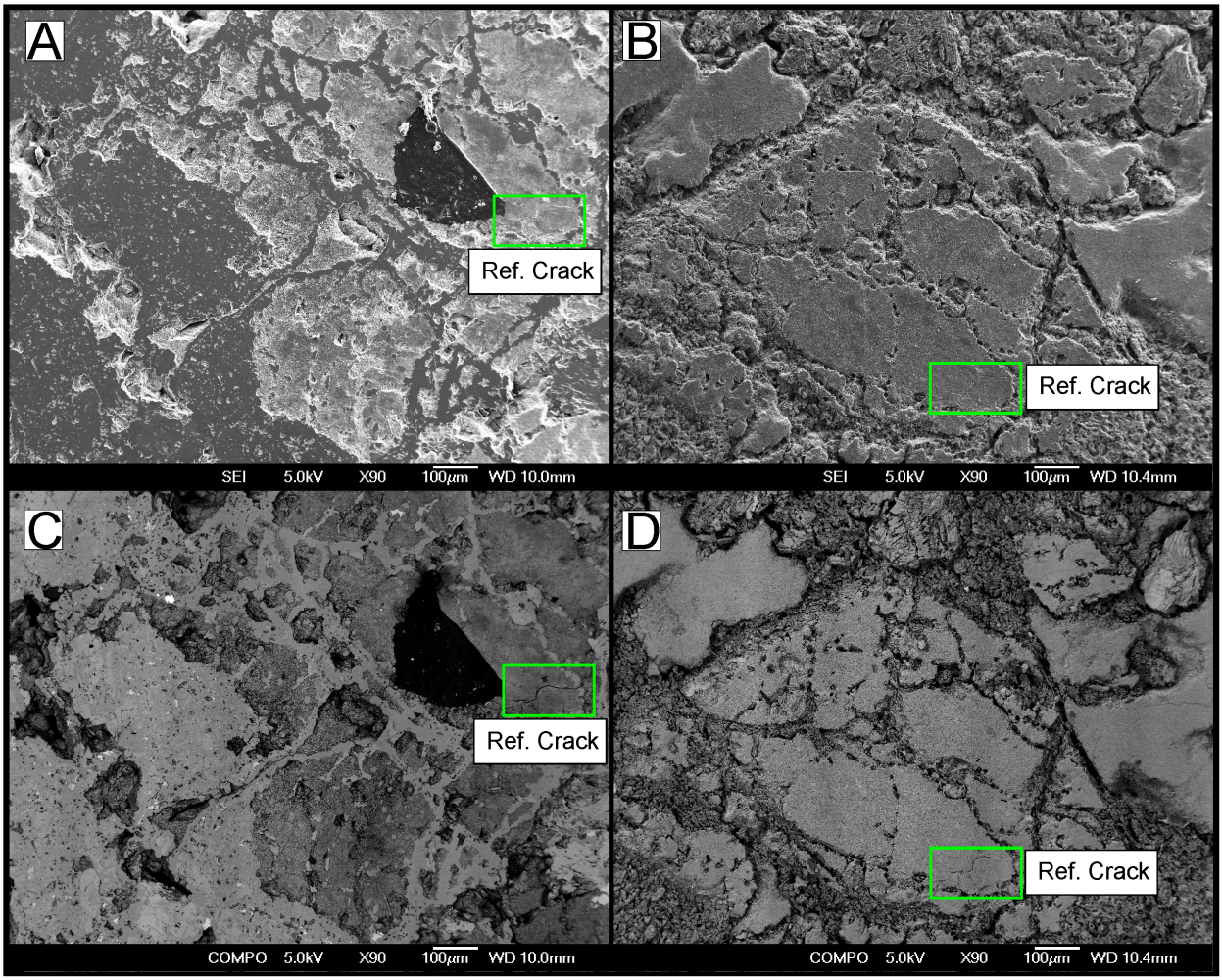

Figure 6.3: Scanning Electron Microsope images of Rotokawa Andesites with reference crack highlighted to orient sample in microscope field of view (A) Pre-treatment secondary analysis image showing likely plagioclase phenocrysts and ferromagnesian ground-mass. (B) Post-treatment secondary analyis image showing greater relief and preferential nature of chemical etching. (C) Backscattered pre-stressing image showing groundmass and hydrothermally altered phenocrysts. (D) Backscattered post-stressing image showing pervasively etched phenocrysts, groundmass and significantly higher fracture density in phenocrysts with preferential etching.

6.4 Discussion

Thermal stressing under laboratory conditions has been carried out on rocks of varying composition at various heating and cooling rates (e.g. Yong and Wang, 1980, Chaki et al., 2008; Keshavarz et al., 2010). In almost all cases where thermal treatments are applied, permeability is increased by the treatment (see David et al., 1999 and Nara et al., 2011 for further discussion). However, many of these studies are carried out on rocks that have been erupted and slowly cooled and been used for quarrying materials and building materials for some years (e.g. Westerly Granite Frederick Diabase, see Yong and Wang, 1980; Fredrich and Wong, 1986). No studies have been carried out on geothermal core with the explicit aim to increase permeability under controlled temperature conditions and fully water saturated environments using high cooling rates and high flow rates. We have demonstrated the ability to enhance permeability through our experiments and this is seen in Figures 6.2 and 6.3.

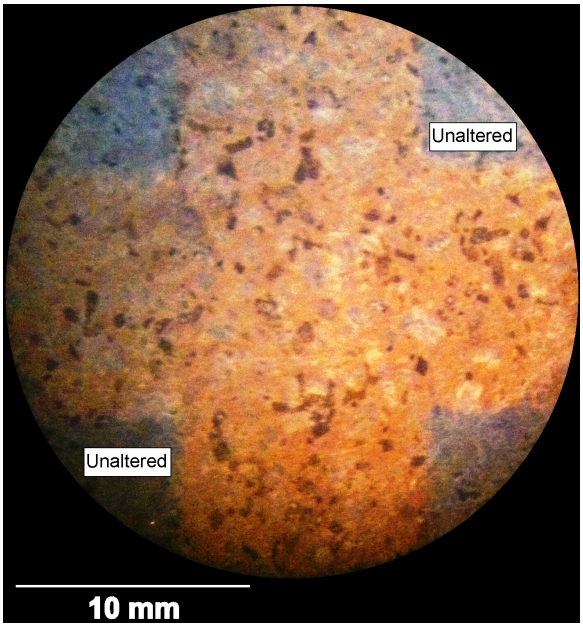

Figure 6.4: Post-Treatment Rotokawa Andesite showing altered and unaltered portions of core where the sample sat on the platen in the pressure vessel.

We have stressed these rocks to temperatures that they would have been subject to prior to exhumation by drilling (Rae, 2007), and do not anticipate that additional damage would result from thermal stressing whatever the heating rate (as observed by Yong and Wang, 1980). It is however possible that during our rapid cooling, we are placing instantaneous stress by thermal gradients on already existing cracks and propagating those cracks. This is evidenced by acoustic emissions that we have observed during the thermal cycling (Chapter 3 for further discussion). As such, we have to consider that significant thermal stress is being imparted on rocks that have a complicated thermal and chemical history.

A close inspection of the SEM images shows that there is significant surface chemical interaction occurring in the samples. There is apparent preferential dissolution of plagioclase and significant dissolution of several other mineral species that are present in the material. This dissolution is extensive and we consider this to indicate that there must be a disequilibrium of the fluids used in our stimulation with those that are the resident in the reservoir, and that this reaction is both thermally and chemically complex. We must also consider that the depth at which the alteration occurs is only a small fraction of the total volume of the

sample. It is possible that the thermo-chemical reactions we see at the surface are able to penetrate into cracks that pervade the rock masses, but that the entire sample is not subject to this alteration as seen in Figure 6.4.

The implications of the thermal and chemical components of this study are significant as in real-world thermal stimulations, when large volumes of water pumped down wellbores sourced from nearby water sources or cooling tower basins, these are largely enriched in oxygen compared to those fluids in the reservoir. We must therefore conclude that there is a significant oxidation of the reservoir rocks and this may serve to work as a chemical 'wedge' of sorts for propagation of fractures. It is widely accepted that thermal cracking is isotropic in nature. However, this does not account for significant chemical changes that may initiate mechanical cracking as a result of weaknesses created by chemical erosion.

Further work should replicate reservoir brine chemistries at ambient temperatures to see if the same chemical erosion occurs. It may be possible that the oxidation and erosion we observe is simply a forced washing of our samples, but at this stage it seems thermal stimulation may be enhanced down-hole at the wellbore face and within reservoir rocks by the introduction of variable fluid chemistries.

Our study has shown that permeability is enhanced by our testing method which is the fundamental goal of any thermal stimulation procedure and has implications for larger scale borehole stimulations. We have shown that permeability is greatly enhanced by cold water stimulation in the laboratory and this reinforces the need to further study how to optimize this procedure and benefit geothermal projects worldwide.

In conclusion, our study is the first of its kind to directly simulate thermal stimulation on cores sourced directly from a geothermal reservoir, with the explicit goal of permeability enhancement through rapid thermal quenching under high flow rates. Our geothermal stimulation device realistically replicates the temperatures and pressures that may be encountered in a down-hole environment. We find that cold water shocking of the core results in an increase of intrinsic permeability as a result of additional thermal cracking, but chemical disequilibrium must be considered when conducting further experiments.

6.5 Acknowledgements

The authours wish to thank the Rotokawa Joint Venture (Mighty River Power Company Ltd. and Tauhara North No.2 Trust) for the core utilized in this study. Mighty River Power Company Ltd. also provided generous financial support. The staff of the Department of Geological Sciences at the University of Canterbury were invaluable in many aspects of this research. The Brian Mason Trust also provided for the transportation and delivery of the core to UC. The authors of this study also acknowledge a Hubert Curien Partnership

(PHC) Dumont d'Urville grant (grant number 31950RK) which has assisted the France-New Zealand collaboration for this and future projects.

6.6 References

Anderson, D.L., Minster, B., & Cole, D. (1976). The effect of oriented cracks on seismic velocities. Journal of Geophysical Research, 79, 4011–4015.

Axelsson, G., & Thórhallsson, S. (2009). Review of Well stimulation Operations in Iceland. Geothermal Resource Council Transactions, 33, 795–800.

Chaki, S., Takarli, M., & Agbodjan, W. P. (2008). Influence of thermal damage on physical properties of a granite rock: Porosity, permeability and ultrasonic wave evolutions. Construction and Building Materials, 22(7), 1456–1461.

Darot, M, Gueguen, Y., & Baratin, M.-L. (1992). Permeability of Thermally Cracked Granite. Geophysical Research Letters, 19(9), 869–872.

David, C., Menendez, B., & Darot, M. (1999). Influence of stress-induced and thermal cracking on physical properties and microstructure of La Peyratte granite. International Journal of Rock Mechanics and Mining Sciences, 36(4), 433–448.

Flores, M., Davies, D., Couples, G., & Palsson, B. (2005). Stimulation of Geothermal Wells , Can We Afford It ? In Proceedings World Geothermal Congress, Antalya, Turkey 24-29 April (p. 8).

Flores-Armenta, M., & Tovar-Aguado, R. (2008). Thermal Fracturing of Well H-40 , Los Humeros Geothermal Field. Geothermal Resource Council Transactions, 32, 8–11.

Fredrich, J. T., & Wong, T. (1986). Micromechanics of Thermally Induced Cracking in Three Crustal Rocks. Journal of Geodynamics, 91(B12), 12743–12764.

Grant, M.A., Clearwater, J., Quinao, J., Bixley, P.F., & Le Brun, M. (2013). Thermal Stimulation of Geothermal Wells: A Review of Field Data. In Proceedings, Thirty-Eighth Workshop on Geothermal Reservoir Engineering. Stanford University, Stanford, California. (p. 7).

Guéguen, Y. & Palciauskas, V. (1994). Introduction to the Physics of Rocks (p. 294). Princeton, New Jersey: Princeton University Press.

Keshavarz, M., Pellet, F. L., & Loret, B. (2010). Damage and Changes in Mechanical Properties of a Gabbro Thermally Loaded up to 1,000°C. Pure and Applied Geophysics, 167(12), 1511–1523.

Kitao, K., Ariki, K., Hatakeyama, K., & Wakita, K. (1990). Well Stimulation Using Cold-Water Injection Experiments in the Sumikawa Geothermal Field, Akita Perfecture, Japan. Geothermal Resource Council Transactions, Vol. 14(Part II), 1219–1224.

Klinkenberg, L.J. (1941). The permeabiltiy of porous media to liquids and gases. American Petroleum Institute, Drilling and Production Practices, 200-213.

Milsch, H., Seibt, A., & Spangenberg, E. (2008). Long-term Petrophysical Investigations on Geothermal Reservoir Rocks at Simulated In Situ Conditions. Transport in Porous Media, 77(1), 59–78.

Nara, Y., Meredith, P. G., Yoneda, T., & Kaneko, K. (2011). Influence of macro-fractures and micro-fractures on permeability and elastic wave velocities in basalt at elevated pressure. Tectonophysics, 503(1-2), 52–59.

Pasikki, R. G., Libert, F., Yoshioka, K., & Leonard, R. (2010). Well Stimulation Techniques Applied at the Salak Geothermal Field. In Proceedings World Geothermal Congress, Bali, Indonesia (Vol. 25–29 Apri, p. 11).

Rae, A. (2007). Rotokawa Geology and Geophysics. GNS Science Consultancy Report 2007/83 (p. 17).

Stanchits, S. A., Lockner, D. A., & Ponomarev, A. V. (2003). Anisotropic Changes in P -Wave Velocity and Attenuation during Deformation and Fluid Infiltration of Granite. Bulletin of the Seismological Society of America, 93(4), 1803–1822.

Stanchits, S., Vinciguerra, S., & Dresen, G. (2006). Ultrasonic Velocities, Acoustic Emission Characteristics and Crack Damage of Basalt and Granite. Pure and Applied Geophysics, 163(5-6), 975–994.

Ulusay, R. & Hudson, J. (2007). The Complete ISRM Suggested Methods for Rock Characterization, Testing and Monitoring: 1974-2006 (1974th–2006th ed., p. 628). Antalya, Turkey: Elsevier.

Vinciguerra, S., Trovato, C., Meredith, P., & Benson, P. (2005). Relating seismic velocities, thermal cracking and permeability in Mt. Etna and Iceland basalts. International Journal of Rock Mechanics and Mining Sciences, 42(7-8), 900–910.

Yong, C. & Wang, C. Y. (1980). Thermally Induced Acoustic Emission in Westerly Granite. Geophysical Research Letters, 7(12), 1089–92.

Chapter 7

Conclusions

7.1 Key Findings of the Thesis

In order to investigate thermal stimulation on the laboratory scale, it was necessary to develop a special device that would allow me to heat and cool rocks under water saturated confined conditions while maintaining pressure in the system. I therefore developed a system that imparts damage on rocks through rapid quenching and is currently unique in laboratory rock deformation techniques (Chapter 3). This thermal damage has been quantifiable through the use of tools that rely on the microstructural characteristics of the rocks to determine physical properties.

In all cases where I have quenched rocks under pressure, acoustic velocities have been attenuated and porosity has increased. These properties have been used by many authors to infer that permeability has been increased through proxy of increased porosity and decreased acoustic velocities by damage to the microstructure. By comparison of my results to those of previous studies, I have demonstrated that through the damaging of the rocks, their permeability has been increased, which is the fundamental goal of the device.

A systematic evaluation of the Rotokawa Andesite was deemed necessary to develop an understanding of the physical properties of this lithology for the application of the thermal stimulation device. Through a rigorous evaluation of the Rotokawa Andesite core (Chapter 4), I was able to develop solid empirical relationships based on strength, porosity, permeability and ultrasonic velocities. These findings were further enhanced by developing a solid understanding of how the microstructure of the Rotokawa Andesite related to these physical properties.

In my investigation, I was able to correlate the microstructure to the physical properties measured and found that the microstructure (specifically with regard to cracks) is the dominant controlling factor on the physical behavior of the andesites. Further, through the application of my microstructural data, I applied classical modeling to develop a damage criterion that gives a close approximation of the strength of the andesite through the use of acoustic velocities.

A further investigation of the thermo-elastic properties of the Rotokawa Andesite helped me to constrain the thermal expansion coefficients of the rock under varied heating rates (Chapter 5). This indicated that regardless of the heating rate, the coefficients were the same, but were coupled with much greater strain on the samples at high heating rate. I was unable to create additional cracking during these experiments which were carried out in a dry atmosphere.

The results of the investigation also show that in the temperature range (20-350^{o}C) of thermal expansion measurements, there was no significant thermo-chemical reaction occurring that could have caused damage in the samples. However, by increasing the temperature range of my thermo-mechanical measurements, there were significant reactions that took place above 450^{o}C. I also attempted to fit thermal expansion behavior to porosity of the rocks but found that there was no correlation to linear thermal expansion behavior both empirically and through classical models that derive thermal expansion from porosity. However, I was able to develop a tensile stress criterion for the Rotokawa Andesite as a function of temperature and the thermomechanical properties measured.

In Chapter 6, I was able to replicate the very process that was envisaged at the onset of planning for this thesis: creating permeability in the Rotokawa Andesite in the laboratory. Through the application of the geothermal stimulation device, the understandings of the physical properties of the Rotokawa Andesite, and the application of my findings, I replicated a thermal stimulation on the Rotokawa Andesite. The results of this experiment were confirmed by evaluation of physical properties before and after thermal stimulation in the laboratory. Permeability was enhanced in rocks that have experienced a very complex thermal and mechanical history. This was therefore a successful laboratory demonstration of the potential effects of thermal stimulation on Rotokawa Andesite.

7.2 Implications for the Geothermal Industry

This research has developed several ideas and pieces of information that are directly applicable to optimization of geothermal resources. The stimulator device is one such development that can serve as a testing ground for processes that are normally carried out at a field scale. Chemical suites to be applied to reservoirs may potentially be tested in the stimulation device on samples of reservoir rock to help reduce risk to the wells and reservoir before being applied at the reservoir scale.

The empirical correlations that we have shown for the Rotokawa Andesite will be useful in the assessment of wells to be drilled in the future by applying our strength criteria and damage criteria. These correlations may also be applied to the results of wireline logging to assess formation strength and permeability, and can

be applied to numerical reservoir simulations using the data that we have derived, giving accurate constraints of physical properties.

Results of our thermal stimulation testing can also be quite useful in the planning of future reservoir stimulation as permeability in our experiments has increased by nearly an order of magnitude, which in a well would be an astonishing result. It would be very beneficial to address how the changes we see in the laboratory correlate to field scale stimulations and what conditions need to be met in the field to achieve such success.

7.3 Future Research Issues and Questions to Address

There are many research issues that I believe can be addressed in future laboratory work on thermal stimulation, and many questions still to answer.

Some of these questions are considered here:

- The relationship between laboratory experiments and the field environment, is there a scale effect?
- The geochemical component of thermal stimulation in the stimulation device. How does the geochemical signature of the waters used in the process change through the thermal cycle? Can we isolate those chemicals that are prone to change and enact purely mechanical changes? Conversely, what conditions are needed to enact pure chemical changes with no mechanical stress component?
- The role of differing fluid temperatures of the stimulation fluid in the stimulation device. Can we determine the ideal threshold at which permeability is increased in reservoir rock through laboratory testing? Is it possible to use fluids other than water to achieve even greater permeability enhancement (i.e. acids, brines, supercritical fluids, etc.)?
- Comparing the response of differing rock types to thermal stimulation testing. Testing on different lithologies of similar physical properties may yield significant information on what parameters change the most from thermal stimulation testing. Are the changes we have observed constrained by mineralogy and chemistry or are they purely mechanical and textural?
- Thermal expansion appears to have no reliance on porosity in this study. What are the factors that constrain thermal expansion in geothermal reservoir rocks? Would high-temperature water-saturated testing yield significantly different results? Can detailed mineralogy and petrology be used to apply geochemical models to constrain thermal expansivity?

- Constraining fracture networks in reservoir samples using high-resolution tomographic studies on pre-stimulation and post-stimulation samples. This will allow very detailed mapping of fracture networks in a non-destructive manner and illustrate which pathways are preferentially stimulated during quenching.
- What are the constraints of the Kaiser effect? To what extent is it controlled by chemistry of the rocks and fluid interactions?

Appendices

Contents of Digital Appendices:

- Appendix A: Spreadsheets of Stress-strain curves and ultrasonic data files used in Chapter 3
- Appendix B: Spreadsheets of Stress-strain curves and ultrasonic data files used in Chapter 4
- Appendix C: Thin-section photomicrographs and spreadsheet for crack density studies in Chapter 4
- Appendix D: Photomicrographs of Rotokawa Andesite (optical microscope and scanning electron microscope)